# Analysis of Ship Motions in Shallow Water

Development of a numerical tool for fluid-structure interaction in shallow water

## W.E. Zwart

**TU**Delft

Delft University of Technology

Delft Offshore and Dredging Engineering

# Analysis of Ship Motions in Shallow Water

**Development of a numerical tool for fluid-structure interaction in shallow water**

MASTER OF SCIENCE THESIS

For the degree of Master of Science in Offshore and Dredging Engineering at Delft University of Technology

W.E. Zwart

February 21, 2017

DELFT UNIVERSITY OF TECHNOLOGY
DEPARTMENT OF
OFFSHORE AND DREDGING ENGINEERING ODE

The undersigned hereby certify that they have read and recommend to the Faculty of Mechanical, Maritime and Materials Engineering (3mE) for acceptance a thesis entitled

ANALYSIS OF SHIP MOTIONS
IN SHALLOW WATER

by

W.E. ZWART

in partial fulfillment of the requirements for the degree of

MASTER OF SCIENCE OFFSHORE AND DREDGING ENGINEERING

Dated:  February 21, 2017

Supervisor(s):                                  prof.dr.ir. R.H.M. Huijsmans

Dr.ir.H.J. de Koning Gans

ir. Daan Scheltens

Reader(s):

# Acknowledgements

This thesis is the result of my graduation internship at Van Oord as final part of obtaining a master's degree for the program Offshore and Dredging Engineering at Delft University of Technology. I could not have done it without the help and support of several people and I would like to thank them sincerely for their contributions.

First and most of all, I would like to thank my supervisor Daan Scheltens for his friendly, professional and insightful assistance. Daan Scheltens has been very helpful, especially with regards to his great programming skills and critical in depth questions and guidance throughout the process.

Furthermore, Kevin van de Leur, thanks for jumping on board. Your expertise, critical questions and constructive criticism have been of great help. It has offered lots of guidance in structuring the project and the final report.

Thirdly, I would like to express my gratitude to Henk de Koning Gans, many thanks for your help and the fact you have given me some confidence in times when I needed it. Furthermore, I would like to thank Prof. RenÃľ Huijsmans for supervising this project. Critical questions during meetings helped to challenge my own thought process and keep the main objective in mind. The academic expertise and feedback from your side helped me a lot during the process.

And of course, this space cannot be left unused to thank everyone I love. Nicole, Anne and mama; idiots and rockstars. Bobbedijnen, OD26, Taco's, Nootje, Miet, Bets, thanks for being the awesome and loving friends you are. Oom Kobus and Jo, my running role models.

Delft, University of Technology W.E. Zwart
February 21, 2017

# Abstract

In order to guarantee safe operations in the offshore industry, at all time it is necessary to predict motion behaviour of structures in specific sea states accurately. Safety is very important for the offshore industry, which can come in jeopardy when motions are either extreme or unexpected with regards to predicted motion behaviour. This thesis aims to establish improved motion behaviour prediction of a barge in shallow water.

A parametric model is developed, in both frequency as well as time domain, which contains flexibility for other, non-linear wave theories, as well as other non-linear effects like viscous damping or an additional inertial force which can atone for the approaching seabed in shallow water motions. It utilises hydrodynamic coefficients from the diffraction analysis in ANSYS AQWA, with which motions are also verified. As no validation data were available, this verification was very important. The accuracy of motion prediction is verified in both Frequency Domain (FD) and Time Domain (TD), which assures its applicability. The model subsequently is wider applicable, as it allows for non-linear wave theories or modifications by other external forces. Parameters Ursell Number (UR), steepness $S$ and relative depth $\mu$ are defined which determine the validity of wave theories. These parameters display theoretical limits of applicability and validity of the Linear Wave Theory (LWT). The parametric model is capable of calculating associated wave forces up to second order, which can modify the predicted motion behaviour for higher waves than the LWT allows. In the model a *Vessel* - object and *Wave* - object are defined. The former is for this thesis a rectangular barge, while the latter contains information on the sea state, defined by input parameters wave height $H$, wave period $T$ and water depth $d$. In both FD and TD vertical displacements of four vertices are calculated, based on the heave, roll and pitch Degree of Freedom (DOF). Subsequently, viscous effects are included based on a factor of the critical damping in each specific DOF, which moderates the vertical motion especially near resonance. A numerical example of an additional inertial force to account for cushioning and sticking is elaborated, which displays effects of an approaching seabed on heave displacement. These values are based on water particle velocities in the Under Keel Clearance (UKC), but is not verified nor validated, so no general conclusion can be drawn. It does show nicely how the model is capable of dealing with additional external forces and subsequently calculates resulting motions. Second order effects increase in significance in shallow water of which set - down is an important non-linear

shallow water effect, which has great significance in predicting ultimate vertical motions. The numerical solutions for a mono-directional bi-chromatic wave group show that these additional displacements are in such an order of magnitude that it should be accounted for in shallow water ship motion hydrodynamics. Viscous moderations are also within this order, although these exist by the grace of the structure's velocity, while set - down is a phenomenon related to the waves, which occurs regardless of a vessel present or not.

# Table of Contents

# List of Figures

# List of Tables

# Glossary

**COG** Centre of Gravity

**DOF** Degree of Freedom

**EOM** Equation of Motion

**FFT** Fast Fourier Transform

**FK** Froude-Krylov

**LWT** Linear Wave Theory

**LF** Low Frequency

**FD** Frequency Domain

**IRF** Impulse Response Function

**TD** Time Domain

**UKC** Under Keel Clearance

**RAO** Response Amplitude Operator

**UR** Ursell Number

**QTF** Quadratic Transfer Function

# List of Symbols

| | |
|---|---|
| $\Phi$ | Velocity Potential |
| $\zeta$ | Wave amplitude $[m]$ |
| $\eta$ | Surface elevation $[m]$ |
| $\epsilon$ | Perturbation parameter [-] |
| $\varepsilon$ | Phase $[rad]$ |
| $\lambda$ | Wave length $[m]$ |
| $\mu$ | Shallow water parameter [-] |
| $\nabla$ | Displaced volume of water $m[m^3]$ |
| $\phi$ | Roll angle $[rad]$ |
| $\theta$ | Pitch angle $[rad]$ |
| $\rho$ | density $[kg/m^3]$ |
| $\psi$ | Yaw angle $[rad]$ |
| $\omega$ | Wave frequency $[rad/s]$ |
| $\omega_n$ | Natural frequency $[rad/s]$ |
| $\xi$ | Damping Factor [-] |
| $A$ | Area $[m^2]$ |
| $A_{ij}$ | Added Mass Matrix for force in $i$ - mode due to acceleration in $j$ - mode |
| $B_{ij}$ | Potential Damping Matrix for force in $o$ - mode due to velocity in $j$ - mode |
| $B_{crit}$ | Critical damping $[Ns/m]$ |
| $B_v$ | Viscous damping $[Ns/m]$ |
| $C_{ij}$ | Stiffness Matrix for force in $o$ - mode due to motion in $j$ - mode |
| $C_D$ | Drag coefficient [-] |
| $F_i$ | External load in $i$ - mode |
| $H$ | Wave height $[m]$ |
| $K(k_{cn})$ | Complete elliptical integral of first kind |
| $L$ | Length of Vessel $[m]$ |
| $R_{ij}(\tau)$ | Retardation in $i$ - mode due to motion in $j$ - mode $[Ns/m]$ |
| $S$ | Wave Steepness [-] |
| $S_H$ | Wetted Hull Surface $[m^2]$ |
| $T$ | Draft of Vessel $[m]$ |

| | |
|---|---|
| $U_R$ | Ursell Number [-] |
| $W$ | Width of Vessel $[m]$ |
| $X_j$ | motion in direction $j$ $[m]$ |
| $\dot{X}_j$ | Velocity in direction $j$ $[m/s]$ |
| $\ddot{X}_j$ | acceleration in direction $j$ $[m/s^2]$ |
| $a_{ij}$ | Added mass coefficients $[kg]$ |
| $b_{ij}$ | Potential damping coefficients $[kg \cdot s]$ |
| $cn$ | Jacobi Elliptical Function |
| $c$ | Wave celerity $[m/s]$ |
| $d$ | Water depth $[m]$ |
| $g$ | Gravitational acceleration $[m/s^2]$ |
| $k$ | Wave number $[rad/m]$ |
| $k_{cn}$ | Elliptical parameter |
| $t$ | time $[s]$ |

# Chapter 1

# Introduction

For fixed offshore platforms it is common procdure to be constructed in shallow water for the exploitation of oil and gas resources. Nowadays, floating structures have also been proposed to be located in shallow waters. For these operations to be safe though, the technical challenges which come along with restricted water depths need consideration in the design state. Incoming waves and vessel motion behavior are generally predicted under assumptions of linearity, i.e. with deep water waves. In shallow water though, this might not be accurate enough for motion prediction. Strong non-linearities in propagating waves and complex wave-structure interactions are important aspects in this issue [6].

The rise of interest in shallow water causes to challenge common way of thinking about hydrodynamics, i.e. whether the assumptions of the potential theory are still valid in these situations. Water depth has significant effects on hydrodynamic coefficients, especially on vertical modes of motions, which could alter validity of presumed methods on motion prediction and subsequently cause bottom touching of barges operating in very shallow waters [7]. Van Oord faced issues with these situations and therefore seeks more understanding in shallow water motion behaviour of vessels, and needs knowledge on the validity of potential theory. Accurate motion prediction of barges in shallow water for safe pipe laying or supply operations is necessary, for which the linearity assumptions no longer hold. Furthermore, Van Oord also invests heavily in wind farms so this knowledge on shallow water operations is very valuable since this part of the industry is growing fast, and these wind turbines are usually built in shallow water. Common procedures of predicting motion behaviour through linear transfer transfer functions of incoming waves forces to vessel motions are challenged in these areas. Forces in such operations in shallow water can usually be split in a linear and non-linear components. The linear part is sufficiently covered in literature, but further research is required in prediction of the non-linear component. Instead of combining linearised characteristics, found by Frequency Domain (FD) based analyses, an approach combining empirical data or other solutions in Time Domain (TD) approach might is required [8].

## 1-1   Van Oord

Van Oord is a Dutch contractor, operating globally in dredging, land reclamation and offshore activities. Van Oord's Shallow Water Pipelay Barge Stingray is an example of a vessel which is subjected to the conditions where shallow water effects might be an issue. In 2013 van Oord complemented its fleet with the Shallow Water Pipelay Barge Stingray. This vessel is in use for the installation of pipelines in very shallow water conditions (10-100 m) in S-Lay. Van Oord has experience in shallow water oil and gas market for decades, with a focus on seabed intervention works as trenching and backfilling for pipeline shore approaches. The Stingray expands Van Oord operations as it allows to offer a wider range of services in a complete one-stop package for shallow water oil and gas developments. Furthermore, with the acquisition of Ballast Nedam in 2014, Van Oord got ownership over Svanen. This vessel is another example for which more insight in seabed interaction could be beneficial.

## 1-2   Problem Statement

Van Oord faces challenges with predicting motion behaviour of structures in shallow water in FD. Operations with the shallow water pipe laying barge the Stingray were forced to be cancelled in water depths of approximately $d = 11$ m, in swell waves of $T \approx 12$ s. The structures moved along with the waves in vertical direction downwards, which increased downtime of the operations and thus lowered overall workability. Motion behaviour of the Stingray was hence non-linear, and could thus not have been safely estimated by linear Response Amplitude Operator (RAO)s. With a design draft $T = 5$ m, the non-linearities clearly influenced its motion behaviour. For the validation of numerical results obtained in shallow water, there is not sufficient benchmark data available this present day, which makes knowledge of the motions of large ships and floating structures in shallow water a challenging issue [9]. Van Oord noticed that FD-based calculations done by diffraction software is not fully trusted in (very) shallow water situations. Motion behaviour can arguably not be predicted accurately any more by RAOs due to non-linearities.

Vast majority of research relies on potential flow theory, which neglects non-linear effects such as breaking waves and viscosity. The effect of depth and wave amplitude on dynamic pressure becomes however increasingly important. Panel methods in such cases can however fail to accurately predict motions due to proximity of the seabed [10]. These effects are more problematic in shallow water and should be included in numerical codes [9]. Moreover, in shallow water the importance of accounting for low frequency second order effects is often emphasized. Slow drift excitation forces can increase seriously with decreasing water depth and the second order velocity potential contribution can be dominant is specific frequency ranges. Low frequency second order effects such as set-down and shoaling can result in significant excitation of the focal vessel. It can cause large resonant motions and related mooring loads and can ultimately cause problems in the shallow water area [11]. Wave amplitudes might furthermore be more significant than those assumed in the Linear Wave Theory (LWT). It is argued that the validity of the linearized theory of surface waves only holds for low values of wave steepness $S$ and Ursell Number (UR) [12]. Furthermore, the linearised boundary conditions under the assumptions of the LWT fail to describe wave kinematics in the wave zone and subsequently disregard of some wave loads. The resulting behaviour is however also affected,

so not only the wave exciting part of the Equation of Motion (EOM), but hydrodynamic coefficient added mass and potential damping are also influenced in shallow water. Added mass is for example important to determine natural periods of structure motions, and known to increase significantly when the seabed approaches [6, 13, 14, 15]. Non-linear effects might be excited and affect steady state oscillations but the diffraction theory does not simulate these effects. To overcome this issue is necessary, as more accurate prediction of in what type of environmental conditions barge like vessels will move more / less in vertical direction is necessary to safely predict when these vessels will approach hitting the seabed. Second order effects like set - down will cause the mean water level to decrease, lowering the clearance between the vessel's keel and seabed simultaneously, but also first order roll and pitch moments can magnify the vertical motions when these are superimposed with the heave displacement. This increases chances of bottom - touching, lowering workability, or worse. This obviously can cause great problems, so with more detailed knowledge on non-linear effects of incoming waves, the policy of Van Oord and its clients on allowing operations in very shallow water can be adjusted to one with a more accurate prediction of operating window. Firstly by improving knowledge on non-linear water waves, because a relationship exists between potential flow and pressure exerted by water waves and some difficulties arise which are not covered by assuming linear waves. Secondly, non-linear effects with lower under keel clearances affects hydrodynamic coefficients which is also not captured by the linear potential theory [6, 9].

For the linear part, a FD based analysis in the diffraction software package suffices. For non-linear parts of the problems in shallow water, the linear FD analysis isn't capable of predicting motions accurately. Second order wave loads need to be taken into account and can only be considered an external force to the EOM in the TD analysis. One of the issues of this is the diffraction analysis software Ansys AQWA itself. The program assumes very small movements of source panels. Moreover, the seabed is assumed to be far away. In reality though, when the body approaches the seabed, particles have less freedom to move, i.e. to escape vertically from the gap.

Because of this, a parametric model is developed which can carry out calculations in both FD and TD. This flexibility allows for verification for the motion modelling, but also for including non-linear external wave forces or other non-linear effects on the hydrodynamic coefficients added mass and potential damping.

## 1-3   Objectives

The main objective is improve workability by more accurately predict incoming wave forces and associated motion behaviour of a barge in shallow water. Preventing the barge to hit the seabed determines this workability, so an analysis is necessary on what additional information is necessary next to linearity assumptions of the potential theory. It has been shown in literature that first order forces due to incoming waves provide information which is not accurately enough, so additions and/or modifications are necessary. For the issues in shallow water, the objective of the thesis is two-fold. To assess safety and workability, it is necessary to gain in depth insight in wave exciting forces on the one hand, and the hydrodynamic coefficients added mass and potential damping on the other hand. The goals which are created for this thesis are:

1. Gain knowledge on wave theories and their applicability based on parameters which can describe certain sea states
2. Describe non-linearities and capture these effects to adapt linear results in such a manner that these effects are included to analyse the hydrodynamic loads on the structure in shallow water
3. Developed a parametric model which can predict motion behaviour and validate it with a deep water case
4. Develop a parametric model which can calculate forces and moments and subsequent motion behaviour in TD to account for non-linearities and/or other additional forces
5. Say something about vertical motions in shallow water, and how and if these differ from motion behaviour by linearised motion prediction

## 1-4    Approach

A parametric model is developed where based on user defined input the motion behaviour of a barge in shallow water can be determined beyond the boundaries where AQWA diffraction analysis is capable of doing so. Unfortunately, no reliable validation data were available, so the research focused heavily on the verification of the methods for computations with the parametric model, to assure validity of results. The model is therefore verified based on deep water situations, for both incoming wave forces as well as resulting vertical motions.

Firstly the range of validity of different wave theories is investigated, to determine when to apply what theory and what the associated forces should be. The parameters Ursell number UR, wave steepness $S$ and relative depth $\mu$ are used to determine the validity of the wave theories.

Linear results are gathered by a FD based analysis in the diffraction software AQWA, from which the hydrodynamic coefficients are used to model motion behaviour in the numerical model in Python. In this model, *Wave* - object and *Vessel* - objects can be created based on user defined parameters. Fluid forces are subsequently estimated through the method of direct integration of the pressure, based on the specified *Wave*, on the wetted surface of the focal *Vessel*. When the model identifies the need for additional pressure terms, second order pressure can for instance be added. Subsequently, another parametric model is created which calculates the forces on the *Vessel*, based on the LWT. The calculation method is validated with displacement RAOs from the diffraction analysis in AQWA.

Even though it is common practice to use the FD analysis to simulate behaviour of floating structures in waves because of its ease of applicability and general accuracy, this study also covers the TD analysis. As mentioned, the FD analysis cannot take into account non-linear effects associated with shallow water. Superposition no longer holds when non-linearities are encountered, and the analysis needs to be done in TD, where the EOM is directly updated every time step. Memory effects are taken into account with the retardation kernel, which is used for the convolution integral. The TD analysis based on the Cummins equation is thus more comprehensive on dealing with non-linear systems. Especially since the second order contribution to the motion behaviour of the vessel is important, its inclusion in the EOM is necessary. Second order forces and moments are determined through with a Quadratic

Transfer Function (QTF) from the diffraction analysis. The resulting second order external wave forces are subsequently superimposed with the first order wave forces in the TD model.

For the lower Under Keel Clearance (UKC) in shallow water and subsequent viscous effects, an additional external force can also be added based on the critical damping of the focal vessel. Factors which determine the additional damping force based on critical damping are based on empirical data from literature and can be applied in the model to account for additional forces.

Furthermore, an additional inertial force is calculated in TD, which accounts for the shallow water effect which occurs with very low UKC. This phenomenon is known as the 'Cushioning' and 'Sticking' effect, which captures the decrease in vertical motions due to increasing pressures in this UKC. The model is capable of including this additional external force in TD and it can therefore be used to as engineering approach for this phenomenon.

## 1-5 Document structure

The documents is structured as follows. Firstly wave theories are discussed and their validity for specific wave parameters in Chapter 2. Next, how motion behaviour of vessels is approximated is explained in Chapter 3. In Chapter 4 firstly the first order FD based model is explained. It explains the model used in AQWA, how the forces and motions are calculated in Python and shows the verification of calculation methods with load and displacement RAOs. It subsequently explains how the second order forces are calculated based on QTFs. The model chapter furthermore elaborates on how the transformation is made to TD, and the verification of calculation method in this domain. In Chapter 5 results from calculations with the created models are given. Finally, in Chapter 6 at the end of the thesis the conclusions and recommendations for future studies are given.

# Chapter 2

# Waves

To determine waveloading and motions responses of offshore structures, common practice in engineering is to rely on two basic descriptions of waves; deterministic, regular waves and random, irregular waves [16]. The periodic (co)sine function defines what is called a regular wave and is defined in terms of its amplitude $a$, wavelength $\lambda$ and period $T$. These regular waves can be represented as function of space $x$ and time $t$ and are used in the Linear Wave Theory (LWT) to solve the flow problem in waves [2]. The distance between two successive crests within such a wave train is the wavelength $\lambda$. The wave period $T$ is the interval between the passing of two successive crests at a certain point in space and time. Regular waves can be described by several theories, among which the LWT is most often used. This, and other wave theories, which can be applied to describe waves in specific conditions are described in this chapter.

In shallow water some phenomena affect waves and subsequently the incoming wave forces and therefore the different wave theories need to be discussed and understood in order to include shallow water effects on the ship motions. With regards to wave exciting motions, wave dynamics show many different phenomena which increase the complexity of reprenting body motions; dispersion, diffraction, refraction, shoaling, reflection, non-linear wave-wave interaction, bound waves, set-down, wave breaking and bottom friction are some examples [11, 17]. In comparison to deep water situations, to predict motions motions accurately is more problematic, due to shallow water effects as strong non-linearities and complex wave-structures interactions [6].

## 2-1   Wave Theories

There is no unique theory that is applicable to all depth regions from very shallow water to deep water. The LWT is the most commonly used theory for engineering applications for first approximations of wave behaviour [18, 19]. As will be explained in section 2-3, this theory assumes the wave surface profile to remain constant, i.e. very small amplitudes. There are however cases in which the small amplitude assumption is not valid, which calls for other

theories to be used to describe the waves. In such cases, one should resort to non-linear or finite amplitude wave theories. In Section 2-2 the range of applicability of different wave theories is shown as a function of water depth $d$, gravity $g$ and wave period $T$.

In developing the wave theory, the boundary value problem with a differential equation and boundary conditions is solved by approximation. There are two types of this approximation, one which is developed around the wave height as parameter of perturbation and one as function of water depth. The LWT and Stokes non-linear wave theory are examples of the first category. Otherwise, the order remains constant and a numerical solution is sought, e.g. the stream theory.

Some general assumptions are made in developing the wave theories. Firstly, water is assumed incompressible and irrotational and continuity of flow is assumed. By means of these assumptions, a velocity potential $\Phi$ is defined which is related to flow velocity components. The derivative of $\Phi$ in any direction equals the flow velocity in that direction. It is a mathematical way to describe flow, and a scalar of space and time. From $\Phi$, pressures and finally hydrodynamic forces and moments on the structures can be calculated, which is explained in Chapter 3. Firstly, $\Phi$ is substituted in the continuity equation, with which the Laplace equation is obtained [2, 19].

$$\frac{\partial^2 \Phi}{\partial x^2} + \frac{\partial^2 \Phi}{\partial y^2} + \frac{\partial^2 \Phi}{\partial z^2} = 0 \tag{2-1}$$

For steady, irrotational flow with a perfect fluid, the Bernoulli equation can be acquired. This equation solves the kinetics (pressures and forces) of the waves. If then the Laplace equation is solved for the boundary conditions, the potential $\Phi$ will be known which can then provide the expression for the pressure from (2-2).

$$p + \rho\, g\, z + \frac{1}{2} \cdot \rho\, (u^2 + v^2 + w^2) = \text{Constant} \tag{2-2}$$

In which $\rho$ = density of water, $g$ = acceleration due to gravity, $[u, v, w]$ = velocity components in direction $[x, y, z]$.

**Boundary Conditions** For $\Phi$ to be applicable in the two dimensional case, it has to satisfy certain conditions:

1. Continuity or Laplace equation.

$$\nabla^2 \Phi = \left( \frac{\partial^2 \Phi}{\partial x^2} + \frac{\partial^2 \Phi}{\partial z^2} \right) = 0 \tag{2-3}$$

2. Seabed Boundary Condition. Vertical velocity of the water particles at the seabed is zero.

$$\frac{\partial \Phi}{\partial z} = 0 \text{ for } z = -d \tag{2-4}$$

3. Free Surface Kinematic Boundary Condition. Vertical velocity of water particles at free surface of the fluid is identical to the vertical velocity of the free surface $\eta(x, y, t)$ itself.

$$\frac{\partial \Phi}{\partial z} = \frac{\partial \eta}{\partial t} + u \frac{\partial \eta}{\partial x} + v \frac{\partial \eta}{\partial z} \text{ for } z = \eta(x, y, t) \tag{2-5}$$

The vertical velocity of a water particle in free surface becomes after linearisation:

$$\frac{\partial \Phi}{\partial z} = \frac{\partial \eta}{\partial t} \text{for } z = \eta(x, t)$$

Which is also valid for $z = 0$. Differentiation to $t$ provides the Cauchy-Poisson condition:

$$\frac{\partial z}{\partial t} + \frac{1}{g} \cdot \frac{\partial^2 \Phi_w}{\partial t^2} = 0 \tag{2-6}$$

4. Free Surface Dynamic Boundary Condition. Pressure at the free surface equals the atmospheric pressure (and is thus constant at the free surface).

$$\frac{\partial \Phi}{\partial t} + \frac{1}{2} \left[ \left( \frac{\partial \phi}{\partial x} \right)^2 + \left( \frac{\partial \phi}{\partial y} \right)^2 + \left( \frac{\partial \phi}{\partial z} \right)^2 \right] + g \cdot \eta = f(t) \quad \text{for } z = \eta(x, y, t) \tag{2-7}$$

Which becomes after linearisation:

$$\frac{\partial \Phi}{\partial t} + g \cdot \eta = f(t)$$

## 2-2 Range of Validity of Different Wave Theories

The parameters wave height $H$, period $T$ and depth $d$ help to determine the validity of wave theories in general. Regions for applicability are in terms of normalized parameters $H/T^2$ and $d/T^2$ and are based on how well the theory satisfies the boundary value problem (see Figure 2-1. Wave parameters which determine the applicability of the theories are according to DNV-RP-C2-5 wave steepness parameter $H/\lambda$ or $S$, shallow water parameter $\mu$ and the Ursell number $U_R$ [5]. $U_R$ is very useful for defining the range to which the wave theories are applicable [18]. There are arguments to combine effects of steepness and water depth, but it is found that effects were approached better when used seperately [20].

In Figure 2-1, the values used on the axes are $h_0$, which is the water depth, the wave height $H$, gravitational acceleration $g$ and the wave period $T$. In shallow water, usually the Airy (LWT) and Cnoidal first order waves are suitable, while in deeper water, the Stokes non-linear theory is more approproiate [19, 16].
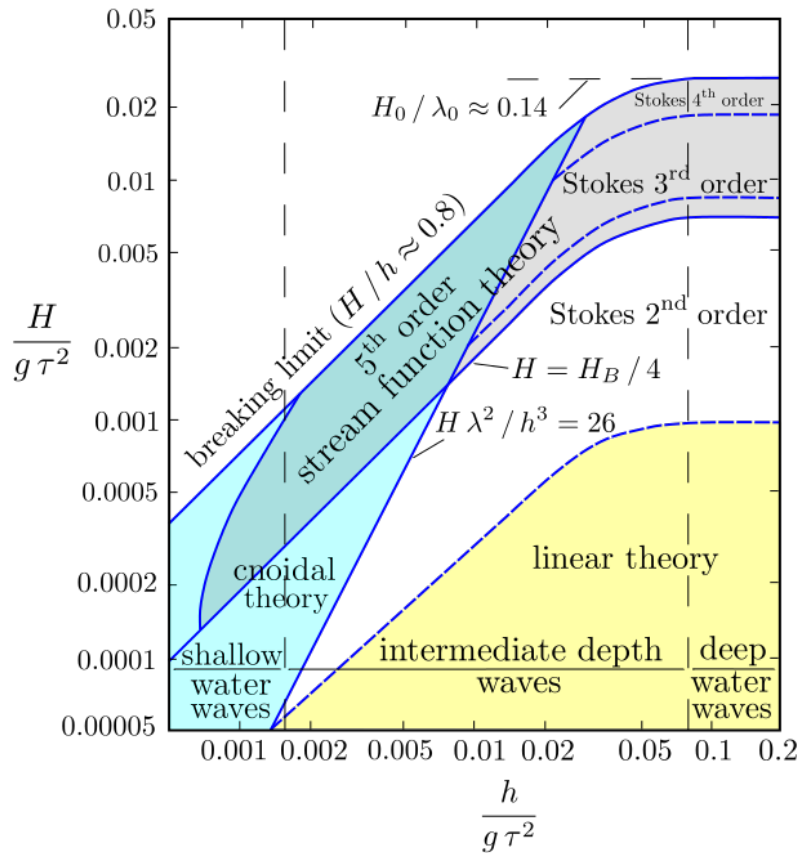
**Figure 2-1:** Applicability Range of Various Waves From LeMeHaute (1970)

### 2-2-1   Parameters for Applicability of Theories

The parameters discussed before to find the right wave theory are shortly explained.

**Wave Steepness**

Wave steepness $S$ is an important parameter in determination of the applicability of the LWT, as it determines whether or not the assumption of small amplitudes is valid. In a simple wave travelling in a single direction, crests are know to travel faster than their associated troughs, causing the front to continually steepen[12]. The sharpened wave crests is the most obvious indication of non-linearity in the ocean, but the detailed description is difficult. When waves show behaviour which departs from the linear description, crests are higher and sharper than expected from a summation of sinusoidal waves with random phase.

$$S = \frac{H}{\lambda} \tag{2-8}$$

**Ursell Number**

To determine whether or not the LWT for surface waves is applicable, $S$ does not suffice as

the only parameter. It is shown that the linearized theory of surface waves is valid only if $U_R$ and $S$ (see (2-8)) are small [12]. The number $U_R$ indicates the degree to which surface gravity waves are non-linear. $U_R$ is the result of studies on waves with small amplitudes $\zeta$ and large wavelengths $\lambda$, and where $\lambda$ is much larger than the water depth $d$. Basically, it is the ratio of the amplitudes at second order to first order according to Stokes' theory. It is commonly used to determine boundaries of wave theories, as shown in 2-1, and one can see that the boundary lies approximately at $U_R = 26$ for LWT. The number is a function of wave height, wavelength and water depth:

$$U_R = \frac{H \cdot \lambda^2}{d^3} \tag{2-9}$$

**Relative depth** The relative depth, or shallow water parameter $\mu$ is used to define the relationship between wavelength $\lambda$ and depth $d$. Depth is not the sole parameter to determine whether waves are considered deep or shallow water waves. It is the relative depth parameter which provides this measure, as the wavelength $\lambda$ (or wave number $k$) determines to which depth to which the orbital velocities, accelerations and pressures are significant. Hence, it is this factor which defines whether interaction with the seabed will influence properties of the waves.

$$\mu = \frac{d}{\lambda} \tag{2-10}$$

## 2-3   Linear Wave Theory - Airy Theory

The LWT is the simplest and most used theory for waves. It is a first order theory, which assumes that amplitude is small compared to $\lambda$, water depth and dimensions of the structures. The regular waves described by the LWT can by means of the superposition principle be used to describe more complex waves systems with irregular waves. It gives useful approximations of kinematic and dynamic properties of surface waves, and under the assumption of small amplitude it allows for the application of dynamic and kinematic boundary conditions to be applied at the still water level instead of at the oscillating, wave disturbed surface level. In Table 2-1 the coefficients are given for the parameters described in 2-2.

| | S | $\mu$ | $U_R$ |
|---|---|---|---|
| LWT | $\ll 1$ | $\simeq > \frac{1}{20}$ or $S/\mu < 0.03$ | $< 26$ |

**Table 2-1:** Parameters for the linear wave theory

For the focal maximum $S$, the relative depth parameter $\mu$ should be larger than 0.2 [5].

**Velocity Potential $\Phi$**
The solution for $\Phi$ is found in the form of a power series in terms of a non-dimensional perturbation parameter $\epsilon$, defined in terms of the ratio between wave height $H$ and length $\lambda$:

$$\epsilon = \frac{k \cdot H}{2} \tag{2-11}$$

The velocity potential $\Phi$ and free surface profile $\eta$ are then defined as:

$$\Phi = \sum_{n=1}^{\infty} \epsilon^n \ \Phi_n$$
$$\eta = \sum_{n=1}^{\infty} \epsilon^n \ \eta_n$$

(2-12)

For the LWT the order is 1, and in order to find the analytical description of $\Phi$ and $\eta$ in this order the boundary conditions as described in the previous need to be solved. In the first order (2-5) and (2-7) reduce to:

$$\frac{\partial \eta}{\partial t} - \frac{\partial \Phi}{\partial z} = 0 \quad \text{at} \quad z = 0$$

(2-13)

$$\frac{\partial \Phi}{\partial t} + g\eta = 0 \quad \text{at} \quad z = 0$$

(2-14)

Combining (2-14) and (2-13)gives the combined free surface boundary condition:

$$\frac{\partial^2 \Phi}{\partial t^2} + g \cdot \frac{\partial \Phi}{\partial z} = 0 \quad \text{at } z = 0$$

(2-15)

Solving $\Phi$ for the boundary conditions stated above, the first order velocity potential becomes:

$$\Phi_W = \frac{\zeta_a g}{\omega} \frac{\cosh k(z+d)}{\cosh(kd)} \sin(kx - \omega t)$$

(2-16)

In the LWT, the first order free surface elevation is regular and follows from (2-13):

$$\eta = \zeta_a \cos(kx - \omega t)$$

(2-17)

And as one can see from (2-17), waves oscillate symmetrically around the mean sea water level. In the LWT only the first order wave steepness is taken into account and terms of higher order are neglected. Substituting $\Phi$ in (2-15) gives the dispersion relationship, which tells that waves with different wavelengths travel at different speeds. For waves with a certain period, or frequency ($f = 1/T$), wave height $H$, and water depth $d$, $\lambda$ is prescribed by this relationship:

$$\omega^2 = g \cdot k \cdot \tanh kd$$

(2-18)

This relationship can be used to determine phase velocities of waves in arbitrary depths. It depends on the depth though whether it affects the phase velocity, or wave celerity $c$. Water is considered deep with respect to the waves when the ratio $d/\lambda > 1/2$, while it is considered shallow when $d/\lambda < 1/20$. Beyond the deep water limit, the water depth effect can be neglected. Below the shallow water limit, the influence of $d$ on $c$ vanishes (they are not dependent on $T$) and waves become non-dispersive, and non-linear [14]. The critical velocity

$c_{shallow} = \sqrt{g \cdot d}$ becomes important considering the possibility of wave breaking, as explained in Section 2-3-3.

**Water Particle Velocity**

Particle velocities are the gradient of the potential in the direction in which the derivative is taken, and can be expressed for horizontal $x$ and vertical $z$ direction as:

$$u = \frac{\partial \Phi}{\partial x} = \zeta_a \cdot \omega \frac{\cosh k(z+d)}{\sinh kd} \cdot \cos(kx - \omega t)$$

$$u_d = \zeta_a \, \omega \, e^{kz} \cdot \cos(kx - \omega t)$$

$$u_s = \zeta_a \omega \cdot \frac{1}{kd} \cdot \cos(kx - \omega t)$$

$$w = \frac{\partial \Phi}{\partial z} = \zeta_a \cdot \omega \frac{\sinh k(z+d)}{\sinh kd} \cdot \sin(kx - \omega t)$$

$$w_d = \zeta_a \, \omega \, e^{kz} \cdot \sin(kx - \omega t) \quad \text{for deep water}$$

$$w_s = \zeta_a \omega \cdot \frac{1}{kd} \cdot \cos(kx - \omega t) \quad \text{for shallow water}$$

Where the subscripts $s$ and $d$ denote the velocities for shallow and deep water respectively.

**Water Particle Motions**

Water particles move in patterns; they have their own orbits, both horizontally as well as vertically, which is illustrated in Figure D-2 in Chapter **??**. These motions are influenced by water depth; as water depths decreases, the motions become more elliptical. For the LWT, the difference in velocities around the mean positions are so small that these differences can be neglected and are thus linearised.

$$x = -\zeta_a \cdot \omega \frac{\cosh k(z+d)}{\sinh kd} \cdot \sin(kx - \omega t)$$
$$z = \zeta_a \cdot \omega \frac{\sinh k(z+d)}{\sinh kd} \cdot \cos(kx - \omega t)$$

$$(2\text{-}19)$$

The change of the particles trajectories as a result of the approaching seabed can considered a primary causation of structure motions [14]. The hyperbolic decay terms for the trajectories can be mathematically expressed as:

$$D_h = \frac{\cosh k(z+d)}{\sinh kd} \quad \text{and} \quad D_v = \frac{\sinh k(z+d)}{\sinh kd} \tag{2-20}$$

Limitations of LWT in shallow water and for high waves in deep water, suggest a need to consider non-linear or finite-amplitude wave theories for some engineering applications. This is because a velocity asymmetry (the distance travel forward under the crest must be done in less time, while travelling back under the trough will be done in more time, peak velocities under the crest will exceed those under the trough) rises which is not predicted by the LWT [18].

### 2-3-1 Pressure

Substitution of the velocity potential in the linearised Bernoulli equation (2-2) yields the following expression for the pressure in the wave:

$$p = \rho g z + \rho g \zeta_a \cdot \frac{\cosh k(z + d)}{\cosh kd} \cdot \cos(kx - \omega t) \tag{2-21}$$

In which $\rho g z$ is the hydrostatic part and the second term contains the dynamic, time-dependent part.

## 2-3-2   Shoaling

As waves travel into shallow water, they begin to be affected by the bottom, making the water particles no longer return to their original position. In shallower water, the free surface elevation $\eta$ is greater than in deeper water, i.e. $H$ changes. Waves start to feel the bottom when $d/\lambda \leq 1/20$; they exhibit a reduction in $\lambda$ and celerity $c$ while keeping the same frequency, which results in sharper crests. Ultimately, the wave shape becomes sharp-crested up until the point particle velocities exceed the group velocity, and break. After breaking, the waves become translatory waves. To adjust for the wave height from deep to shallow water, it is argued that the energy flux must be equal for both cases, which results in the following coefficient [2, 14]:

$$\frac{H_{shallow}}{H_{deep}} = \sqrt{\frac{1}{\tanh(kd[1 + \frac{2kd}{\sinh 2kd}])}} \tag{2-22}$$

As one can see in (2-22), the shoaling coefficient is a function of water depth and affects the wave height subsequently [14]. in Figure 2-3 $K_S$ is plotted over a depth range, and it can be seen that indeed this coefficient approaches one for deeper water. In the right figure it can be seen that the coefficient is higher for lower frequencies, and highest for a difference frequency $\Delta\omega$.
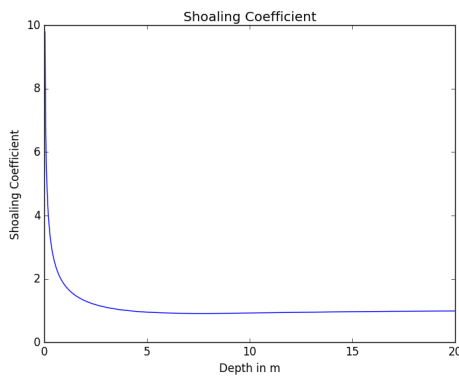


**Figure 2-2:** Shoaling Coefficient
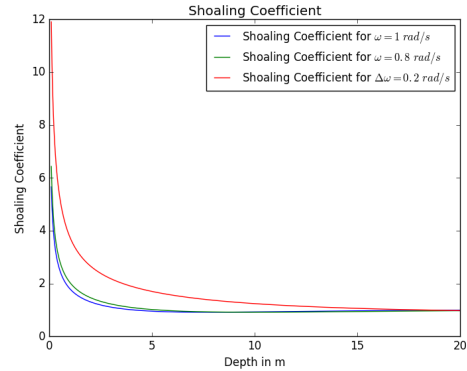


**Figure 2-3:** Shoaling Coefficient two frequencies

In shallow water waves thus steepen and this implies that the waves will break ultimately. Higher parts of the waves thus travel faster. The balance between steepening in shallow water and the acceleration of water particles is expressed in terms of $U_R$, i.e. when the steepness grows faster than the wave height, the wave will break.

### 2-3-3    Breaking

The mentioned shallow water steepening is the primary cause for waves to break [21]. For a given $d$ and wave period $T$, there is a limit to $H$ before the wave becomes unstable and breaks. The Stokes criterion for wave breaking is that the velocity of the particles at the crest reaches the celerity. A higher velocity will make these particles pass the crest, and cause the wave to break [2].

General assumptions for the breaking wave is firstly that the breaking wave is the highest possible wave and that breaking occurs when the maximum water particle velocity in the wave equals the wave speed. When waves approach breaking, the presence of non-linearities in waves increases, which, during breaking, redistributes energy within the spectrum. In shallow water the maximum wave height is usually limited by this breaking limit. A rough estimate for a wave to break is when its height becomes approximately 0.78 times the depth in place (2-23). For the entire range of relative depths, the breaking wave height is given by (2-24).

$$H_b = 0.78 \cdot d \tag{2-23}$$

$$H_b = 0.14 \cdot \lambda \cdot \tanh\left(\frac{2\pi d}{\lambda}\right) \tag{2-24}$$

### 2-3-4    Irregular Waves

The former described the regular waves, while in reality the ocean surface is highly irregular. An irregular wave model enables realization of stochastic sea state which will offer a better representation. The relationship between frequency and amplitude in this superposition can be characterized by a wave spectrum, which defines how the wave energy is distributed over a frequency range which is representative for a certain sea state. Spectra can be used in developing a wave elevation time series, consisting of the sum of many regular waves of different frequencies. The non-linear wave elevation is then a summation of first order solution and second order correction terms. In this manner surface elevation can be represented as a function of time, see Figure 2-4.

The wave elevation of a irregular sea can because of superposition written as a summation of of the individual amplitudes, frequencies and phases:

$$\zeta(t) = \sum_{n=1}^{N} \zeta_{a_n} \cos(k_n x - \omega_n t + \varepsilon_n) \tag{2-25}$$

### 2-3-5    Bi-Chromatic Wave

Regular waves are waves with one frequency, i.e. they are monochromatic. The presence of a regular wave group induces a wave with a Low Frequency (LF) long wave, which is important for second order wave forces. The simplest form of irregular waves is the bi-chromatic wave.
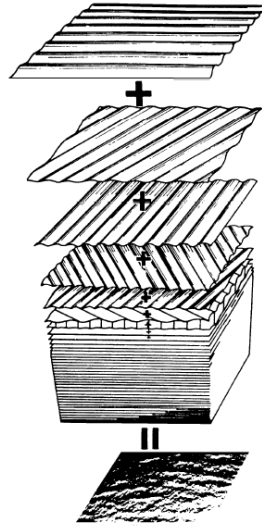
**Figure 2-4:** Superposition of regular waves

The difference of $\omega_i$ of the components of the bi-chromatic waves, makes that the LF part of the wave elevation results in:

$$\left(\zeta^{(1)}(t)\right)^2 = \sum_{i=1}^{N}\sum_{j=1}^{N} \frac{1}{2}\zeta_i^{(1)} \cdot \zeta_j^{(1)} \cdot \cos\left((\omega_i - \omega_j)t + (\epsilon_i - \epsilon_j)\right) \tag{2-26}$$

The simplest form is a 'group' of two waves:

$$\zeta(t) = \sum_{i=1}^{2} \zeta_i \cdot \sin(\omega_i t + \epsilon_i) = \zeta_1 \cdot \sin(\omega_1 t + \epsilon_1) + \zeta_2 \cdot \sin(\omega_2 t + \epsilon_2) \tag{2-27}$$

In modulated form this becomes:

$$\zeta(t) = A(t) \cdot \sin(\omega_0 t + \epsilon) \tag{2-28}$$

Where the summation over all $\zeta_i$ squared is the wave envelope $A(t)$, which contains information with respect to grouping of waves, see (2-29) in Section 2-3-5.

$$A(t) = \sqrt{\sum_{i=1}^{N}\sum_{i=1}^{N} \zeta_i \zeta_j \cdot \cos\left((\omega_i - \omega_j)t + (\epsilon_i - \epsilon_j)\right)}. \tag{2-29}$$

The wave envelope is an imaginary curve joining successive wave crests within a wave group and contains information with respect to the grouping of waves. The entire water surface motion takes place with the area enlosed by these two cruves [2].

## 2-4   Finite amplitude waves

For the application of the LWT the requirements of $H/d$ and $S << 1$ must be satisfied. When $S$ becomes higher though, one should resort to finite amplitude tehories. Basic feature of the finite amplitude is that the amplitude cannot be considered small any more compared to either wavelength or depth. In the LWT, crests and troughs are equal, so the wave is evenly distributed among the still water level. In the finite amplitude theories however, this distribution is no longer equal, the crests are more peaked while the troughs are flatter, meaning that the crests are higher above the mean water level than the troughs are below this level. It becomes necessary to use higher-order approximation to take the non-linear aspect of the wave into account. The physical difference with the LWT is that in these theories the influence of the wave itself on its properties is considered. Properties are in this theory functions of the actual wave height $(d + \zeta_a)$ [18, 22]. Most finite amplitude wave theories are developed for a specific range of wave height $H$, wave period $T$, and water depth $d$ as can be seen in Figure 2-1.

### 2-4-1   Stokes

In Stokes' derivations, perturbation is commonly used. At $z = 0$, a Taylor expansion is applied, which linearises the wave potential. This can be justified for small surface elevations, but in extreme sea states wave kinematics must be included to describe wave loads. The accuracy of the potential problem increases as more terms are added in the perturbation technique, allowing for better prediction of wave loads. Stokes found a method to extend the validity range of theory by taking non-linear terms into consideration for wave kinematics and boundary conditions, which were neglected in the development of the LWT. Stokes assumed all variation can be written as perturbation expansions in terms of a parameters which incresases with wave height [4].

A disadvantage of the perturbation techniques is that the potential loses its superposition property. Furthermore, it is only applicable for wave amplitudes smaller than all other length scales. Despite these shortcomings, higher order Stokes is still helpful in studying non-linear wave kinematics. In interacting wave components, Stokes second order theory accounts for the positive and negative interaction terms, meaning that terms are included in the equations of sum of the frequencies and negative interaction terms by the difference of the frequencies of the first-order components. The positive terms produce the sharpening of the crests and the flattening of the troughs which is associated with second-order Stokes waves. Negative interaction terms give the set-down of the water level under wave groups [20].

Wave characteristics (velocity potential $\Phi$, celerity $c$, surface profile $\eta$, etc.) are described by means of higher orders of $\epsilon$. The Stokes theory is applicable for waves that are not very long and not very high and mostly applicable in deep water and in a portion of the intermediate depth range. The Stokes theory should be applied for values where $\epsilon$ and $U_R$ small, and is generally applicable for $U_R < 10$ [19, 18, 4].

**Stokes Second Order**

For the Stokes' theory, the Laplace equation looks similar as described by (2-1) as well as the seabed boundary condition (2-4). The free surface conditions however are different for higher terms of $\epsilon$.

|  | S | $\mu$ | $U_R$ |
|---|---|---|---|
| Stokes Second Order | < 0.04 [19] | $\frac{1}{7} - \frac{1}{10}$ [18] | 26 - 40 |

**Table 2-2:** Parameters for Stokes Second Order Theory

The first order terms as given in (2-14) and (2-15) are the same, but they are extended by the second-order term by:

$$\frac{\partial^2 \Phi_2}{\partial t^2} + g \cdot \frac{\partial \Phi_2}{\partial z} = -\eta_1 \frac{\partial}{\partial z} \left[ \frac{\partial^2 \Phi_2^2}{\partial t^2} + g \frac{\partial \Phi_1}{\partial z} \right] - \frac{\partial}{\partial t} \left[ \left( \frac{\partial \Phi_1}{\partial x} \right)^2 + \left( \frac{\partial \Phi_1}{\partial z} \right)^2 \right] \quad \text{at } z = 0 \quad (2\text{-}30)$$

and

$$\eta_2 = -\frac{1}{g} \left[ \frac{\partial \Phi_2}{\partial t} + \eta_1 \frac{\partial^2 \Phi_1}{\partial z \partial t} + \frac{1}{2} \left( \frac{\partial \Phi_1}{\partial x} \right)^2 + \frac{1}{2} \left( \frac{\partial \Phi_1}{\partial z} \right)^2 \right] \quad \text{at } z = 0 \quad (2\text{-}31)$$

**Velocity Potential**

Under the assumption of weak non-linearity the potential of the wave train is perturbed in the order of $\epsilon = \eta k \ll 1$; $\eta = \eta^{(1)} + \epsilon \eta^{(2)} + \epsilon^{(2)} \eta^{(3)} ....$

The Stokes expansion can be used to describe steeper crests and flatter troughs, the increase in phase velocity with the increase in $S$ and non-linear wave characteristics up to second order. This is presented in terms of the velocity potential by:

$$\Phi = \epsilon \Phi_1 + \epsilon^2 \Phi_2 \quad (2\text{-}32)$$

Both $\Phi_1$ and $\Phi_2$ satisfy the boundary conditions, and $\Phi_2$ should thus give similar solutions except that $k$ is replaced by $2k$ and the $\cos(x)$ part by $\cos(2x)$. The wave potential is then given by [18]:

$$\Phi_w = \frac{\zeta_a g}{\omega} \frac{\cosh k(z+d)}{\cosh(kd)} \sin(kx - \omega t) + \frac{3}{g} \frac{\pi C}{kT} \frac{H}{\lambda} \left( \frac{\pi H}{\lambda} \right) \cdot \frac{\cosh kd(z+d)}{\sinh^4 kd} \cdot \sin 2 (kx - \omega t) \quad (2\text{-}33)$$

It is reasonable to suppose that non-linear wave surface elevation could be approximated by an amplitude modulated wave [19, 18].

$$\eta = \eta_1 + \frac{1}{2} \cdot \eta_a^2$$

$$\eta = \zeta_a \cos(kx - \omega t) + \frac{\pi H^2}{8\lambda} \frac{\cosh kd}{\sinh^3 kd} \cdot [2 + \cosh 2kd] \cdot \cos 2(kx - \omega t) \tag{2-34}$$

**Water Particle Velocities**

The water particle velocities are given by (2-35).

$$u = \frac{\pi H}{T} \cdot \frac{\cosh k(z+d)}{\sinh kd} \cdot \cos(kx - \omega t) + \frac{3(\pi H)^2}{4T\lambda} \cdot \frac{\cosh 2k(d+z)}{\sinh^4 kd} \cdot \cos 2(kx - \omega t)$$

$$w = \frac{\pi H}{T} \cdot \frac{\sinh k(z+d)}{\sinh kd} \cdot \sin(kx - \omega t) + \frac{3(\pi H)^2}{4T\lambda} \cdot \frac{\sinh 2k(d+z)}{\sinh^4 kd} \cdot \sin 2(kx - \omega t) \tag{2-35}$$

**Pressure field**

From here, the dynamic pressure is obtained by the substitution of $\Phi_w$ into the complete Bernoulli equation (2-2) for $f(t) = 0$ and without hydrostatic pressure [19].

$$\begin{aligned}
p &= \rho g \zeta_a \frac{\cosh k(z+d)}{\cosh kd} \cos(kx - \omega t) \\
&+ \frac{3}{4} \rho g \frac{\pi H^2}{\lambda} \frac{1}{\sinh 2kd} \cdot \left[ \frac{\cosh 2k(z+d)}{\sinh^2 kd} - \frac{1}{3} \right] \cdot \cos 2(kx - \omega t) \\
&- \frac{1}{4} \rho g \frac{\pi H^2}{\lambda} \frac{1}{\sinh 2kd} \cdot [\cosh 2k(z+d) - 1]
\end{aligned} \tag{2-36}$$

In Stokes second order the linear dispersion relationship is still valid. The solution of the second order boundary value problem is valid if the convergence criterion and the 'no bump' criterion are met. The convergence criterion means that the second part of (2-33) should be much smaller than unity. Second, the physical properties of the wave profile requires that in the trough of the wave no small second wave exists, i.e. there should be no 'bump' in the trough. An example is given in Figure 2-5.
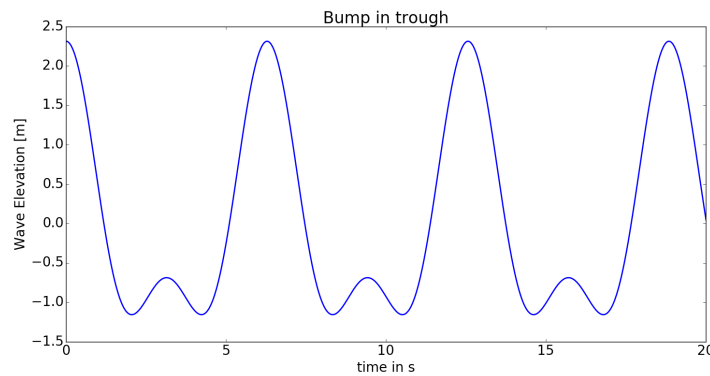


**Figure 2-5:** An example of a wave modelled with Second Order Stokes wave elevation, with large $S$. This creates the hump in the trough

Increasing $S$ in the second order causes peaking at crests when two components are in phase, and flatter troughs when they are out of phase. The through becoming horizontal is a limit beyond which this theory is no longer valid. At this point, $S$ can be approximated by (2-37). This can be expressed in terms of a maximum $S$:

$$S = \frac{\sinh^3 kd}{\pi \cosh(kd) \cdot (2 + \cosh 2kd)} \tag{2-37}$$

In deep water this limit is approximately $S_{max} = \frac{1}{7}$. When the relative depth $\mu \leq 0.1$, $_{limit}$ becomes 0.021. This restricts the application of the second order theory [18].

An lastly, with the increasing $S$, the other effect to consider is of course the breaking limit. These three limits are shown in Figure 2-6, which can be helpful in distinguishing whether or not the waves can be approximated by this theory.
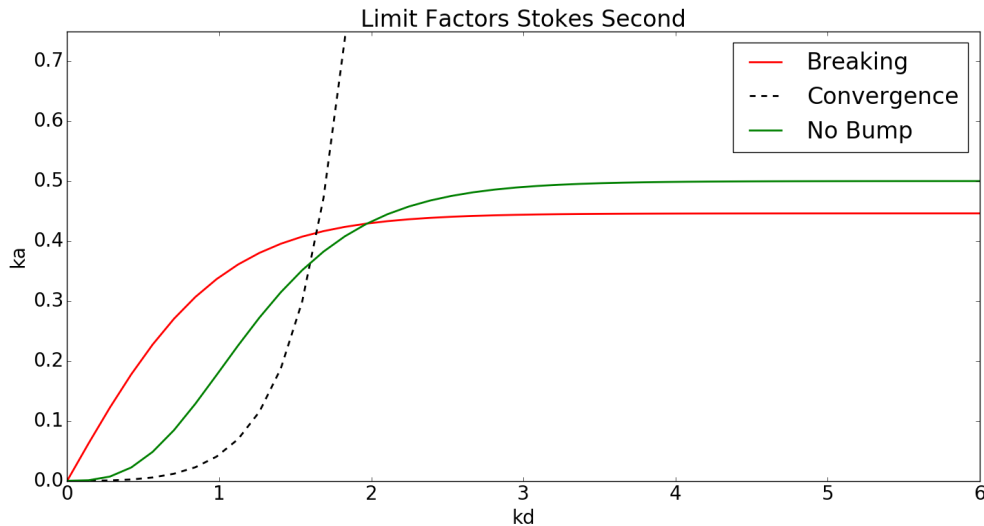


**Figure 2-6:** Limiting Conditions for applicability of Stokes Second Order Theory

Values on the right of the crossing lines are valid values for the focal theory. To model for this limitations, numerical models should be given these limits.

## Stokes Fifth Order

The Stokes fifth order wave theory is applicable for fairly long waves, in deep water with a large wave height [23]. In shallower water it requires many terms to approach the right solutions [4]. As such, the theory is not considered for this study. The theory only has significant effect close to the free surface, which makes it useful for analysing floating structures. The theory has been popular for design, but it fails to converge for shallow water conditions [24]. When waves become relatively longer, the Cnoidal theory is argued to be more applicable in shallow water, see also Figure 2-1 [4, 19]. For completeness however, the values for determining parameters are given in this section.

| | S | $\mu$ | $U_R$ |
|---|---|---|---|
| Stokes Fifth Order | < 0.14 [18] | $\frac{1}{10}$ [4] | < 40 [**?**] |

**Table 2-3:** Parameters for Stokes Fifth Order Theory

**Velocity Potential**

The fifth order velocity potential is written as:

$$\Phi = \frac{c}{k} \sum_{n=1}^{5} L \cosh nk(z+d) \sin n(kx - \omega t) \tag{2-38}$$

Where $L$ is a function of $kd$. The details are beyond the scope of this thesis and can be found in [19].

## 2-4-2   Cnoidal Theory

Finite amplitude long waves of permanent form in shallow water are hard to be described by the Stokes theory. The Cnoidal Theory is in these case better applicable. It is describes a periodic, long, sharp crested wave [4, 25]. The period of a Cnoidal wave depends on both the wavelength and amplitude, while the wave period of a linear sinusoidal wave is only dependent on the wave length. However, for a given wavelength, the period of a Cnoidal wave converges to the linear, sinusoidal wave when the amplitude of the Cnoidal wave tends to become infinitesimally small.

| | S | $\mu$ | $U_R$ |
|---|---|---|---|
| Cnoidal Theory | < 0.125 | $\frac{1}{50}$ <d< $\frac{1}{8}$ [19, 5] | 26 - 40 [**?**, 19] |

**Table 2-4:** Parameters for Cnoidal Theory

For values of $10 < U_R < 26$ both Stokes and Cnoidal theory are equally applicable [18]. Depending on $S$, the cut-off point lies either in the intermediate water depth region $d/\lambda > 0.1$ or ultimately at the shallow water limit $d/\lambda = 0.1$ [18]. The Cnoidal waves are solutions of the Korteweg - de Vries equation in Jacobi elliptic functions $cn$. The Jacobian elliptical function is periodic and modulus lies in between 0 and 1. The wave profile can be described in terms of these functions $cn$ by:

$$\eta = \eta_t + H cn^2 [2K(k_{cn}) \left( \frac{2\pi}{\lambda} - \frac{2\pi}{T} t \right), k_{cn}] \tag{2-39}$$

In which $\eta_t$ is the elevation of the trough, $K(k_{cn})$ the complete elliptical integral of the first kind. Both $K(k_{cn})$ and $cn$ are functions of the elliptical parameter $k_{cn}$ which determines the shape of the Cnoidal wave. The applicability of the theory is extremely complex, so it is often recommended to use other theories to cover as much information as possible. Figures by Wiegel as shown in Figure 2-7 (1964) help find the basic parameters [18, 19].

For Cnoidal theory in the first order the pressure distribution is essentially hydrostatic. It is a function of the distance below the water surface:
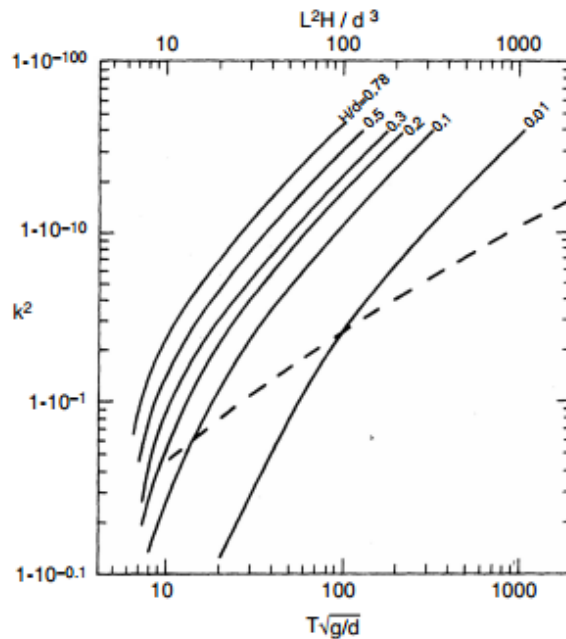
**Figure 2-7:** Solution for basic parameter of Cnoidal Wave Theory. Modified by Sorensen from Wiegel 1964.

$$p_{cn} = \rho \ g \ (\eta - z) \tag{2-40}$$

Calculation of water particle velocity and acceleration components can be found in literature, but are very difficult involving becuase of $cn$. Due the complexity, the solitary wave theory has often been used to calculate characteristics in very shallow water [18].

### 2-4-3   Solitary Waves

The Cnoidal wave becomes a solitary wave in the limiting case of infinite wave length and period, thus when the modulus becomes 0. The profile only exists above mean water level and consists of a single crest [18]. In reality, waves will break before a true solitary wave is reached. As the solitary wave does not represent a train of waves, it is not applicable for offshore design [24]. An example is given in Chapter D.

## 2-5   Stream Function Waves

Dean's stream function is a numerical non-linear wave theory which is used for finite amplitude waves throughout the range of relative water depths. The stream function $\Psi$ is used to define the wave field rather than the velocity potential $\Phi$ [18]. It is a purely numerical procedure for approximating a wave profile. So, instead of assuming perturbation expansions for the coefficients as done by Stokes, the coefficients are calculated numerically by solving non-linear equations [5]. The stream theory has a wider range of applicability than Stokes

waves, up to nearly breaking. However, the stream function applicability is not ideal for design purposes [4, 19, 18]. More details on the theory are given in Chapter D.

**Summary Applicability**

A good starting point for selecting which theory to apply is Figure 2-1. The first modification to be done is by predicting $H$ change from one depth to another by the shoaling coefficient (2-22), which is argued to be valid for $S$ not to be too large. Given a new wave height $H$ with known $T$ and $d$, this allows for calculation under assumptions of LWT. For finite amplitude wave theories, the change in wave height also depends on initial steepness, i.e. on $\mu$ as well as $S$. The application range for the LWT is usually extended as far as possible, because of its ease of application. The parameters which determine the theory of choice, are summarized in Table 2-5 [5, 4, 18, 19]:

|                        | S        | $\mu$                                      | $U_R$    |
|------------------------|----------|--------------------------------------------|----------|
| LWT                    | < 0.01   | $\frac{1}{20}$ or $S/\mu < 0.03$           | < 26     |
| Stokes Second Order    | < 0.04   | $\frac{1}{10} - \frac{1}{7}$               | 26 - 40  |
| Stokes Fifth Order     | < 0.14   | $\frac{1}{10}$                             | < 40     |
| Cnoidal Theory         | < 0.125  | $\frac{1}{50} <d< \frac{1}{8}$             | 26 - 40  |
| Stream Function Theory | -        | -                                          | -        |

**Table 2-5:** Parameters for the applicability of right wave theory

In the next chapter is explained how the motion behaviour of offshore structures can be determined.

# Chapter 3

# Ship Motions

What loads enforce the waves upon a floating structure within those waves is an important question and detailed information on hydrodynamic properties is necessary for accurate motion prediction.

Research has shown that effects of wave steepnesss $S$, wave frequencies $\omega$ and body dimensions affect wave exciting forces on barges. A reduction of $d$ from deep to finite water enhances all wave exciting forces. Second order harmonics of heave force and pitch moment increase, but second order effects can generally be neglected for the surge Degree of Freedom (DOF). When the body is allowed to move, influence of water depth on surge and heave force is that these reduce in first order harmonics, while pitch moments tend to increase, especially when $\lambda$ approaches the dimensions of the structure of interest. Furthermore, in heave DOF the water depth effect for first-order harmonics is significant, i.e. it has great impact on motions [1]. This chapter explains therefore how diffraction analyses approximate motions and what additional or adjusted calculation need to be performed of shallow water ship motion behaviour. It firstly explains how this is done linearly (first order), after which second order motions are discussed because these can cause large loads in shallow water.

## 3-1 Frequency Domain

Potential theory is a Frequency Domain (FD) based approximation of the motions of vessels, based on the assumption of Linear Wave Theory (LWT). The hydrodynamic coefficients $a_{ij}$ and $b_{ij}$ depend on $\omega$ only and wave exciting forces have a linear relation with wave amplitude $\zeta$. In irregular waves, the response of a body can be determined by using the superposition principle.

### 3-1-1 Degrees of Freedom

The first order motions of a vessel can be described after an analysis in the FD. Resulting motion in irregular waves are summations of the vessel's response to regular harmonics waves

| DOF | Name | Symbol | Unit | Description |
|:---:|:---:|:---:|:---:|:---:|
| 1 | Surge | x | [m] | Motion in x |
| 2 | Sway | y | [m] | Motion in y |
| 3 | Heave | z | [m] | Motion in z |
| 4 | Roll | $\phi$ | [rad] | Rotation around x-axis |
| 5 | Pitch | $\theta$ | [rad] | Rotation around y-axis |
| 6 | Yaw | $\psi$ | [rad] | Rotation around z-axis |
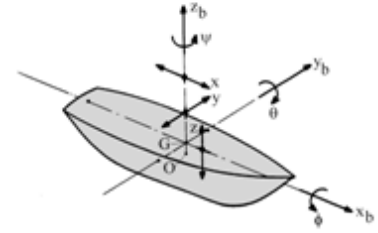


**Figure 3-1:** Degrees of Freedom Ship Motions

with different amplitudes and phases. For a wave energy spectrum, this results in response spectrum in one of the DOF. These DOF are shown in Figure 3-1.

### 3-1-2 Motions

These motions are calculated around the Centre of Gravity (COG). Responses in regular waves are according to LWT are given by the following:

$$z = z_a \cos(\omega t + \varepsilon_{z,\zeta}) \tag{3-1}$$

Where $z_a$ the amplitude of the heave response and $\varepsilon_{z,\zeta}$ the phase shift between wave elevation and heave displacement of the COG of the vessel. The associated velocity and acceleration for this degree of freedom are given in (3-2).

$$\dot{z} = -\omega \ z_a \ \sin(\omega t + \varepsilon_{z,\zeta})$$
$$\ddot{z} = -\omega^2 \ z_a \cos(\omega t + \varepsilon_{z,\zeta}) \tag{3-2}$$

The phase shift of ship motion is considered positive when the ship motion passes zero at a specific moment in time $t$, before the wave elevation passed zero at this same $t$. Decreasing water depth can have a great impact on motions of structures due to the phenomena mentioned in Chapter 2, but also on the frequency dependent coefficients directly. Shallow water conditions make the importance of non-linearities bigger, which changes the accuracy of motion prediction by the linear response amplitude operators [6]. In shallower water, heave and pitch motions decrease due to increasing added mass. In the Low Frequency (LF) region though, pitch motions can increase [9, 1]. It is furthermore shown that pitch is relatively most sensitive to wave steepness [1].

The effect in shown in Figure 3-2. It can be seen that all forces increase when $d$ decreases.

## 3-2 Response Amplitude Operators

Ship motions are usually initially calculated in FD, which gives an adequate first approximation of motion behaviour. Wave exciting forces, added mass and potential damping are terms
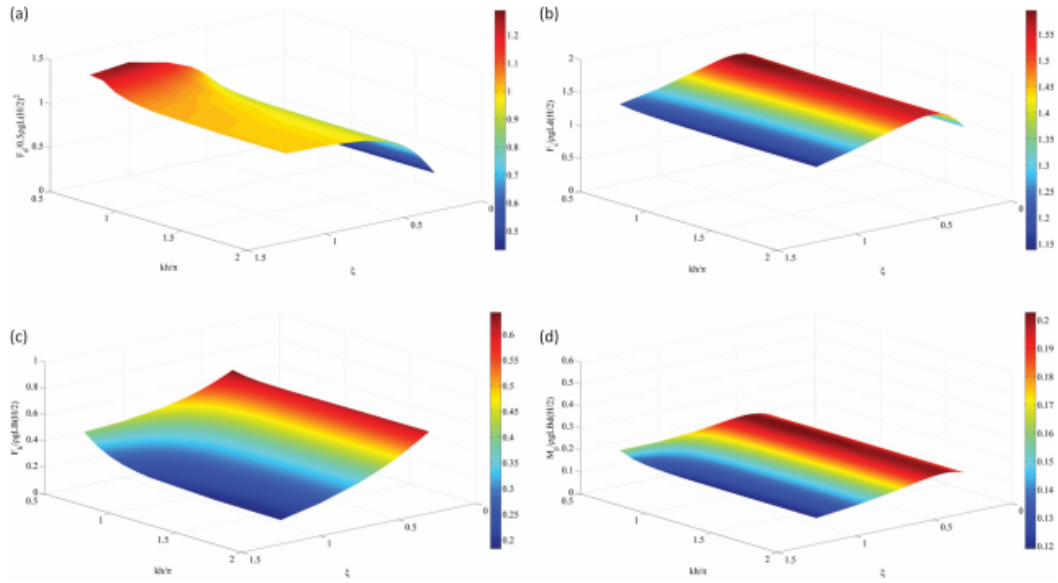
**Figure 3-2:** Effect of water depth and incident wave frequency on wave exciting forces. (a) Drift Force (b) Surge Force (c) Heave Force and(d) Pitch Moment. Obtained from Wang et al. (2016) [1]

in (3-3) which are dependent on wave frequencies [9, 6]. The motion amplitude, for example heave $z_a$ and phase shift $\varepsilon_{z,\zeta}$ can then be written in proportion to the wave amplitude $\zeta_a$. These transfer functions are known as Response Amplitude Operator (RAO)s and define the first order motion of a vessel in response to waves with given period and amplitude. They are found using potential theory. The amplitude relates the amplitude of the vessel motion to the amplitude of the wave ($z_a/\zeta_a$) and the phase defines the phase lag from the time the wave crest passes the RAO origin until the maximum positive excursion is reached ($\varepsilon_{z,\zeta_a}$). Load RAOs represents the magnitude and phase of the force (surge, sway, heave) or moment (roll, pitch, yaw) ($F_a/\zeta_a$). RAOs are obtained through the analysis of dynamic behaviour of a vessel as a result of an incoming harmonic wave. The displacement RAOs for the six DOF are determined by solving the following relation for $X_j$:

$$\{-\omega^2 \cdot (M_{ij} + A_{ij}(\omega)) + i\omega \cdot B_{ij}(\omega) + C_{ij}\} \cdot X_j(\omega) = F_i(\omega) \quad \text{for } i = 1, ..6 \tag{3-3}$$

The right hand side of the Equation of Motion (EOM) consists of wave exciting forces and moments by waves coming in on the restrained body, around the COG. Finally, when the RAOs are calculated, the motion response spectra are found. With a given wave spectrum, and frequency characteristics of a vessel, motion responses can be determined by:

$$S_i(\omega) = \int_{-\pi}^{\pi} S_\zeta(\omega, \mu) \cdot RAO_i(\omega, \mu)^2 d\mu \tag{3-4}$$

Where the subscript $i$ denotes the DOF, $S_i$ the response spectrum and $S_\zeta$ the wave spectrum.

Specifications of the RAO can be crucial in determining whether or not to operate in specific sea states. As mentioned in Chapter 2, incoming waves might change by moving into shallower
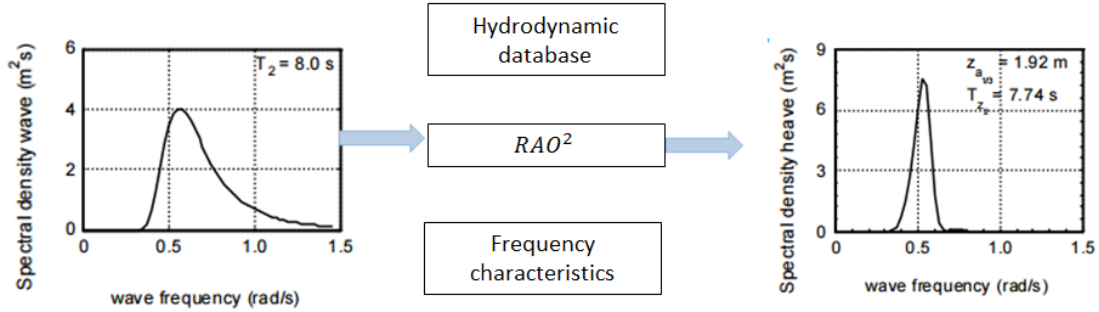
**Figure 3-3:** Calculation of motion responses for a floating structure

water (with reference to the above deep water equations). The hydrodynamic coefficients in $A_{ij}$ and $B_{ij}$ however might also change due to shallow water. These hydrodynamic coefficients and their sensitivity to shallow water conditions are discussed in the following. Firstly, the wave exciting forces are explained as this external factor induces motions. Next, the radiation force is discussed, containing $A_{ij}$ and $B_{ij}$.

## 3-3 Forces and Moments

Wave exciting forces are those on a body due to the unsteady fluid pressure of water waves, where the body is retained from moving. The forces consist of the Froude-Krylov (FK) and diffraction forces and follow from integration of pressure on the submerged part of the body $S_H$. Assuming a structure is subjected to linear waves, the total first order velocity potential $\Phi^{(1)}$ can be written as a summation over the velocity potentials at each $\omega$:

$$\Phi^{(1)}(x, y, z, t) = \text{Re}\left[\sum_{j=1}^{6} \phi_j e^{i\omega_j t}\right] \tag{3-5}$$

The lower case velocity potential $\phi_j$ is the space dependent part belonging to one specific frequency $\omega_j$. The potential under the assumption of the LWT is the superposition of three parts, the potential of the undisturbed incoming wave $\Phi_I$, the radiation potential $\Phi_R$ and the diffraction potential $\Phi_D$ [6, 2]:

$$\Phi = \Phi_I + \Phi_D + \Phi_R$$

$$\Phi(X, Y, Z)\, e^{-i\omega t} = \left[(\Phi_I + \Phi_D) + \sum_{i=1}^{6} \Phi_j x_j\right] e^{-i\omega t} \tag{3-6}$$

The incident wave potential $\Phi_I$ used to describe to flow of the undisturbed incoming waves, the FK forces. $\Phi_D$ is the diffraction potential and is used to describe the disturbances of flow due to a body in this flow. Added to the undisturbed wave potential, it describes the total potential of the incoming waves, $\Phi_W$. $\Phi_R$ is the radiation potential and exsists for each of the six DOF of a body in waves and it is calculated for oscillation in still water [2, 26].

**The Diffraction Problem**

As a watertight body is considered, the kinematic boundary condition on the body must be zero. The potentials $\Phi_I$ and $\Phi_D$ can be written in a space and time dependent part for the undisturbed wave and diffraction potential respectively:

$$\Phi_I = \text{Re}\{\phi_W \cdot i\omega\zeta_a e^{i\omega t}\}$$
$$\Phi_D = \text{Re}\{\phi_D \cdot i\omega\zeta_a e^{i\omega t}\} \tag{3-7}$$

With the space-dependent part:

$$\phi_W = \frac{\zeta_a g}{\omega^2} e^{kz} e^{i(kx\cos\mu + ky\sin\mu)} \tag{3-8}$$

The velocity potential given by (2-16) where $x$ is the space dependent part given in (3-8). The diffraction potential is determined through diffraction analysis in software intended to do so. For this thesis Ansys AQWA is used, which uses Green's theorem. Through the Haskind relations the diffraction potential then only depends on incoming wave potential $\phi_I$ and radiation potential $\phi_R$. $\Phi_I$ is subsequently used to find pressures due to incoming and diffracted waves, which ultimately gives the description for total wave forces by (3-9). The forces and moments on the body also include the radiation forces $F_R$, which is discussed in Section 3-3-1.

$$F_D + F_W = -\iint\limits_{S_H} (p \cdot \vec{n_k})\,\mathrm{d}S = \rho\omega^2\zeta_a e^{i\omega t}\iint\limits_{S}(\phi_W + \phi_D)\,\mathrm{d}S_H \tag{3-9}$$

$$\vec{M} = -\iint\limits_{S_H} p \cdot (\vec{r} \times \vec{n})\,\mathrm{d}S_H \tag{3-10}$$

In which $\vec{n}$ is the outward normal vector on the surface and $\vec{r}$ the position vector of surface $\mathrm{d}S_H$ in the coordinate system. For the LWT, the steepness of the wave is considered small, and the second order terms in the above equation are ignored. The resulting pressure due to water waves is then:

$$p = -\rho\frac{\partial\Phi}{\partial t} - \rho gz = -\rho\left(\frac{\partial\Phi_I}{\partial t} + \frac{\partial\Phi_R}{\partial t} + \frac{\partial\Phi_D}{\partial t}\right) - \rho gz$$

$$p = -\rho gz + \rho g\zeta_a \cdot \frac{\cosh k(d+z)}{\cosh(kd)} \cdot \cos(kx - \omega t) \tag{3-11}$$

For a complete determination of forces and moments of the body in waves, the hydrodynamic loads need to be included. As can be seen from (3-3), the pressure is split in four parts. Therefore, forces and moments $\vec{F}$ and $\vec{M}$ are split in those four parts as well:

$$F_{total} = F_I + F_D + F_S + F_R \tag{3-12}$$

- $F_I$: hydrodynamic forces and moments on the body due to undisturbed incoming wave
- $F_D$: hydrodynamic forces and moments due to the diffracted waves.
- $F_S$: hydrodynamic forces and moments due to hydrostatic buoyancy and loads due to changes in water plane area.
- $F_R$: hydrodynamic forces and moments due to radiating waves from the oscillating body

Diffraction analysis calculates displacement and load RAOs respectively of incoming wave loads. This load RAO is used to describe the wave exciting force on the vessel:

$$F_W = F_{A,\zeta_a} \cdot \zeta_a \; cos(\omega t - \varepsilon_{F,\zeta}) \tag{3-13}$$

Where $F_{A,\zeta_a}$ is the amplitude of the load RAO at $\omega$, and $\zeta_a$ the incoming wave amplitude. The linear hydrodynamic and hydrostatic forces are also based on coefficients determined in the diffraction analysis, which is discussed in the Section 3-3-1.

### 3-3-1   The Radiation Problem

Incoming wave forces will cause the floating structures to oscillate, inducing wave creation which will radiate from the body. The associated force in six DOF can be expressed as the radiation force $F_R$. These radiation forces contain the coefficients of added mass and potential damping, $a_{ij}$ and $b_{ij}$. Added mass is the additional force necessary to accelerate the fluid particles surrounding the vessel, compared to oscillation in air, and potential damping is the damping due to generation of waves by oscillation of the vessel, which withdraws energy from the motions of the vessel. These terms are shown in the $A_{ij}$ and $B_{ij}$ respectively as function of frequency of oscillation, as shown in (3-3) [2].

Shallow water affects added mass and potential damping significantly by firstly the proximity of the seabed and secondly the more intensive free surface fluctuations [6, 15, 9, 27]. Especially in the vertical modes of motion the effects are noteworthy. Research has shown that a fundamental change of motion behavior is observed due to great increase of added mass [14, 7]. Several phenomena discussed in Chapter 2 can thus cause challenges for accurate prediction of these coefficients, which affects the degree to which a good analysis of motion responses of floating bodies in waves can be done [6, 28].

With regards to damping, potential damping might not suffice and an additional damping term might be needed. Especially near resonance this is important, as the damping term dominates the equation of motion near these frequencies [2]. LF effects such as set-down and shoaling can result in significant excitation when hulls have little damping against these motions. This combination can cause significant resonant motions and related mooring loads [11].

In the following the determination of the hydrodynamic coefficients is discussed, after which the effect of shallow water is further elaborated.

#### Added Mass and Potential Damping

The accuracy of $a_{ij}$ and $b_{ij}$ directly influences the numerical simulations of the motions of a vessel. Using the velocity potentials, hydrodynamic pressure can be calculated from the

linearised Bernoulli equation, and added mass and potential damping terms are subsequently calculated by the pressure distribution on the hull. The radiation potential $\Phi_R$ can be written in potential in each DOF:

$$\frac{\partial \Phi}{\partial n} = \sum_{j=1}^{6} v_j \cdot f_j(x, y, z) \quad \text{with} \quad f_j = \frac{\partial \phi_j}{\partial n} \tag{3-14}$$

The mean wetted part $S_H$ of the hull is approximated by panel elements, representing a distribution of source singularities. These sources contribute to the velocity potential, describing the flow at any point in the domain. The total radiation force $F_R$ on $S_H$ is follows from integration of the pressure:

$$F_R = \iint\limits_{S_H} (p \cdot n_k) \, \mathrm{d}S = \rho \iint\limits_{S_H} \left( \frac{\partial \Phi_R}{\partial t} \right) \overrightarrow{n} \, \mathrm{d}S_H \tag{3-15}$$

In which $\overrightarrow{n}$ is the matrix including the direction cosines on the partial surface elements. It should be noted that the forces and moments which are the solution of the $\Phi_R$ can be expressed in terms of added mass and potential damping in the EOM:

$$M_{ij} \cdot \ddot{X}_j(\omega) = F_{W_i} + F_{D_i} + (-C_{ij} \cdot X_j(\omega)) + (-A_{ij}(\omega) \cdot \ddot{X}_j(\omega) - B_{ij}(\omega) \cdot \dot{X}_j(\omega)) \tag{3-16}$$

In which the following can be recognized:

$$\begin{aligned} F_{S_i} &= (-C_{ij} \cdot X_j(\omega)) \\ F_{R_i} &= (-A_{ij}(\omega) \cdot \ddot{X})j(\omega) - B_{ij}(\omega) \cdot \dot{X}_j(\omega)) \end{aligned} \tag{3-17}$$

The only unknown is the space dependent term of the radiation potential $\phi_j$. The potential $\phi$ can be found by the panel method. According to this method, $S_H$ is approximated by a large number of panel elements to use for calculations. Once $\Phi_R$ for the six DOF is known, calculation of $a_{ij}$ and $b_{ij}$ is next:

$$\iint\limits_{S_H} \left( \rho \frac{\partial \Phi_j}{\partial t} \cdot n_i \right) \, \mathrm{d}S_H = -a_{ij} \ddot{X}_j - b_{ij} \dot{X}_j \tag{3-18}$$

$$a_{ij} = \mathrm{Re} \left\{ -\rho \iint (\phi_j \cdot n_i) \, \mathrm{d}S_H \right\} \tag{3-19}$$

$$b_{ij} = -\omega \mathrm{Im} \left\{ -\rho \iint (\phi_j \cdot n_i) \, \mathrm{d}S_H \right\} \tag{3-20}$$

These coefficients $a_{ij}$ and $b_{ij}$ are sensitive to water depth for shallow water conditions. Most significant changes in hydrodynamics will affect the vertical DOF, with the seabed becoming closer [17, 6, 10, 7]. The heave added masss and pitch added mass are underestimated by the linear radiation-diffraction calculations when viscosity is not taken into account. Experiments

with barges in wave basins have shown that the added mass is highly sensitive to reduction of water depth for values lower than $d/T \leq 1.35$ [6]. In the case of determination where a vessel might hit the seabed, heave added mass plays an important role. Not only because of the possible bottom grounding, but also its effect on the other DOF. Roll added mass is for example little changed by shallow water effect, but the main contribution on its added mass comes from the heave induced component (while the roll-induced component is small) [15, 27]. Added mass is furthermore a critical factor to determine natural periods of structure motions, as its magnitude is comparable to other terms in the EOM [29]. These natural periods could decrease significantly, inducing the LF wave exciting forces. The fact that added mass is affected by shallow water, is shown in Figure 3-4.
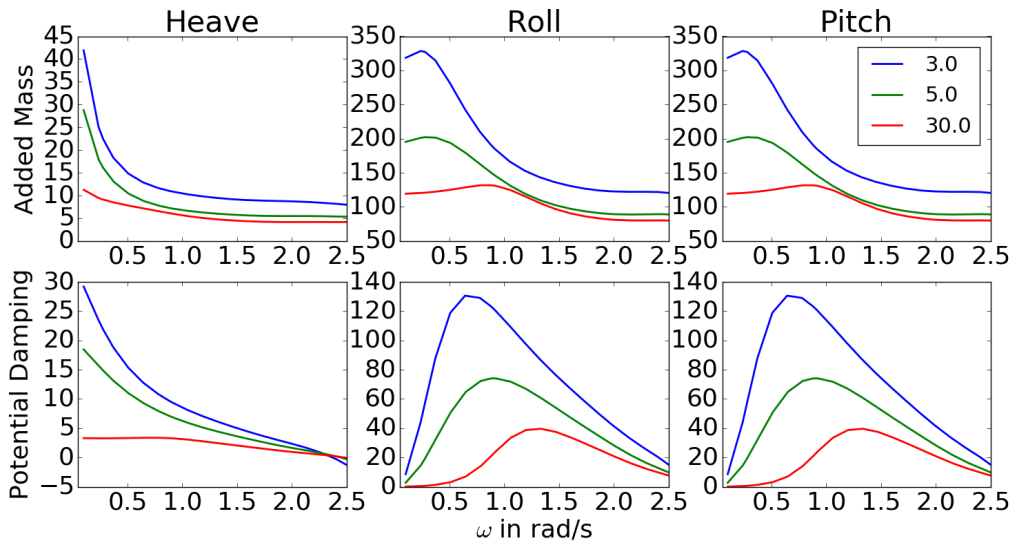


**Figure 3-4:** Increase in added mass in shallow water

Behaviour of the added mass at three different DOF is shown in top three plots, at three different water depths: $3, 5$ and $30$ m, for a draft $T$ of $1$ m. The shallow water effect on $B_{ij}$ is shown in the lower three plots. One can see that the coefficients gradually increase and converge to a constant value as $\omega$ gets higher for added mass, while radiation wave damping decreases and ultimately goes to zero, which is also shown by literature [28]. This increase in added mass in vertical DOF causes the motions in these directions to decrease. Wave frequency motions, i.e. heave and pitch, are found to decrease with decreasing water depths, which can be explained by the fact that the added mass indeed increases as can be seen in Figure 3-4, i.e. more force is needed to move the structure. The water column thus pushes the vertical moving structures, the 'Cushioning Effect'. Pitch motions are also known to decrease at shallower water. For the LF range however, vertical motions and pitch especially have shown to become significantly [9]. These results are agued to be due to the increasing wave drift forces, which will be explained further on [7, 30].

It however also gets harder for the barge to move upwards again: the water needs some time to flow back into the gap which will be created for the upwards movement. This phenomenon is known as the 'Sticking Effect'. The approaching seabed can hence have a dramatic effect particularly when the body is being raised from the seabed [31]. This could arguably be approached by the method developed by Brennen (1982) [31], which is explained in Chapter 4.

Here is firstly viscosity discussed, since this is ignored in potential theory, and becomes of greater importance in shallow water, especially near resonance.

### 3-3-2   Viscous Damping

Research has demonstrated that the effect of water depth on damping is very clear, where generally trends are that the damping increases with a decreasing water depth [29]. In shallow water, motions are often over predicted by diffraction analysis, or in other words; the damping is under predicted. Complex hydrodynamic effects play a role to the viscous damping due to the small distance between the structure and the seabed which causes large velocities of flow around it. Especially for mooring in shallow water, it has shown that viscous damping is one of the major issues in the LF area due to the LF reaction forces. And since the focus of this thesis lies on shallow water motion behaviour, where LF second order wave effects increase, the viscous effects increase in significance.

Resulting discrepancies in diffraction theory prediction and reality found motions are argued to be a consequence of neglecting these viscous effects, and therefore a viscous damping factor needs to be added to the EOM [14, 13]. The assumption of inviscid low limits amount of hydrodynamic damping, and the potential flow solution needs to be augmented with viscous effects.

Research by Clauss et al. (2009) has shown that motion behaviour already changes in shallow water ($d/T \leq 1.3$) due to neglectence of viscous damping [14]. Other experiments have shown similar results, with a rectangular barge in a basin with adjustable depth, where the damping significantly increased for [$2.72 \geq d/T \geq 1.36$] [29]. So in shallow water, viscous effects need consideration, as they can possibly affect significance of results, especially in motion modelling near resonance [2, 29, 14, 32, 6]. It is however not an easy task to find the proper viscous damping coefficient owing its non-linearity. The contribution can be derived experimentally, as factor of critical damping $\xi$, or as a term based on drag as an empirical input [13, 14]. The viscous effects can subsequently be added to the EOM as an external damping force in Time Domain (TD)[14, 22].

**Critical Damping Factor**
Common practice is to add a linearised viscous damping term to account for non-linearities in damping. This term is taken as fraction of the critical damping [33]:

$$B_{vi} = \xi \cdot B_{crit} = \xi \cdot 2 \cdot \sqrt{(A(\omega) + M(\omega) \cdot C}$$
(3-21)

The damping factor $\xi$ is usually obtained from experimental data or estimated from simplified hydrodynamic models [5]. In their research, Clauss et al. [14] derived $\xi$ experimentally and found 1.2 % and 2 % for heave and pitch motion respectively. The resonance peak in the LF of heave RAO due to heave-pitch coupling was eliminated as a result. Other research on damping has found values of approximately 4% of the critical roll damping to be added to the radiation damping [34, 33].

The viscous damping coefficient is widely investigated for cylindrical bodies, with or without heave plates of different diameters. But also for a diameter ratio of 1, a viscous damping coefficient (as fraction of critical damping) is found. These damping ratios $\xi$ lie in the range

of $1\% - 2\%$ [35, 14].

**Roll viscous damping factor based on decay tests**

Based on free decay test, of pure rolling in still water $B_{4v}$ is obtained as the viscous damping coefficient in roll motion. For rectangular barges experiments have resulted in an empirical estimation for roll $\xi$:

$$\xi = \xi_1 + \xi_2 \cdot \phi_a \tag{3-22}$$

In which $\phi_a$ is the roll angle and constants $\xi_1$ and $\xi_2$:

$$\xi_1 = 0.0013 \cdot \left(\frac{B}{T}\right)^2 \quad \text{and} \quad \xi_2 = 0.50 \tag{3-23}$$

In which $B$ is the breadth and $T$ the draft of the barge [36]. From the figure it can be concluded that an approximation of $\xi = 1\% - 4\%$ would be valid. Generally, for large $B/T$ ratios, potential damping dominates. It could however be a manner to model viscous damping due to shallow water effects. In Figure 3-5 these coefficients are shown for a range of roll angles.
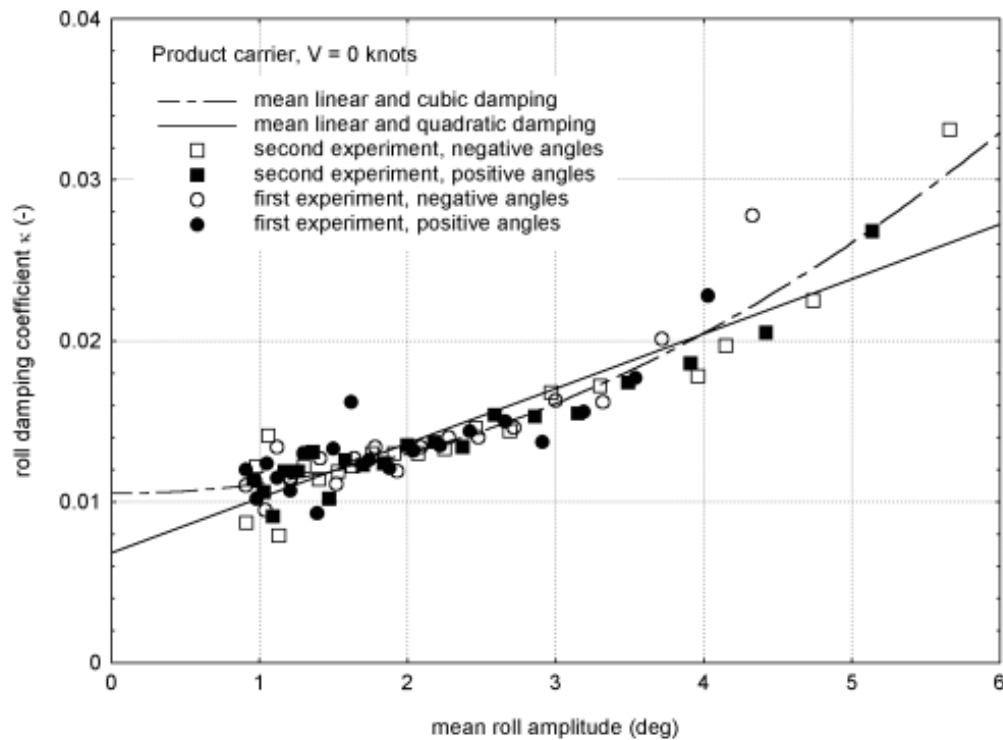


**Figure 3-5:** Roll Damping Coefficients Based on Experiments. From: Journée [2]

**Viscous Drag Constant** $C_D$

Another method to determine viscous effects on the motions is by including a drag force. A widely used approach to calculate these forces is the Morison's equation. The drag load on a body is by definition the component of the force in the direction of the velocity of the flow. These forces are then directly calculated from wave kinematics and it thus does not require the velocity potential to solve this. The method is however usually applicable for slender structures, where the characteristic length scale is smaller than $\leq \frac{1}{5}$ shortest wavelength [18, 2]. More details on this method are given in Chapter D.

## 3-4    Second Order Wave Forces and Moments

Generally speaking, magnitudes of first order harmonics are the large part of the wave exciting moment, but in shallow water second order harmonics increase in significance. In shallow water, first order analysis usually isn't sufficient in predicting a particular vessel's motions accurately enough. Especially for the heave force and pitch moment these nonlinear effects cannot be ignored [1]. In second order approximations fluid pressures and wave loads are either linear with wave amplitude or proportional to the square of this amplitude. The solution of the second order results in a mean force and forces oscillating with the difference and sum frequencies in addition to the linear solution. Especially the occurrence of wave set-down in irregular waves demands for wave force description up to second order, as shallow water effects play an important role in these wave drift forces [6].

Non-linear second order motions in the horizontal DOF $(x, y, \psi)$ have often been subject of research. Horizontal drift forces are major contributor on practical applications in the offshore shallow water operations, and in particular for mooring lines design these are heavily investigated. Second order drift forces in the vertical plane however are much less widely investigated [37, 7].

Response of a structure in irregular waves includes three important components:

*First Order*

1. An oscillating displacement of the vessel at frequencies which correspond to those of the waves, caused by the first order waves forces.

*Second Order*

1. A mean displacement of the vessel as a result from a constant load, caused by the mean drift force. This is caused by second order wave potential effects. This mean wave drift force is proportional to the incident wave amplitude squared. These loads determine a new equilibrium position.
2. An oscillating displacement of the structure of the vessel at frequencies lower than those of the irregular waves, caused by low-frequency drift forces.

The first order loads are discussed in the previous sections. Both contributions of the second order loads are a result of non-linear behaviour in waves. The first part is time-independent and causes a mean off-set of the average position of the body in waves. The difference frequency component will induce slowly varying motions [38]. The contributions of wave phenomena on the resulting wave forces is schematically given in Figure 3-6 and explained in the following.

### 3-4-1    Set-Down

Freely propagated waves generated by wind are complemented by bound waves, which are a significant population of the total ocean surface. Wave set-down is a non-linear effect in irregular waves, when long waves bound to short waves. Set-down produces a depression of
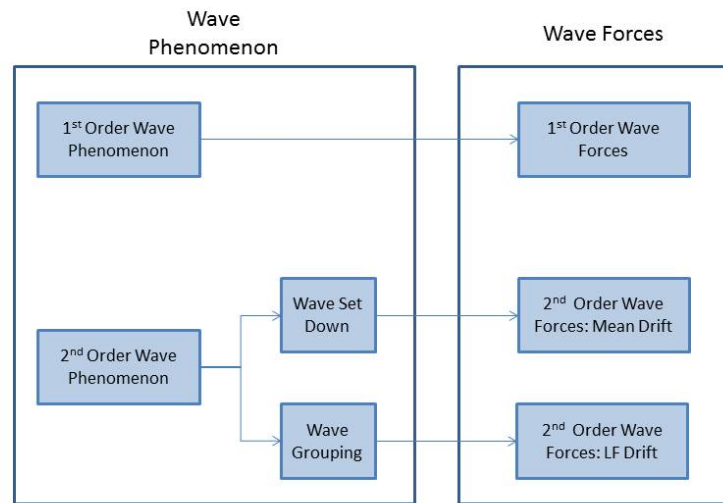
**Figure 3-6:** Wave Phenomena

the mean water surface level, which subsequently affects drift forces [30, 39, 11, 6]. Wave elevations are then related to second order pressure disturbance in the wave field. Bound waves move at speeds near those of their parents waves and appear to affect LF forces more than first order forces. This effect is in shallow water is dominated by the second order potential $\Phi^{(2)}$. The set-down phenomenon does not affect the mean value of second order forces, but only slowly varying part.
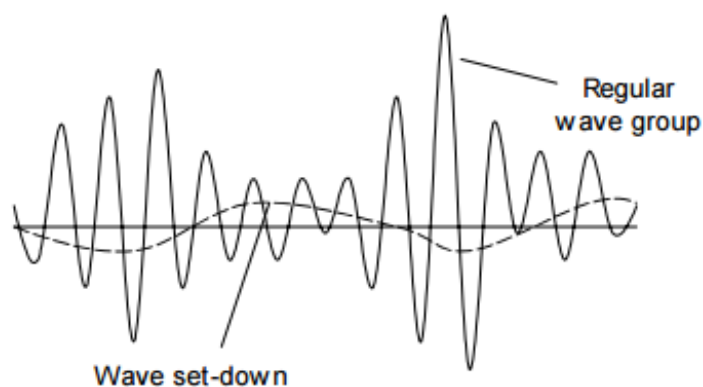


**Figure 3-7:** Set-Down

Set-down will stimulate large wave exciting forces at the LF area [17, 6, 37, 40, 41]. The effect is widely known to be necessary to consider in the design for mooring systems, but also

for the vertical DOFs, it surely is important [17, 6, 37, 7]. It is a contribution proportional to first order wave heights squared, i.e. it can be calculated from quadratic products of first order quantities [2, 38]. In the bi-chromatic wave of two regular Airy waves, the second order potential implicitly includes the second order incident potential effects.

**Set-Down Calculation** Interactions between the waves can help to explain the mechanism which creates the higher crests and flatter troughs in shallow water. The second-order wave elevation, set-down, can be approximated through a correction of the first order wave elevation. The model by Longuett-Higgins, and later extended by Sharma and Dean (1979), for the second-order waves with amplitudes $A_m$ and $A_n$ has $N^2$ corrections over sum-frequencies and $N^2$ corrections over difference-frequencies helps to do so. The second order wave is then modelled as $\eta_2 = \eta_1 + \triangle\eta_2$ with the second-order correction:

$$
\begin{aligned}
\triangle\eta_2 &= \sum_{m=1}^{N}\sum_{n=1}^{N} A_m A_n E_{mn}^{(+)} \cos\left[(\omega_m + \omega_n)\,t + (\varepsilon_m + \varepsilon_n)\right] \\
&+ \sum_{m=1}^{N}\sum_{n=1}^{N} A_m A_n E_{mn}^{(-)} \cos\left[(\omega_m - \omega_n)\,t + (\varepsilon_m - \varepsilon_n)\right]
\end{aligned}
\tag{3-24}
$$

With sum and difference frequency contributions respectively:

$$
E_{mn}^{(+)}(\omega_m, \omega_n) = \frac{1}{4g}(\omega_m^2 + \omega_n^2) \quad \text{and} \quad E_{mn}^{(-)}(\omega_m, \omega_n) = -\frac{1}{4g}\mid \omega_m^2 - \omega_n^2 \mid
\tag{3-25}
$$

These equations are for infinite water depths, and that's where the correction by Sharma and Dean (1979) gives a better description for the wave surface. These waves have shown by experiments that the difference frequency drift forces increase dramatically for small depth over wavelength ratios [38]. The second order correction by Sharma and Dean for finite water depth is the following [42, 20]:

$$
\eta^{(2)} = \frac{1}{4}\sum_{m=1}^{N}\sum_{n=1}^{N} A_m A_n \left\{ K^- \cos(\psi_m - \psi_n) + K^+ cos(\psi_m + \psi_n) \right\}
\tag{3-26}
$$

Where $K^-$ and $K^+$ are complicated kernels, which express interactions between the frequencies and water depth, and details are given in Chapter **??**. The positive kernels are associated with the sharper crests and flatter troughs which are associated with Stokes second order waves. The negative parts describe the set-down effect [20]. The positive interaction has a frequency approximately double that of the linear component waves, and have positive peaks in phase with both crests and troughs of linear parts. The negative interaction term has a frequency of the difference frequency. The interaction kernel $K^-$ for these is negative, which causes this second-order wave to be negative under high wave groups.
Another formulation of the set - down is developed by Voogt (2005) [43]. The additional second order term his work is the following:

$$
\zeta^{(2)} = \sum_{i=1}^{N}\sum_{j=1}^{N} \zeta_i \cdot \zeta_j D(\omega_i, \omega_j, k_i, k_j, d) \cdot \cos((\omega_i - \omega_j)t + \epsilon_i - \epsilon_j - (k_i - k_j)x)
\tag{3-27}
$$

The transfer function $D$ can also be read from Figure 3-8. The figure also shows that the effect is in phase with wave group, and that it amplifies in shallow water (dotted arrow) [43, 37, 41].
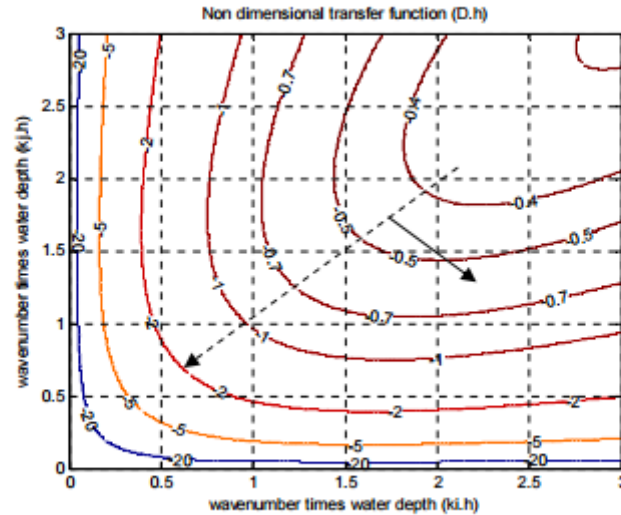


Figure 1 Non dimensional transfer function for wave setdown

**Figure 3-8:** Set-down Voogt

In Chapter D, in Section D-3-1 the details for $A$ are given.
The total second order wave forces and moments are given in Section 3-4-2. When two non-linear Stokes waves are considered, the set-down needs an additional correction by the work of [44]. In Stokes second order waves there is often a term neglected which accounts for an additional free surface decrease, i.e. set-down, which adds to the set-down resulting from quadratic product of the first order potential. Ignoring this additional set-down related to a monochromatic second order Stokes wave causes inconsistency in the vertical drift force where the difference frequency is zero [38, 44]. For this thesis, these cases are not considered, but the correction is given in Chapter D.

### 3-4-2   Wave Drift Forces and Moments

Wave drift forces are generally assumed to be second order wave forces, where forces are quadratic functions of wave height [2, 37]. Second order difference frequency forces (drift forces) increase significantly in shallow water [6, 38, 7]. Where the mean drift froces are calculated from first order quantities, this osciallatory component requires the calculation of the second order potentials. This contribution is avoided in deep water, but this cannot be done in shallow water situations [7]. These require full Quadratic Transfer Function (QTF)s, which can become time-consuming [38]. As mentioned in Section 3-3-1, wave frequency motions decrease in shallow water, while LF increase [17, 14, 41]. Shallow water effects thus play an important role, both in horizontal as well as in vertical drift forces [6, 39, 38, 7].
Second order potential effects are large contributing aspect to this increase of drift forces, and should be included in the calculations. Newman's approximation does not consider these

second order potential effects and subsequently underestimates heave LF drift forces in shallow water [6, 38, 40]. It can underestimate second order wave loads and provide wrong phase shifts since the approximation is a real function while the QTF is a complex function.

The second order wave forces and moments are defined as in (3-28). For the derivation and explanation of these, reference is made to the work of Pinkster [37] Journée et al. [2]. After the perturbation analysis over the wetted surface, the second order wave exciting forces and moments can be written as:

$$
\begin{aligned}
\overrightarrow{F}^{(2)} \;=\; & -\frac{1}{2} \cdot \rho\, g \oint_{WL} \left(\zeta_r^{(1)}\right)^2 \cdot \overrightarrow{n} \cdot \mathrm{dl} \\[2mm]
& +\frac{1}{2} \cdot \rho\, g \iint_{S_0} \left(\overrightarrow{\nabla}\Phi^{(1)}\right)^2 \cdot \overrightarrow{n} \cdot \mathrm{dS} \\[2mm]
& +\rho \iint_{S_0} \left(\overrightarrow{X}^{(1)} \cdot \overrightarrow{\nabla}\frac{\partial \Phi^{(1)}}{\partial t}\right) \cdot \overrightarrow{n} \cdot \mathrm{dS} \\[2mm]
& +m \cdot R^{(1)} \cdot \overrightarrow{\ddot{X}_g^{(1)}} \\[2mm]
& +\rho \iint_{S_0} \left(\frac{\partial \Phi^{(2)}}{\partial t}\right) \cdot \overrightarrow{n} \cdot \mathrm{dS}
\end{aligned}
$$

$$
\begin{aligned}
\overrightarrow{M}^{(2)} \;=\; & -\frac{1}{2} \cdot \rho\, g \oint_{WL} \left(\zeta_r^{(1)}\right)^2 \cdot (\overrightarrow{r} \times \overrightarrow{n}) \cdot \mathrm{dl} \\[2mm]
& +\frac{1}{2} \cdot \rho\, g \iint_{S_0} \left(\overrightarrow{\nabla}\Phi^{(1)}\right)^2 \cdot (\overrightarrow{r} \times \overrightarrow{n}) \cdot \mathrm{dS} \\[2mm]
& +\rho \iint_{S_0} \left(\overrightarrow{X}^{(1)} \cdot \overrightarrow{\nabla}\frac{\partial \Phi^{(1)}}{\partial t}\right) \cdot (\overrightarrow{r} \times \overrightarrow{n}) \cdot \mathrm{dS} \\[2mm]
& +I \cdot R^{(1)} \cdot \overrightarrow{\ddot{X}_g^{(1)}} \\[2mm]
& +\rho \iint_{S_0} \left(\frac{\partial \Phi^{(2)}}{\partial t}\right) \cdot (\overrightarrow{r} \times \overrightarrow{n}) \cdot \mathrm{dS} \quad (3\text{-}28)
\end{aligned}
$$

As can be seen from (3-28), the second order force and moments consists of five parts:

- The first part is caused by the effect of relative wave height
- The second part is caused by the pressure drop due to first order velocity potential
- The third part is caused by the pressure due to the product of the gradient of first order pressure and first order motion
- The fourth part is caused by the effect of the product of first order rotational motion and the inertia force
- The fifth part is the second order potential term and is related to the long wave induced by the presence of regular wave groups

The first four contributions depend on first order quantities, and these are referred to as the quadratic forces and moments. These second order wave exciting forces/moments due to first order waves and motions responses result in pairs of regular incident waves. Sum and difference frequency components result from interaction of the first order velocities. For analyses done in frequency domain, the time independent QTFs of second order forces and moments are used, which is explained in Section 3-4-4 [45, 39].

The fifth part depends on the second order potential $\Phi^{(2)}$, it is therefore referred to as the second order potential force or moment. This contribution must be considered in shallow water to find accurate results [46, 7]. Pinkster made an extensive investigation on three dimensional bodies and found an approximatino of the $\Phi^{(2)}$ which was good when the difference frequency of components in bi-chromatic waves was small [37, 7]. The velocity potential related to a case with two incident harmonic waves, must also satisfy the Laplace equation, as well as bottom and radiation conditions. Furthermore, $\Phi^{(2)}$ must comply with the free surface and

body boundary conditions and it must satisfy the radiation condition on vertical boundaries and bottom impermeability condition . This method has been proven not too differ too much from a full second order potential calculation and can thus be used [38].

### 3-4-3   Approximation Second Order Potential

The LF part represents a long wave induced by the presence of the regular wave group. It is assumed that a first order wave of which the frequency equals the difference frequency of a bound wave can be used to describe this bound wave.
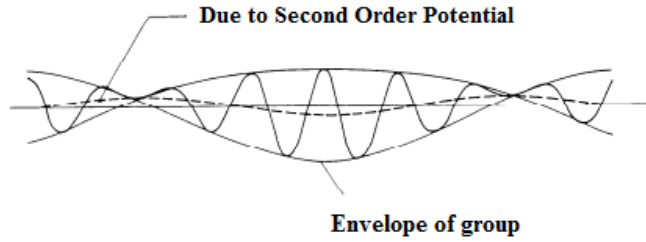


**Figure 3-9:** Second Order Potential Contribution. From Journee (2001) [2]

In shallow water difference frequency drift force can increase significantly due $\Phi^{(2)}$ and cannot be ignored [39, 38]. The non-linear nature of free surface condition and complexity of body boundary conditions makes calculation of the contribution due to the second order potential difficult. There have been succesful efforts though which can estimate the velocity potential of incoming second order LF bound wave that belongs to the bi-chromatic wave group as a function of first order wave numbers, frequencies and water depth [37, 47]: The combination of two first order waves carry a second order wave with wavenumber $k_i - k_j$. The second order wave potential can then be approximated by [37, 39]:

$$
\begin{aligned}
\Phi^{(2)} \;=\; & -\sum_{i=1}^{2}\sum_{j=1}^{2} \zeta_i \cdot \zeta_j \cdot A_{ij} \cdot \frac{\cosh((k_i - k_j) \cdot (z - d))}{\cosh((k_i - k_j) \cdot d)} \\
& \times \sin\left[(k_i - k_j)x - (\omega_i - \omega_j)t + (\varepsilon_i - \varepsilon_j)\right]
\end{aligned}
$$

Where $\Phi^{(2)}$ is the LF part of the second order incoming wave potential, $(k_i - k_j)$ the wave number of the LF bound wave. The vertical drift force ultimately can then be approximated by:

$$
F_z^{(2)}(\omega_i - \omega_j) \approx \zeta_i \cdot \zeta_j \cdot \frac{A_{ij}(\omega_i - \omega_j)}{g} \cdot F_z^{(1)}(k_i - k_j) \tag{3-29}
$$

Where $F_z^{(1)}(k_i - k_j)$ is the first order vertical wave induced force and $A_{ij}$ a function of $(\omega_i, \omega_j, k_i, k_j, d)$, which is explained in more detail in Chapter D. In short, it assures the functions to assure that the wave transformed wave force to one with a difference frequency still meets the dispersion relationship, and that the right first order wave potential is used. This approximation $\Phi^{(2)}$ as part of the total second order wave forces can also be expressed in terms of contributions to $P_{ij}$ and $Q_{ij}$ [39, 2]. These transfer functions are explained in the following.

### 3-4-4   Quadratic Transfer Functions

Where RAOs are linked to each individual wave, QTFs are applied to each pair of wave components to translate that pair's contribution to the second order wave load. It is composed of two distinct parts; one dependent on quadratic product of first order wave fields and another contributed by second-order incoming and diffraction potentials [48].

$$F^{(2)}(\omega_1, \omega_2) = F_q^{(2)}(\omega_1, \omega_2) + F_p^{(2)}(\omega_1, \omega_2) \tag{3-30}$$

LF QTF is defined as second order wave loads occurring at $\Delta\omega$ of two frequencies ($\omega_1$ and $\omega_2$) in bi-chromatic waves. The contribution from this bi-chromatic wave has a frequency equal to the difference between $\omega_1$ and $\omega_2$. Wave pairs of equal frequencies give a constant, zero frequency contribution, and the sum of these give a mean static offset of the vessel, i.e. set-down. Component pairs near each other in frequency give LF load contributions; the slowly varying part of the wave drift load causing slow drift motions. Larger differences are generally less important. It is shown that a full QTF approach is needed, as the Newman approximation underestimates LF responses of floating vessels in shallow water [6, 38]

For the LF part, $P_{ij}$ and $Q_{ij}$ are time-independent in- and out-phase part of the quadrature parts of QTF. QTF$_{ij}$ describes the force amplitude and phase (QTF $= P + i\,Q$) with respect to the incoming wave group. The second order force becomes:

$$
\begin{aligned}
F_q^{(2)}(t) = \sum_{i=1}^{N} \sum_{j=1}^{N} \zeta_i \zeta_j \cdot P_{ij} \cdot \cos\left[(\omega_i - \omega_j)t + (\epsilon_i - \epsilon_j)\right] \\
+ \sum_{i=1}^{N} \sum_{j=1}^{N} \zeta_i \zeta_j \cdot Q_{ij} \cdot \sin\left[(\omega_i - \omega_j)t + (\epsilon_i - \epsilon_j)\right]
\end{aligned}
\tag{3-31}
$$

The amplitude of the QTF is defined as:

$$T_{ij} = \sqrt{P_{ij}^2 + Q_{ij}^2} \tag{3-32}$$

The spectral density of the LF part of the wave drift force is then:

$$S_F(\omega_i - \omega_j) = 8 \int_0^\infty S_\zeta(\omega_1) \cdot S_\zeta(\omega_2) \cdot |T(\omega_1, \omega_2)|^2 \cdot \mathrm{d}\omega \tag{3-33}$$

### 3-4-5   Second Order Motions

Vertical motions are affected by vertical second order drift forces. These are calculated by applying pressure integration over the hull wetted surface $S_H$, with the five contributions in (3-28). It is shown that the fifth contribution due to $\Phi^{(2)}$, dominates in case of zero forward speed in shallow water [39]. A steady drift offset occurs in surge DOF mainly, and increases in shallow water [38]. Usually, second order heave motion is very small, it is however shown that it incresases significantly for shallow water, especially around $\omega_n$ [38].

## 3-5   Time Domain Calculations

When considering irregular waves the FD EOM (3-3) is no longer applicable. The hydro-dynamic coefficients however can be used to derive the TD coefficients [2, 16]. The linear frequency response functions are transformed to TD, after which the TD-functions will contain a convolution integral to account for memory effects. The formulation of EOM in TD relates the instantaneous values of forces, moments and motions. This allows for non-linearity and coupling between components [34]. To calculate motions, velocities and accelerations, a solution of the EOM based on Newton's second law is sought:

$$\overrightarrow{F} = \frac{d}{dt}(m \cdot \overrightarrow{U}) \tag{3-34}$$

In which $\overrightarrow{F}$ is the force acting of the COG of the vessel and $\overrightarrow{u}$ is the instantaneous velocity of the COG. The interaction and influences of surrounding fluid on a vessel's motion are captured in the Cummins' equation through a reduced radiation impedance Impulse Response Function (IRF) and infinite frequency added mass terms, as explained in Section 3-5-1. The hydrodynamic coefficients are calculated at a position representing an equilibrium position at still water level. However, once the body and fluid are in motion, things change dynamically and this effect is not captured in FD analyses.

### 3-5-1   Cummins equation

The advantage of analysis in TD is the fact that external forces can be embellished with non-linear components taking into account. A popular approach in TD analysis is the hybrid FD - TD analysis in which radiation forces are calculated through a convolution integral of motion history and the IRF [3]. Cummins proposed the hydrodynamic formulation in TD, where radiation forces are calculated using infinite frequeny added mass, convolution of the memory function with the velocity of the vessel and the hydrodynamic restoring coefficient based on geometry [49, 50]. Hydrodynamic coefficients are frequency-dependent but when the system contains multiple frequencies, these frequency-dependent parameters lose their deterministic meaning. For this reason, the second step is introduced, where these parameters are transformed to TD and the Cummins method is applied to solve the time-dependent problem [51, 2, 3, 52]. The latter approach is used here. Usually use is made of classic formulation by Cummins [53] with FD solution of Ogilvie [54]. Basically, the formulation starts with an impulsive displacement. The floating object is at rest at initial position $t = t_0$, after which it is given an impulsive displacement $\triangle x$ over constant velocity $V$.

$$\triangle x = V \cdot \triangle t \tag{3-35}$$

This impulsive displacement affects motions of the fluid during this period, but also further on in time, for which is retardation function $R_{ij}$ is used. For an arbitrarily time-dependent varying motion, this motion can thus be considered to be a succession of all small impulse displacements, while still accounting for previous displacements. For TD analyses, the retardation functions $R_{ij}(t)$ and $R_{kj}(\tau)$ are included in the equation of motion, which represent the fluid-memory effects that capture the energy transfer from motion of structure to the radiated waves [6, 2]. These retardation functions and the additional inertia can be approximated by a numerical solution of the integral up to a certrain $\omega$ and the values for frequency dependent damping and added mass values at one frequency [54]. The linear EOMs which

describe motion of ships and offshore structures provided linearity assumption is satisfied, in TD become:

$$\sum_{j=1}^{6}\{(M_{ij} + A_{ij}) \cdot \ddot{x}_j + \int_{-\infty}^{t} R_{ij}(t-\tau) \cdot \dot{x}_j(\tau)\mathrm{d}\tau + C_{ij} \cdot x_j\} = F_{ext}^{(1)}(t) \qquad (3\text{-}36)$$

Knowing the displacement and its time derivatives, a simulation can be continued with a small time step predicting the velocity from acceleration and known time histories [55]. Supposing that the velocity is a unit impulse, the radiation forces in (3-36) are represented by the convolution integral [56].

$$F_{rad}(\dot{x}, t) = -A_{\infty} \cdot \ddot{x}_j - \int_{-\infty}^{t} R_{ij}(t-\tau) \cdot \dot{x}_j(\tau)d\tau \qquad (3\text{-}37)$$

The convolution operation is commutative, i.e. $x[n]*v[n] = v[n]*x[n]$ [57], and after replacing $\tau$ with $t-\tau$ while changing the integration boundaries, the radiation part can be rewritten in a more convenient form [2, 52].

$$F_{rad}(\dot{x}, t) = -A_{\infty} \cdot \ddot{x}_j - \int_{0}^{\infty} R_{ij}(\tau) \cdot \dot{x}_j(t-\tau)d\tau \qquad (3\text{-}38)$$

The first part represent pressure forces due to accelerations and $A_{\infty}$ is the constant positive definite added mass matrix. The second term represent the fluid-memory effects, which capture energy transfer from motion of the vessel to radiated waves. The convolution part is known as the fluid-memory model. The relation between TD amd FD quantities is given by Ogilvie [54, 52].

$$
\begin{aligned}
a_{ij}(\omega) &= A_{ij}(\infty) - \frac{1}{\omega}\int_{0}^{\infty} R_{ij}(t)\ sin(\omega t)\ dt \\
b_{ij}(\omega) &= B_{ij}(\infty) + \int_{0}^{\infty} R_{ij}(t)\ cos(\omega t)\ dt
\end{aligned}
\qquad (3\text{-}39)
$$

Where $B_{ij}(\infty) = 0$. The damping coefficient $b_{ij}(\omega)$ holds for individual frequencies, so damping coefficients are needed for all possible frequencies $B(\omega) :\in [0, \infty)$.

**Convolution Integral**

What can be recognized in (3-37) is the following convolution integral of input signal $u(t)$ with output $y(t)$ [56, 57]:

$$y(t) = \int_{-\infty}^{t} H(t-\sigma)u(\sigma)d\sigma \qquad (3\text{-}40)$$

When both functions overlap, the numerical values are multiplied over this specific range. Before solving the convolution integral of Cummins' equation, the IRF, $R_{ij}(t)$ must be computed for every instant $t$. These follow from the Fourier transform in FD and TD respectively [52, 56]:

$$R_{ij}(\tau) = \frac{2}{\pi} \int_0^\infty b_{ij}(\omega) \cdot cos(\omega\tau) \cdot d\omega$$

$$R_{ij}(j\omega) = \int_0^\infty R_{ij}(\tau)e^{-j\omega t}d\omega = b(\omega) + j\omega\left[A(\omega) - A_\infty\right]$$

(3-41)

# Chapter 4

# Model

In predicting motions of vessels, the linearised Frequency Domain (FD) analysis is a common procedure and therefore extensively studied, the time-dependent problem has however gotten less attention. The Linear Wave Theory (LWT) allows for calculations to be done in FD, because the system behaves linearly dependent on displacement, velocity and acceleration. For the shallow water problem however, a Time Domain (TD) analysis is necessary to account for non-linearities in either the wave exciting forces or the radiation problem. For the current study, firstly a FD analysis is done though. The aim of this FD analysis is to validate the calculation method of the code developed in Python, where the hydrodynamic loads are evaluated numerically. This Python-model is created which evaluates what theory to apply and helps predict ship motions. It allows to include memory, where motions in a specific interval are also influenced by what has happened through motions before this interval [2].

This chapter firstly explains the model in AQWA which is used to obtain data. Secondly, the model in Python is described and how it is used to compute motions and forces by pressure integration. Next, it is explained how calculations are transformed from FD to TD, and how this method is applied for this research. After that the second order problem is explained, and how Quadratic Transfer Function (QTF)s are used to determine the second order wave loads. Then, it is explained how motions are evaluated in TD including these second order effects. At the end of the chapter a section is given where the verification of the model is shown for the different domains.

## 4-1 Frequency Domain Calculations

In Chapter 3 the methods for FD analyses are described. The preliminary analysis for this study is based on these assumptions, and a model is developed in the diffraction software AQWA.

### Model in AQWA

In AQWA, a model is created of a rectangular barge with dimensions $B \times L \times W = 20 \times 20 \times 1$ in $m \times m \times m$. The mass of the vessel is $m = 410000$ kg. The hydrodynamic analysis is performed on a discretized geometric model of these dimensions. The potential flow is described on the principle of Green's theorem. In AQWA the water depth, range of wave frequencies, frequency

step and position of the body in global coordinate system are defined. The mesh parameters and tolerance define the allowable frequencies and computation time. The accuracy depends on the size of the panels, and AQWA has set up requirements for each panels, which is further explained in Chapter B. Most important restrictions are the fact that its sizes should be small compared to the wavelengths and that the centres of the panels should be above the seabed:

$$d_{max} = \frac{1}{7} \cdot \lambda \text{and} \quad z_p + d \geq r_p \tag{4-1}$$

The following mesh input is used:

| Tolerance | Max Element Size | No. of Nodes | No. of Elements |
|-----------|------------------|--------------|-----------------|
| $1\ m$    | $0.5\ m$         | 5696         | 5561            |

**Table 4-1:** Mesh Details Used in AQWA

The focal mesh input allowed for the vessel to be analysed in the diffraction software package at a water depth op $d = 1.09$ m in the most shallow situation. The model in Python is developed to analyse ship motion behaviour beyond the limits of the diffraction analysis of AQWA. It allows for including non-linear waves, but also viscous forces or other non-linear external loads because it can do analyses both in FD as well as TD. The latter, as explained, allows for this flexibility of adding multiple external forces at every time step. The total model is shown in Figure 4-1 below.

For a clear understanding of how it can be used and what it can give as output, it is explained step by step. Firstly, the first order motions and forces are highlighted, after which the transformation to TD is explained.

## 4-2   First Order Motions

To calculate the forces on the rectangular barge over time, a model is created which calculates forces and moments through multiplying the pressure with the area of the (created) panels. These forces are compared to load Response Amplitude Operator (RAO)s as calculated by AQWA, and the associated displacement are compared to the displacements as predicted by displacement RAOs. These should be the same for deep water cases, to assure validity of the calculations in the model.

Python is an object-oriented language, which makes the creation and application of class and objects an easy manner to work with. A class is a variable which defines the set of attributes that characterize any object in the class. Within the class, methods, definitions are created which help solve the problems. For the determination of motions of a vessel in waves two classes are created: a *Wave* and a *Vessel*-object. With those classes, objects are constructed; waves and vessels with parameters which can be defined by its user.

In Figure 4-2 the work flow to determine the motions responses by the model in Python is given by a schematic overview. Firstly, a hydrodynamic analysis has been set up in AQWA in order to calculate the hydrodynamic coefficients and first order wave forces and moments. This output is used in Python to calculate the wave forces and motions with the model, in combination with the environmental conditions, which are stored in the *Wave* - object. The orange box in Figure 4-2 displays these conditions and in Python the model is capable of determining what theory to apply, recalculate wave numbers and wavelengths, the shoaling
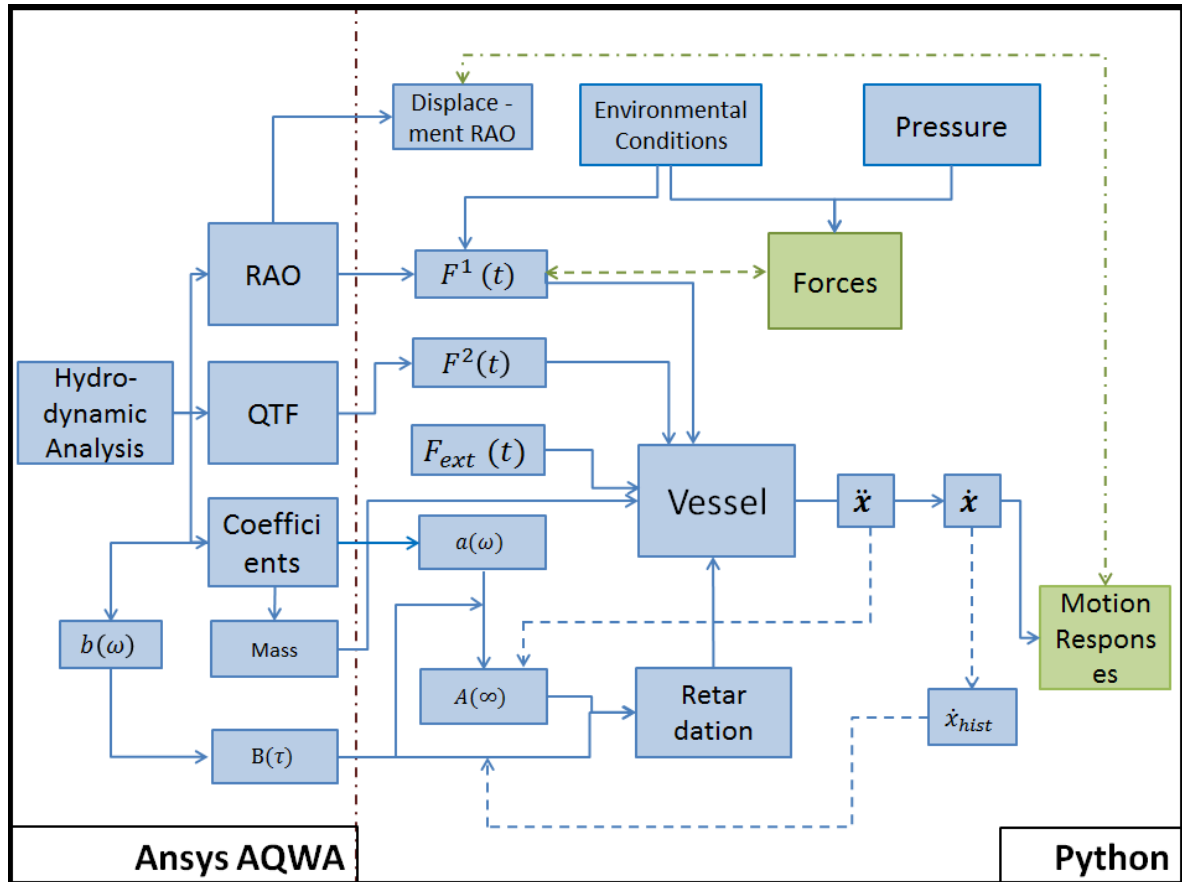
**Figure 4-1:** Flowchart model in Python

coefficient, waves, and pressures and give these as output for the user defined input. The wave amplitude is subsequently multiplied with the load RAO to find first order incoming wave force, with which the *Vessel* is excited. A hydrostatic force is also applied, after which the acceleration is calculated with the total mass (mass + added mass). The resulting acceleration is integrated, which gives the velocity at that time step. This is multiplied with the potential damping coefficient to give the damping force $F_D$, which is then also applied at the *Vessel*. This velocity is simultaneously integrated to give the displacement. The relative displacement to the initial position of the Centre of Gravity (COG) is used to calculate the hydrostatics $F_S$. To assure the calculation method is done correctly, the displacement computed in this manner should equal the displacement RAO, which is highlighted in Figure 4-2 by the green boxes. That this is indeed the case is shown in Section 4-6.

The model is capable of calculation these forces and displacement for every Degree of Freedom (DOF). From the diffraction analysis in AQWA the $6 \times 6$ - matrices are obtained and used to calculate the $F_S$, $F_D$, $F_{total}$ by taking the inner products with the displacements, velocities and accelerations. This process is repeated for every time step $t$.
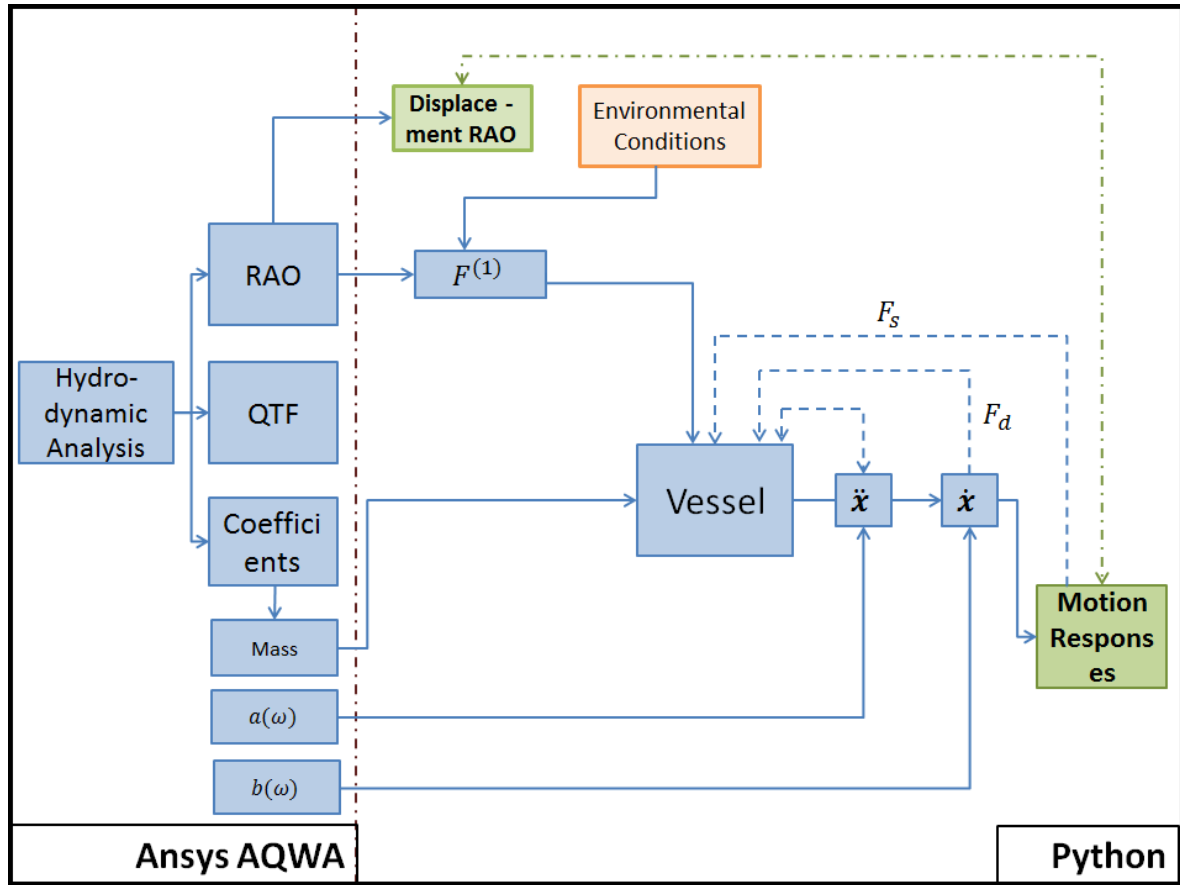
**Figure 4-2:** Flowchart of FD analysis to determine motions responses

### 4-2-1   Environmental Conditions

In the *Wave* - object in the Python model the environmental conditions are stored. The user defines a wave height $H$, wave period $T$ and water depth $d$. Current and wind forces are not taken into account. The body is subjected to forces resulting from fluctuations in water surface elevation over time. As discussed in Chapter 2 wave surface elevation can be created based on a summation of multiple regular waves. For this thesis, the spectrum is constructed based on the frequencies used in AQWA. An example what such a time series of surface elevation looks like is shown in Figure 4-3.

### 4-2-2   Rotation Matrix

To account for both translational as well as rotational displacements, the rotation matrix is applied to the motions in DOFs roll, pitch and yaw mode:

$$R_x(\phi) = \begin{bmatrix} 1 & 0 & 0 \\ 0 & \cos\phi & -\sin\phi \\ 0 & \sin\phi & \cos\phi \end{bmatrix}, \ R_y(\theta) = \begin{bmatrix} \cos\theta & 0 & \sin\theta \\ 0 & 1 & 0 \\ -\sin\theta & 0 & \cos\theta \end{bmatrix}, \ R_z(\psi) = \begin{bmatrix} \cos\psi & -\sin\psi & 0 \\ \sin\psi & \cos\psi & 0 \\ 0 & 0 & 1 \end{bmatrix} \quad (4\text{-}2)$$

After matrix multiplication, where the inner product of the three rotation matrices in (4-2),

**Figure 4-3:** Time Series of Surface Elevation, $H = 1\ m$, $[0.6 \leq \omega \leq 1.3]\ rad/s$
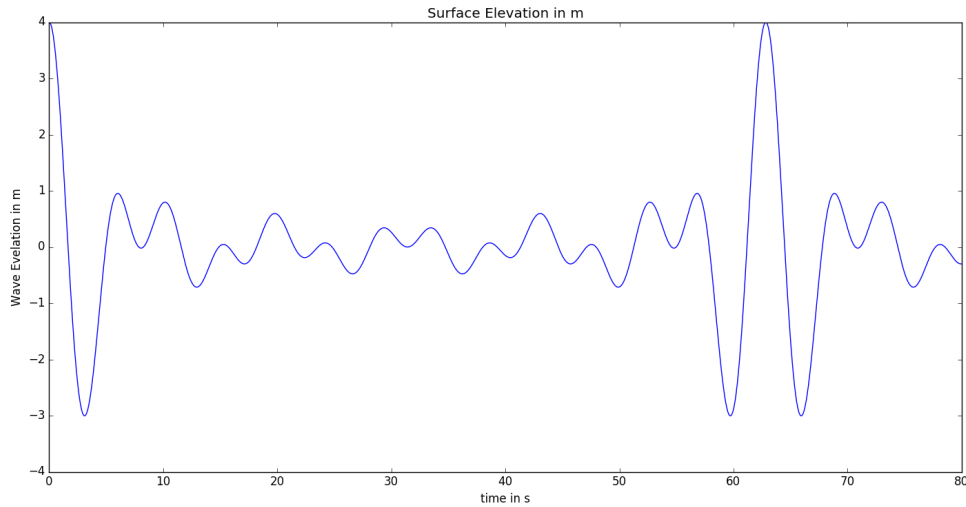
a rotation can be obtained where $phi, theta, psi$ are used to find the new coordinates in $x, y, z$ due to these rotations.

$$R = R_z(\psi) \cdot R_y(\theta) \cdot R_x(\phi) \tag{4-3}$$

## 4-3   First Order Forces

Wave exciting are calculated at each time step, by multiplication of the pressure with the area of the *Vessel*. This part of the model is used to calculate incoming wave forces by integration of pressure over the number of panels.

### 4-3-1   Pressure Integration

The Froude-Krylov (FK) - force associated with the incident wave potential is calculated by the direct integration method, so integration of associated pressure over the wetted hull $S_H$ under the undisturbed wave profile. It is hereby assumed that the moments due to vertical forces and horizontal levers are substantially larger than the horizontal forces and vertical levers in the estimation of the roll and pitch rotating moments. Therefore, these are assumed to be dominated by vertical pressures on the bottom of the discretized *Vessel* - object. This is done in the Python model to allow for higher order non-linear waves as input for the wave force. In order to do so in a later stadium, firstly the first order wave forces are calculated which should be equal to the wave force as computed by the load RAO. The incident wave forces are evaluated by integration of incident wave pressure and hydrostatic pressure $\rho \cdot g \cdot z$ over $S_H$ by the instantaneous position of the hull under this incident wave surface. This position is gathered by the position vector and rotation matrix and obtained at every time step as explained in the previous.

In Figure 4-4 the work flow is shown for the verification of the first order wave forces. The wave forces are in the model evaluated at every time step $t$, and compared to values from
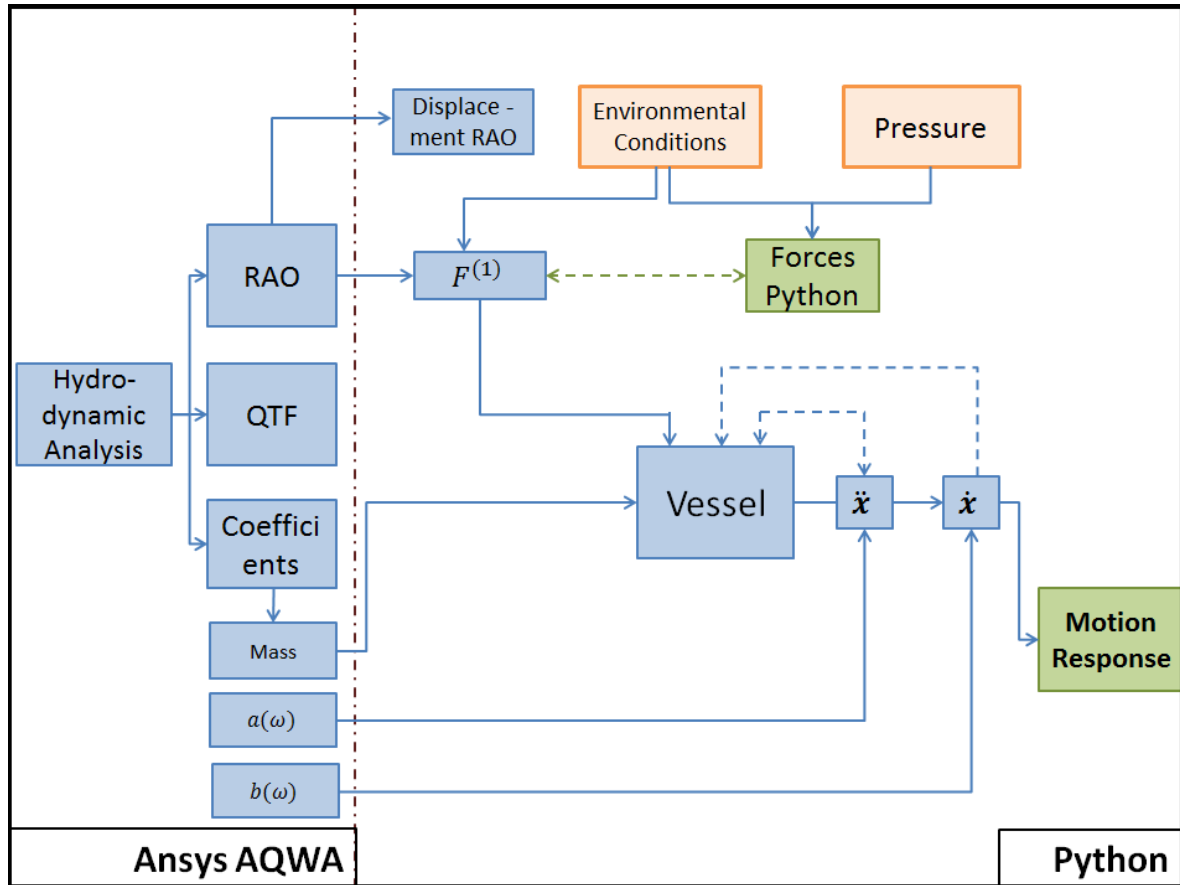
**Figure 4-4:** Flowchart of FD analysis to determine motions responses

AQWA's diffraction analysis. This method implicitly assumed that the structure responds linearly to the loads, i.e. the relationship between the load and responses remains linear given by the response functions. This assumption might no longer be valid as the wetted hull surface changes a lot. Just like with the determination of motion responses by Python, this work-flow starts with the same diffraction analysis in FD in AQWA. With the environmental conditions in the *Wave* - object the model gets the pressure for the focal *Vessel* - object. For a position $x$ and depth $z$ on the vessel, the pressure is calculated and multiplied by the bottom area of the vessel. The resulting force is superimposed with the gravitational force, to get the total incoming force on the structure. Subsequently, the damping force is calculated with the structure's velocity due to these incoming forces, which gives the total force acting on the structure with which the acceleration, velocity and displacement are calculated.

### 4-3-2   The Radiation Problem

Not only the wave exciting forces are sensitive to changes in water depth, but also hydrodynamic loads related to added mass and potential damping [6, 14]. Some thoughts one these phenomena are evaluated in the model.

**Added Mass**

In potential theory masses are assumed to stay in position. Forces are assessed at this position and related motion behaviour is calculated. In shallow water however, added masses are known to increase altogether [6]. What the potential theory neglects to represent, is the deviation of added mass over the course of the movement of the vessel. Taken this into account is however not easily done, as more phenomena come in play. For instance, one should think about the relocation of water, the mass flow rate, thus the fact that a body pushes water away which demands some additional force. This also means that somewhere else, the amount of water increases (as it cannot vanish). Another variable what ought to be considered in that case is the impulse in place. The linear momentum is calculated in a constrained control volume, where the mass flow is calculated assuming a constant flow rate. The amount of mass leaving this control volume minus the amount of mass entering this control volume per unit of time thus determines the linear momentum rate. Newton's second law in (3-34) assumes mass to be constant, while as soon as this linear momentum rate is taken into consideration, this no longer holds:

$$\vec{F} = \frac{d}{dt}(m \cdot \vec{U}) = \frac{d}{dt}\vec{G}$$

$$\vec{F} = \frac{dm}{dt} \cdot \vec{U} + \frac{d\vec{U}}{dt} \cdot m$$

(4-4)

The linear momentum is calculated for a specified control volume, with a flow rate $Q$ which is equal everywhere:

$$\frac{d}{dt}\vec{G} = \sum_{out} \dot{LM} - \sum_{in} \dot{LM}$$

(4-5)

Where the linear momentum flow rate equals the mass rate times the velocity of the fluid:

$$\vec{LM} = \dot{m} \cdot \vec{U}$$

$$= \rho \cdot Q \cdot \vec{U}$$

(4-6)

For the scope of this thesis, only some research is done on how much the hydrodynamic coefficients added mass and potential damping alter because of the motion, but difficulties mentioned prior are not considered and no further conclusions can be drawn. Shortly a description is given, which can be used for further research.

**Position dependency of hydrodynamic coefficients**

As the vessel moves in heave, it could be argued that coefficients are needed to be expressed as functions of time, or position. In Figure 4-5 this is schematically drawn. This is done by firstly examining the hydrodynamic coefficients of a barge in a single, regular wave in FD-analysis. The hydrodynamic coefficients are determined and used to evaluate the motion behaviour. Next, the $a_{ij}$ and $b_{ij}$ are determined at the most extreme position in this motion, and applied for a second analysis to determine the effects of these changes on the hydrodynamic behaviour. The hydrodynamic coefficients are extrapolated over the range of motion with some data points and established as functions of position. For a water depth of $d = 5\ m$ and wave
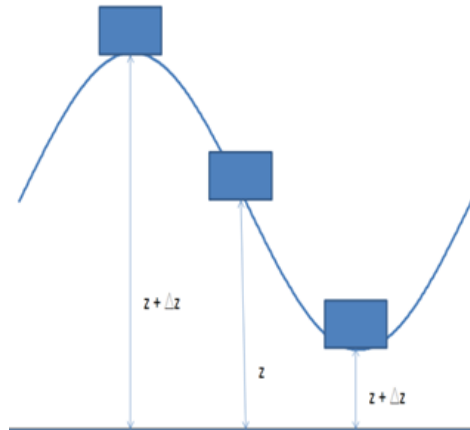
**Figure 4-5:** Actual Motion of Body Based on heave RAO

frequency $\omega = 0.7$ rad/s, the following values for $a_{ij}$ and $b_{ij}$ are obtained from AQWA in Table 4-2:

| Depth in [m] | Added Mass [kg] | Potential Damping [kg/s] | AM % - change | PD % - change |
|---|---|---|---|---|
| 4.3 | 3770200 | 2753700 | 9.9 | 10.1 |
| 4.475 | 3668100 | 2681700 | 7.0 | 7.2 |
| 4.65 | 3580200 | 2618400 | 4.4 | 4.7 |
| 5 | 3429700 | 2501800 | 0.0 | 0.0 |
| 5.35 | 3303500 | 2395200 | -3.7 | -4.3 |
| 5.525 | 3258400 | 235000 | -5.0 | -6.1 |
| 5.7 | 3208100 | 2302600 | -6.5 | -8.0 |

**Table 4-2:** Added Mass and Potential Damping Deviations

What can be concluded from these data is that on the course of the motion of the vessel in waves, added mass and damping do experience some reasonable change, even though this is only based on assumptions of potential theory. For the sake of visualization, the motions of the vessel are evaluated at these 'extreme' conditions, i.e. for the highest values of added mass and potential damping the vessel *can* experience. The results of this analysis are shown in Chapter D

**Cushioning and Sticking Effect**    The cushioning and sticking effect as explained in Chapter 3 is a phenomenon which can be considered to alter over course of its motion as well: especially the sticking part. It could be argued that it seems that in shallow water, the vessel in heave remains longer in the lowest positions (closest to seabed) due to this effect. It is however difficult to determine what this should actually should be. Furthermore, one should be aware not to account for these effects twice. Hence when for example viscosity effects are considered in damping, the 'stickiness' might already be captured to some degree.

**Potential Damping**

Also for the potential damping value, this could be considered not only as a function of frequency, but also of position. For the same reasons discussed before, only research is done on the degree to which these values could differ, but no further analysis and subsequently conclusions are drawn.

## 4-4   Second Order Forces

The second order wave forces are frequency dependent, and the transfer functions in this degree are quadratic. The computed vertical wave drift force can be translated into the TD by using Impulse Response Function (IRF) techniques [39]. For this thesis, waves of same directions are assumed. When multi-directional waves are considered, the problem's complexity increases, as a small difference in the direction of two first order wave components can already lead to a very different direction for the bound second order wave [47].

### 4-4-1   Quadratic Transfer Functions

The second order loads are calculated corresponding to the wave pairs in (3-31). The QTFs account for all five contributions of the second order wave load. AQWA includes the contributions of the undisturbed incoming waves as well as diffracted waves for the second order velocity potential. TheQTFs are obtained from AQWA and used in Python to calculate forces and motions for the bi-chromatic wave. The time series for the wave force due to difference frequencies, is a summation of all incident wave pairs:

$$F^{(2)}(t) = Re \left( \sum_{i=1}^{N} \zeta_i \zeta_i \ \mathrm{QTF}_j^-(\omega_i, \omega_i) + \sum_{(i-j)}^{N-1} \sum_{j}^{N-(i-j)} \zeta_i \zeta_j \ \mathrm{QTF}_j^-(\omega_i, \omega_j) \cdot e^{j(\omega(i-j))t} \right) \quad (4\text{-}7)$$

In which the first term corresponds to the mean drift loads and equals the sum of the terms of the diagonal of the QTF. The second term represents the slow drift load and corresponds to the off-diagonal terms in the QTF. To obtain the force in a real sea state, the coefficients must be multiplied by the complex amplitude of both waves [16].
The first second order term, the mean drift load, is a result from quadratic interactions of the first order problem and can therefore be computed without requiring solution of the second order potential. It is only dependent on diagonal terms of the difference frequency QTF.
For a bi-chromatic system, with components $(\zeta_i, \omega_i, \epsilon_i)$ , $(\zeta_j, \omega_j, \epsilon_j)$ the second order wave force of the incident bi-chromatic wave group can be described as function of the first order parameters for $\omega_i > \omega_j$ as follows:

$$\begin{aligned}
F_{ex}^{(2)} = {} & \zeta_1^2 \cdot P_{11} + \zeta_2^2 \cdot P_{22} \\
& + \zeta_1 \cdot \zeta_2 (P_{12} + P_{21}) \cdot \cos\left((\omega_1 - \omega_2)t + (\varepsilon_1 - \varepsilon_2)\right) \\
& + \zeta_1 \cdot \zeta_2 (Q_{12} - Q_{21}) \cdot \sin\left((\omega_1 - \omega_2)t + (\varepsilon_1 - \varepsilon_2)\right)
\end{aligned} \quad (4\text{-}8)$$

The case where $\omega_i = \omega_j$ is the mean drift force, and thus independent of second order potential:

$$F_{ext}^{(drift)} = \zeta_i^2 \cdot P_{ii} + \zeta_j^2 \cdot P_{jj} \quad (4\text{-}9)$$

## 4-4-2   Frequency range

For the determination of the drift force, the difference frequencies $\Delta\omega$ are calculated. Firstly, simulations in AQWA are done with frequency steps of 0.1 rad/s for a frequency range of $[0 \leq \omega_i \leq 2.5]$ $rad/s$. The focal frequencies are used to distinguish the hydrodynamic coefficients of the *Vessel* of interest. Their importance of motion behaviour of the body in waves rises near the resonance area, i.e. around $\omega_n$. When these are calculated in FD, these change as a result of the frequency dependence of $a_{ij}$. This gets easier in TD, where the added mass is calculated to a single value for frequneices of interest, and one can thus distinguish what the $\omega_n$ is to focus on for these second order drift forces. For a preliminary analysis, the values for three different water depths are shown, to get a sense of the effects of water depth on the resonance area. These are given for a barge in $d = 5, 2, 1.09$ m, which is subject to the wave force of an incoming wave with direction $-180°$ for DOF heave $z$ and pitch $\theta$.

| d in [m] | $\omega_{nh}$ in [rad/s] | $\omega_{np}$ in [rad/s] |
|:--------:|:------------------------:|:------------------------:|
| 5 | 0.57 - 1.2 | 1.28 - 1.88 |
| 2 | 0.4 - 0.74 | 0.77 - 1.25 |
| 1.09 | 0.21 - 0.26 | 0.34 - 0.42 |

**Table 4-3:** Natural frequencies for heave and pitch

Where subscript $h$ and $p$ represent heave and pitch respectively. The QTF should be calculated where the difference frequency, $\Delta\omega$ of the bi-chromatic wave is equal to these natural frequencies $\omega_n$. The difference frequency should thus lie in the range of the natural frequencies. This means that for the $d = 5$ m case in heave motion one should focus on the case where the differences are somewhere in between $\Delta\omega = 0.6 - 1.2$.

## 4-5   Time Domain Calculation

For the TD analysis in Python, firstly, the FD parameters are obtained; the RAOs and the QTFs. Hydrostatic terms are furthermore calculated. Next, the retardation function $R_{ij}$ in TD from $a_{ij}$ and $b_{ij}$ in FD are obtained. With these data the transformation to TD can be done, which will be explained in this section. This allows for simulating the motion behaviour of the *Vessel* - object in TD, where reality can better be approximated by means of adding external forces which simulate non-linear effects in shallow water. After this first order analysis, the method to determine second order wave forces and moments is explained, which can be added to the first order solution in TD.

In Figure 4-6 the calculation loop is shown for the Equation of Motion (EOM) which includes the convolution integral.
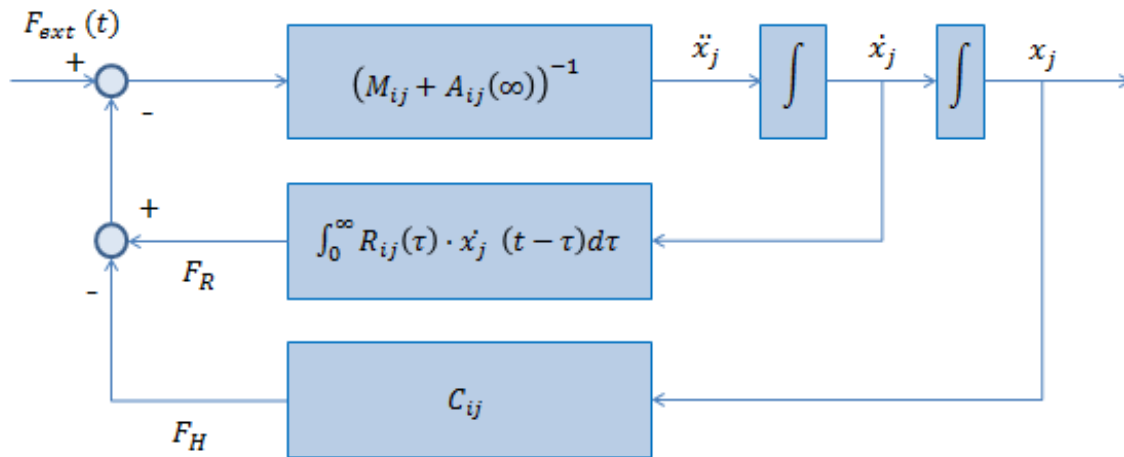


**Figure 4-6:** Simulation Scheme for Including Retardation Function with Convolution Integral

In Figure 4-1 the total calculation scheme is shown, where the retardation function is used to calculated $F_rad$, as shown in the figure above.

Firstly, the solution for $R_{ij}(t)$ as given in (3-41) is evaluated in Python for potential damping values available after the diffraction analysis in AQWA. These values are multiplied by the matrix of cosine associated with the focal frequency and moment in time of defined time range $\tau$ :

$$M_{cos} = \cos\left\{\begin{bmatrix} \omega_1 \\ \omega_2 \\ \vdots \\ \omega_N \end{bmatrix} \cdot \begin{bmatrix} \tau_1 & \tau_2 & .. & \tau_N \end{bmatrix}\right\} \tag{4-10}$$

Which gives a matrix of size $N_\omega \times N_{tau}$, which is subsequently used to determine the retardation functions for all DOF by taking the dot product of the potential damping matrix with the calculated cosine matrix, as shown in (4-10), multiplied by $\triangle \omega$ and $\frac{2}{\pi}$, see (3-41). This gives the $6 \times 6$ matrix for the retardation function $R_{ij}(\tau)$ at every value of $\tau$. The total

damping force is then calculated by re-creating the convolution integral, thus the velocity over time is 'flipped', and multiplied by the values of the retardation function $R_{ij}$. This is done because values closest to time $t$, i.e. those at $t-1$ should count more than those further away in history of motion. The resulting force matrix gives the forces in every DOF.

The spring coefficient is based on ship geometry and is thus equal to the value used in FD analyses. The added mass coefficient needs to be re-calculated though following (3-39). The hydrodynamic mass coefficient follows from:

$$A_{i,j} = a_{i,j}(\omega = \infty)$$

When this coefficient is not available for an infinite frequency, it can be calculated from a mass coefficient at a frequency $\Omega$.

$$A_{ij} = a_{ij}(\Omega) + \frac{1}{\Omega} \cdot \int\limits_0^{T_c} R_{ij}(\tau) \cdot sin(\Omega t) \cdot d\tau \qquad (4\text{-}11)$$

Where $T_c$ is the cut-off time for the time lag to store sufficient memory. The chosen integration length of the convolution integral is at least the time for waves with shortest wavelengths to travel to a different structure [58]. This is to assure every wave its impact is considered in the simulation. The added mass term in TD can then be determined using equation 3-39. A disadvantage of TD identification is that the integral (3-41) can only be computed up to finite upper frequency $\Omega$, and that the starting point is only a distortioned version of the true impulse response $R_{ij}(t)$. When determining $R_{ij}(\omega)$ a tructation error might subsequently occur in this limited frequency range $0 \leq \omega \leq \Omega$ instead of $0 \leq \omega \leq \infty$ [3, 50, 52]. The response should therefore be expressed as:

$$R_{ij}(\tau) = \frac{2}{\pi} \int_0^\infty W(\omega) \cdot b_{ij}(\omega) \cdot \cos(\omega\tau) \cdot d\omega \qquad (4\text{-}12)$$

Where $W(\omega)$ is a window function which entries for different frequency range are defined as:

$$W(\omega) = \begin{cases} \frac{n}{N_\omega} \cdot b_{ij}(\omega_1) & \text{if } 0 < \omega \leq \omega_1 \\ 1 & \text{if } \omega_1 < \omega \leq \Omega \\ b_{ij}(\Omega) \cdot \left(\frac{\Omega}{2\pi}\right)^{-3} & \text{if } \omega > \Omega \end{cases}$$

Where $N_\omega$ is the number of frequencies, $n$ the element in $N_\omega$, $\omega_1$ and $\Omega$ are the first and last potential damping values respectively in the output diffraction analysis data. $W(\omega)$ is assumed to decay linearly to zero, while for the higher frequencies in the tail the values are approximated based on the highest frequency by a factor, which is normalized for the value at $\Omega$ [50, 52]. The window function $W(\omega)$ is necessary, as numerical approximation show errors for $R_{ij}$ when time series exceed a certain value related to $\Delta\omega$ used in the AQWA ($T_{rep} = \frac{2\pi}{\Delta\omega}$). $W(\omega)$ causes this $T_{rep}$ to increase significantly, allowing for this function to be applied.

Furthermore, IRF is multiplied by a cut-off scaling function, to assure the IRF decays to zero as $\tau$ goes to infinity. This coefficient is dependent on $\tau$ and a user defined cut-off time $T_c$:

$$c(\tau) = e^{-\left(\frac{3\tau}{T_c}\right)^2} \qquad (4\text{-}13)$$

The scaling is smoothly over $t$, and is assumed to be justified when sufficient time lag is taken to account for enough memory. It improves results over sudden truncation, as no residual

value causes negative damping and thus unexpected acceleration (free energy), which would not be present in real life situations.

### 4-5-1   Second Order Forces Time Domain

The second order forces are included in the formulation of motion for the vessel in TD, as in this manner the external forces are evaluated at each time step. After the QTFs are obtained and used to calculate the second order wave forces $F^{(2)}$, this force is considered an external force in TD analysis with memory effects, for the determination of the motion behaviour. The motions computations are carried out in irregular waves under influence of first order wave loads and low frequency second order drift forces $(F(t) = F^{(1)}(t) + F^{(2)}(t))$. Second order sum frequency wave loads are not included in this evaluation. The TD equation is similar to the first order TD equation (3-36), but with second order wave excitation force on the right hand side [16]:

$$\sum_{j=1}^{6}\{(M_{ij} + A_{ij}) \cdot \ddot{x}_j^{(2)} + \int_0^t R_{ij}(t-\tau) \cdot \dot{x}^{(2)_j}(\tau)\mathrm{d}\tau + C_{ij} \cdot x_j^{(2)}\} = F_{ext}^{(2)}(t) \qquad (4\text{-}14)$$

To calculate the total motions, these can be superimposed. Alternatively, these motions can be included in the equation of motion simultaneously by including the first- and second order wave excitation forces on the right hand side:

$$\sum_{j=1}^{6}\{(M_{ij} + A_{ij}) \cdot \ddot{x}_j^{(tot)} + \int_0^t R_{ij}(t-\tau) \cdot \dot{x}^{(tot)_j}(\tau)\mathrm{d}\tau + C_{ij} \cdot x_j^{(tot)}\} = F_{ext}^{(1)}(t) + F_{ext}^{(2)}(t) \quad (4\text{-}15)$$

The second order wave loads are calculated with the use of QTFs. The model in Python takes the difference frequency QTFs from AQWA, after determination of frequencies by the user. Two waves are created with the *Wave* - Object. The model calculates both mean and Low Frequency (LF) drift forces and these forces are superimposed with both first and second order wave loads. The damping forces are subsequently with the retardation functions.

## 4-5-2   Viscous Damping

Viscous damping needs to be added to the EOM in shallow water, the issue is however that AQWA doesn't account for the viscosity effects. The model in Python in TD is capable of calculating an additional damping term, based on empirical data and the potential flow hydrodynamic coefficients. The TD method allows for inclusion of an additional force to account for viscosity effects in shallow water. Viscous damping can then be included in the term $\int_{0}^{\infty} R_{ij}(t-\tau)\dot{X}$, by re-evaluation of the damping coefficients in the matrix calculations as they are related to the motion velocity of the vessel [6].

The EOM including the viscous forces becomes:

$$\sum_{j=1}^{6}\{(M_{ij}+A_{ij})\cdot\ddot{x}_j + \int_{0}^{t} R_{ij}(t-\tau)\cdot\dot{x}_j(\tau)\mathrm{d}\tau + b_{visc}\cdot\dot{x}_j(t) + C_{ij}\cdot x_j\} = F_{ext}(t) \qquad (4\text{-}16)$$

The non-potential damping effects are usually obtained from model tests. Since for this study these tests are not carried out, coefficients are obtained from literature.

### Critical Damping Factor

As discussed in Section 3-3-2 in Chapter 3 an additional damping factor can be included based on the critical damping for a DOF. Based on empirical data from literature, a damping ratio should lie in the range of $\xi = 4-5\%$ to account for viscosity. [14, 34, 13]. A preliminary estimate is taken from research from Clauss et al. (2009) [14]:

$$\xi_2 = 2\ \%$$
$$\xi_4 = 1.2\ \%$$

### Viscous Drag Damping Factor

Another method to be applied is calculation an additional damping force based on a drag constant $C_D$. A viscous drag load can subsequently be calculated with (D-17). Based on several empirical models for the calcuation of quadratic heave, pitch and roll damping, this drag term can be included with value $C_D = 2$ [13].

The method applied in this study is a viscous damping term based on the critical damping factor $\xi$, as the one based on $C_D$ is one which is usually applied for long slender structures in the Morison equation. More data is available therefore on the viscous damping term related to the critical damping in literature and therefore this value seems more reliable.

### 4-5-3 Approaching Seabed

As discussed in Section 3-3-1 the cushioning effect causes the floating structure not to hit the seabed. It is argued that this phenomenon can be captured by including an additional force in the acceleration part of the EOM, i.e. as some sort of additional added mass term. This can benefit motion prediction, as AQWA fails to calculated hydrodynamic added mass and potential damping coefficients when the seabed approaches, see Chapter **??**. Reference can be made to the work of Brennen (1982) [31], which concentrates on fluid inertial forces due to acceleration and discusses the forces due to the creates of a low Under Keel Clearance (UKC) when approaching the seabed. It comes up with an engineering approaching with the associated forces, for the lifting of a plate near the seabed, which can be a comparable situation to the one of the barge in shallow water. It derives a force where to body width needs to be very large compared to the UKC, which is the case in this study. The velocity and acceleration in positive $z$ - direction are $dh/dt$ and $d^2h/dt^2$, see Figure 4-7
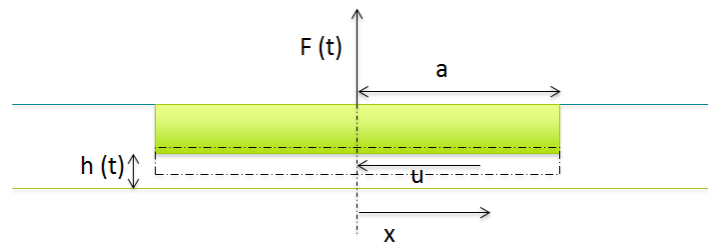


**Figure 4-7:** Plate near the seabed

The heave motions induces a horizontal velocity which increases as the UKC gets lower:

$$h \cdot u_x = -\frac{dh}{dt} \cdot x \tag{4-17}$$

The pressure distribution in the gap is the following for the case where frictional forces and viscous forces are not present:

$$p = p_{edge} + \frac{\rho}{2}(a^2 - x^2) \cdot h \cdot \frac{\partial(\frac{1}{h})^2}{\partial t^2} \tag{4-18}$$

By integration the added mass for the fluid on the plate per unit length becomes:

$$F = \frac{2}{3} \cdot \rho \frac{a^3}{h} \left\{ \frac{\partial h^2}{\partial t^2} - \frac{2}{h} \left[ \frac{\partial h}{\partial t} \right]^2 \right\} \tag{4-19}$$

Where a is the width, as shown in Figure 4-7. The UKC $h(t)$ is replace by $d - T$, where $d$ is the water depth and $T$ the draft of the *Vessel* - object. The re

$$F = \frac{2}{3} \cdot \rho \frac{a^3}{d - T} \left\{ \ddot{z} - \frac{2}{(d + z)} \cdot \dot{z} \right\} \tag{4-20}$$

The resulting additional force can be included in the EOM:

$$\sum_{j=1}^{6} \{(M_{ij} + A_{ij}) \cdot \ddot{x}_j + \int_0^t R_{ij}(t-\tau) \cdot \dot{x}_j(\tau) \mathrm{d}\tau + b_{visc} \cdot \dot{x}_j(t) + C_{ij} \cdot x_j\} = F_{ext}(t) - \frac{2}{3} \cdot \rho \frac{a^3}{d+z} \left\{\ddot{z} - \frac{2}{(d+z)} \cdot \dot{z}\right\}$$

$$(4\text{-}21)$$

The value for $h(t)$ is in the model defined as 'gap', and equals $d - T + z$ and is thus dependent on the oscillation vertically. As one can see, the force is dependent on both acceleration and velocity of the body. The additional inertial force is only determined for vertical motions, and the first part is included in the function which calculates the acceleration.

This force is added as an additional function in the model, as function of wave height in the *Wave* - object and water depth in the *Vessel* - object.

## 4-6   Verification

To allow for addition of non-linear parts, i.e. non-linear wave forces or non-linear reaction forces, one must be sure that the model calculates the desired output. In this section the verification is shown by considering a deep water case, thus a case where the wave can surely be seen as a regular wave based on the parameters Ursell Number (UR), $S$, $\mu$.

This section shows that for both FD and TD wave forces and resulting shop motions are predicted well by the numerical model. Time series plots of motions calculated and those prescribed by RAOs overlap nicely. However, to be sure that the results hold for all $\omega$, the Fast Fourier Transform (FFT) is performed. For every $\omega$, a *Wave* is created for with which forces acting on the *Vessel* are calculated in a time loop. The FFT is explained in Chapter B. The Fourier transform decomposes the time signal into the frequencies that contribute to it and shows its magnitude and phase. In this manner the amplitudes of displacements and the associated phases can be plotted as function of $\omega$ of the focal *Wave* and these can be compared to the displacement RAOs.

### 4-6-1   First Order Motion

The accelerations, velocities and displacements calculated in the Python model are verified by comparing these with the RAO amplitude obtained from the diffraction analysis at the specific frequencies. A deep water case is considered, to assure calculation method.

$$
\begin{aligned}
z &= \zeta_a \cdot RAO \cdot cos(\omega\ t - \varepsilon_{z,\zeta}) \\
\dot{z} &= \omega \cdot \zeta_a \cdot RAO \cdot cos(\omega\ t - \varepsilon_{z,\zeta} + \pi/2) \\
\ddot{z} &= -\omega^2 \cdot \zeta_a \cdot RAO \cdot cos(\omega\ t - \varepsilon_{z,\zeta})
\end{aligned} \tag{4-22}
$$

In Figure 4-8 a time series of heave displacement as calculated by the model and by the displacement RAOs. As one can see lines overlap. In Figure 4-9 the amplitudes and phases for all frequencies are shown, and one can see that the calculation method is verified for all frequencies. In Figure 4-10 and Figure 4-11 is shown that the same holds for pitch and roll DOF. The results hence show that the displacement of the created *Vessel* - object, based on values in the *Wave* - object are the same as those determined through RAOs, and it can thus be concluded that the model can be used to determine ship motion behaviour.

### 4-6-2   First Order Forces

To compare results calculated with the model with the results from AQWA, the pressure are calculated as if the barge would lay still in water. The pressure equals the amount of water pushed away by the vessel, with a hydrostatic part (draft) and dynamic part (oscillation).

An incoming wave is considered with $H = 0.1$m, $\omega = 1$rad/s at a water depth of $d = 30$m. The water wave parameters are:

- UR = 0.004
- $S = 0.01$
- $\mu = 3$

Which thus fall in within the limits of LWT.

The incoming wave forces are calculated based on pressure distribution on the hull. As shown in Figure 4-4, this wave force should equal the load RAO. In Figure **??** both wave forces are
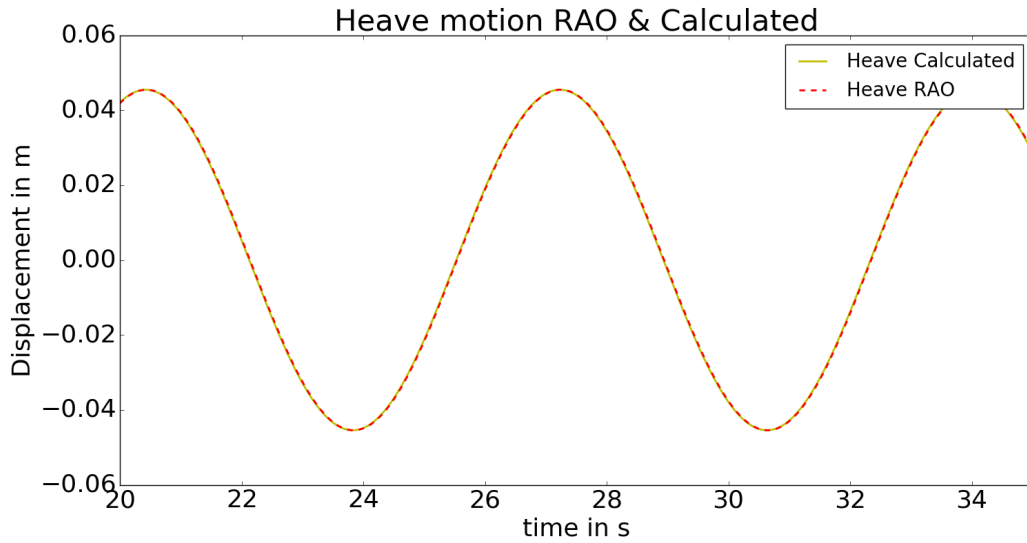
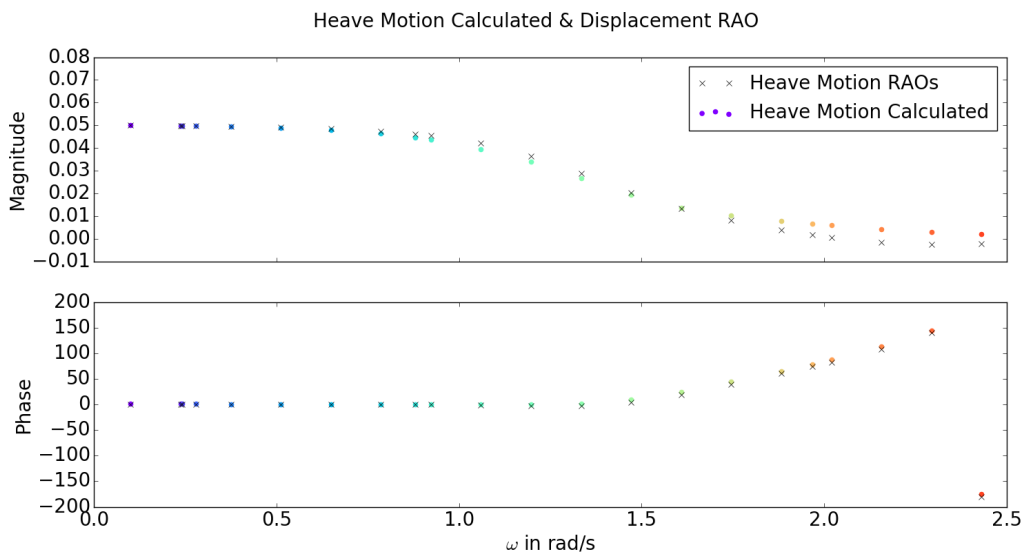**Figure 4-8:** Heave Motion Time Series Caculated and Estimated with RAOs



**Figure 4-9:** Heave motions calculated with model and with RAO for a range of $\omega$

shown, i.e. the one calculated by the pressure distribution in the Python model and the one with the load RAO.

A FFT is done to determine these wave forces for all $\omega$. In Figure 4-13 the results are shown. In the upper plot the wave forces are shown when calculated with the load RAO, where the coloured dots show the wave force and the crosses identify the direct calculation of load RAO with wave amplitude. The lower plot shows the same for the crosses, while the coloured dots identify the wave forces calculated through pressure integration.

Ultimately, one is interested in resulting motions at all frequencies, so these are also compared to the displacement RAOs, at every $\omega$. These results are shown in Figure 4-15 and Figure **??** for heave and pitch respectively.
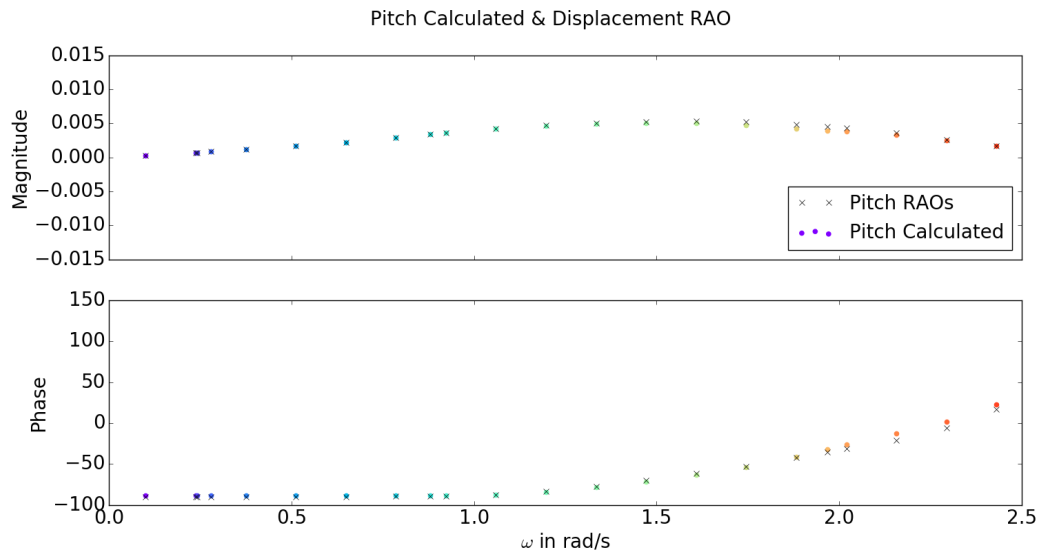
**Figure 4-10:** Pitch calculated with model and with RAO for a range of $\omega$
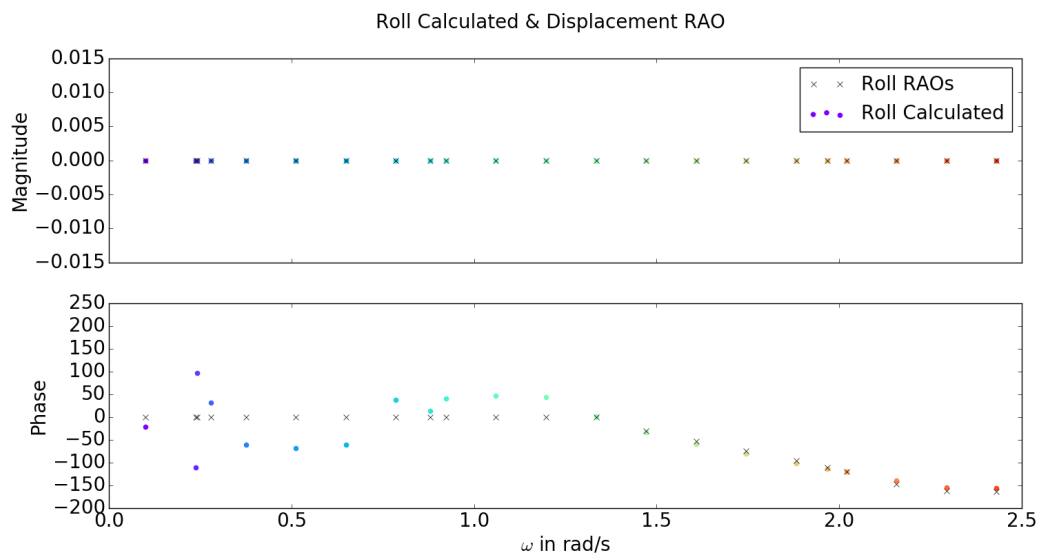


**Figure 4-11:** Roll calculated with model and with RAO for a range of $\omega$

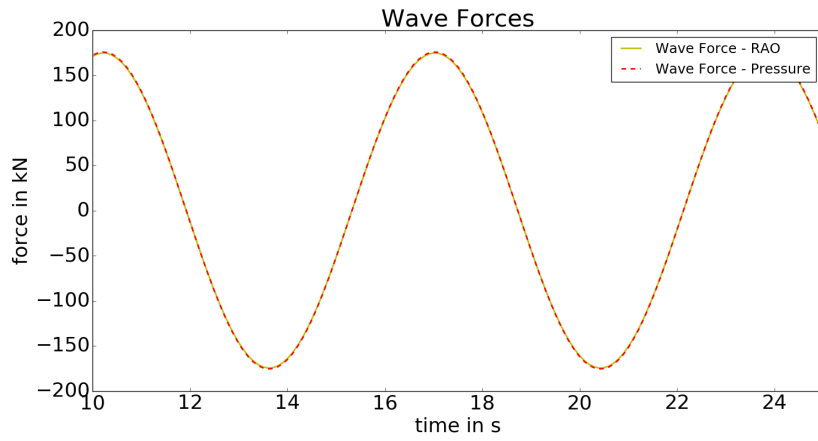This implies the computation strategy is right and can be utilized for other conditions or dimensions of *Vessel* - objects.
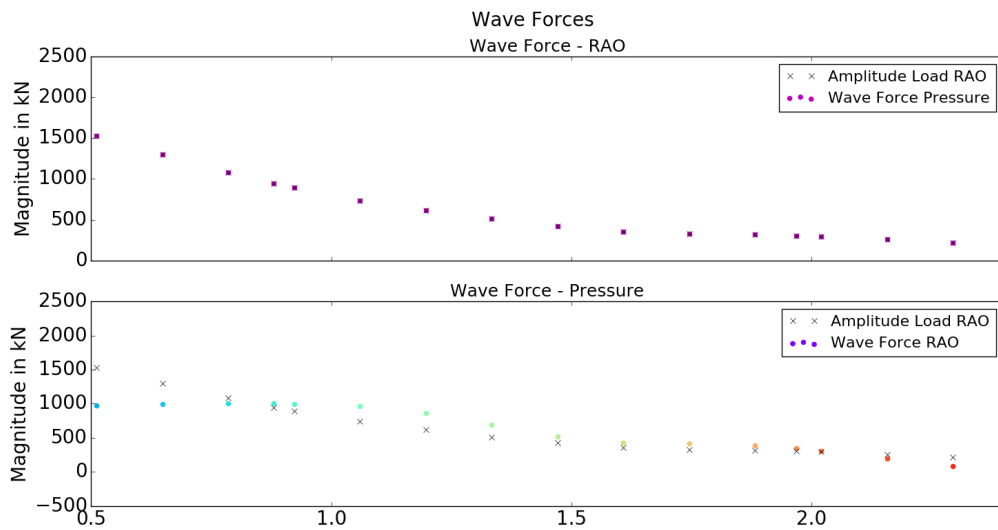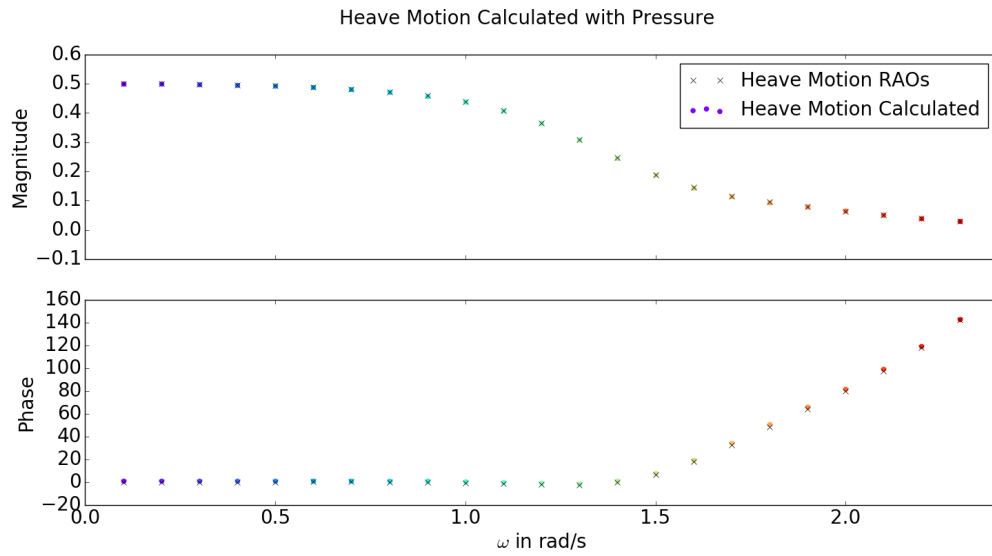
**Figure 4-12:** Wave Forces



**Figure 4-13:** Wave Forces

**Figure 4-14:** Wave Forces
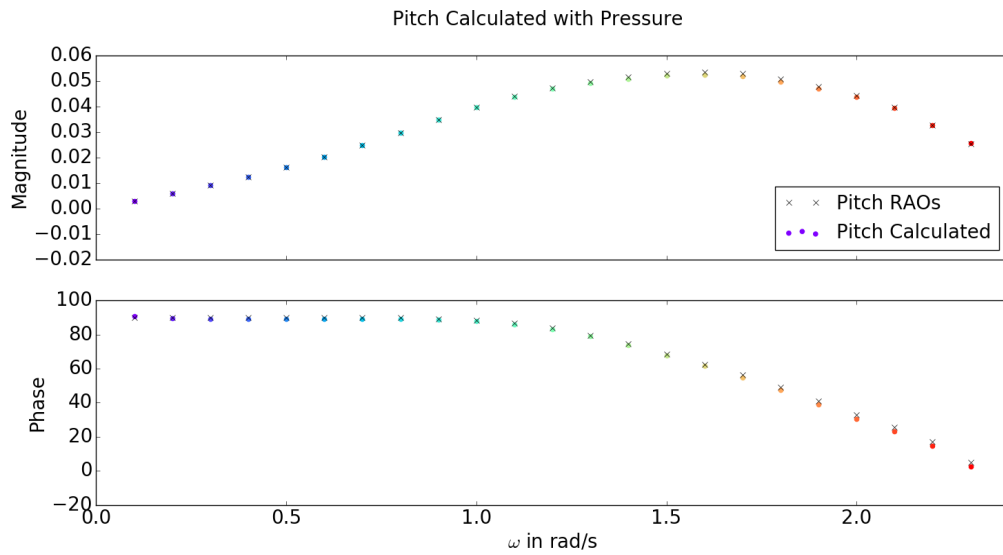


**Figure 4-15:** Wave Forces

### 4-6-3   Time Domain

After transforming the EOM to TD, the resulting motion behaviour should be approximately be the same as the analysis done in FD.

In Figure 4-16 the retardation function for heave is shown as calculated with the described method in Section 4-5. This figure is given to show what this damping function does: it gives most damping to the system at $t = 0$, and lesser through the course of time. This could be expected and should give the right results when applied in the EOM.



**Figure 4-16:** Retardation for heave for $d = 5\ m, \omega = 1\ rad/s$

**Forces**  In Figure 4-17 the forces are compared individually, calculated by the model in FD with the RAOs and the one with the retardation function in TD.



**Figure 4-17:** Forces Comparison FD and TD calculation

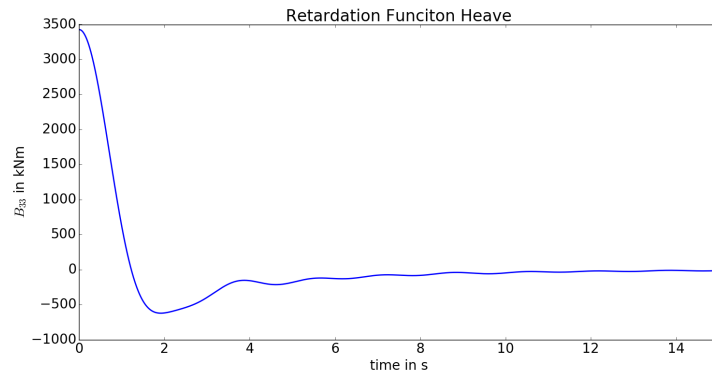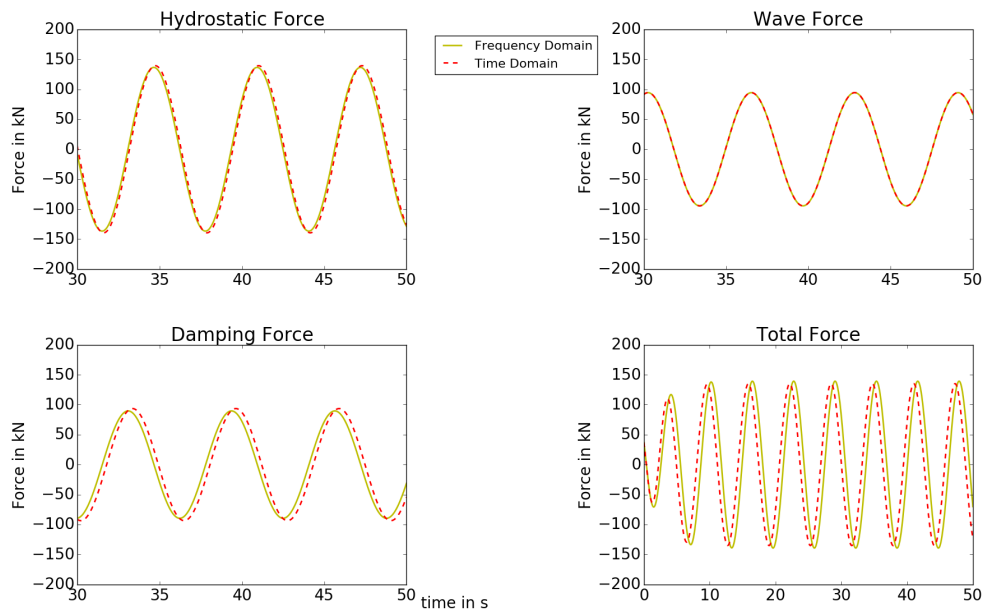**Motions**   Memory effects should cause the system to damp out when an impulse is applied to the *Vessel* - object. As shown in Chapter 4, the retardation function is developed correctly, so it should give approximately the same results for the damping when multiplied with the velocity and integrated over time. The system should be damped when no additional external forces are applied to it. An impulse is given to the *Vessel* - object, to see whether motions indeed approach zero. The result of this impulse for both heave and pitch motion are shown. For $d = 5\ m$ and $\omega = 1$ rad/s (at which the initial velocity is determined in the velocity RAO) the following impulse responses are calculated:
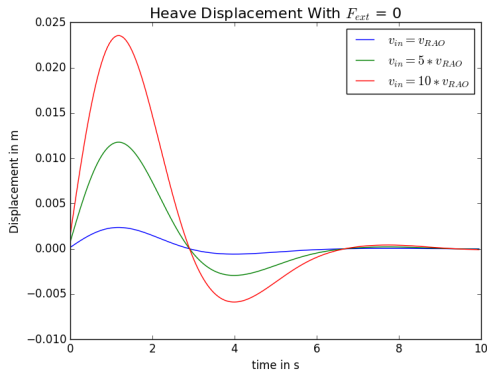


**Figure 4-18:** Heave
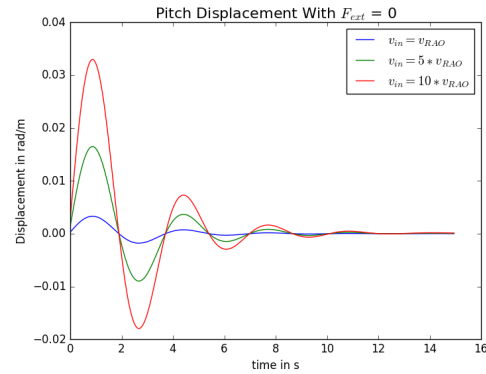


**Figure 4-19:** Pitch

So, also with regards to motion behaviour, the model correctly applies the largest force and calculates the associated largest displacement at the moment in time this force is applied. The system damps out nicely, and does so faster for smaller external forces than larger external forces. The next step would be to see if the motion behaviour indeed is the same in this TD analysis as it is in FD, for same, - deep water - , input values.

In Figure 4-20 the magnitude and phases of the heave displacement are shown for the deep water case as explained in the previous, with damping used which is calculated by the convolution integral. Two Vessel - objects' displacements are evaluated and compared and one can see that the retardation function computes approximately the same as when the displacements is approximated by the hydrodynamic coefficients directly.

It differs a little, which is not surprising as the added mass has increased and the damping has also changed somewhat. The deviations are reasonable though, the displacements are not very far apart, 6 % at the most. The retardation function can thus be used to evalute motions in TD with the purpose of allowing additional non-linear forces.

**Figure 4-20:** Heave Displacement with potential damping and with retardation function

# Chapter 5

# Results and Discussion

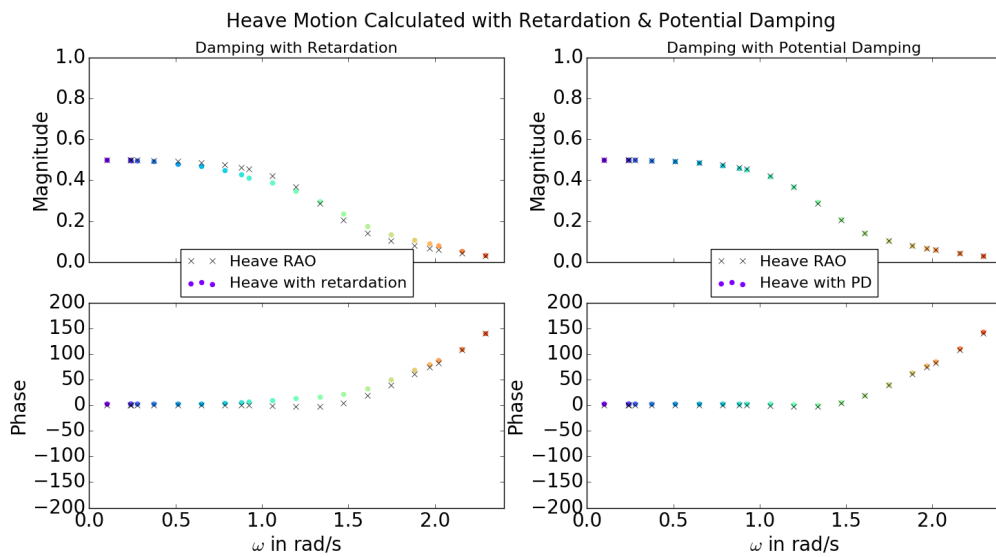In this chapter the results are given of the parametric model developed Python to approximate motion behaviour in shallow water. It firstly describes the Frequency Domain (FD) results, and gives a numerical example of the application of Stokes second order wave theory on a *Vessel* - object. Next, Time Domain (TD) analysis is elaborated and how the results are in line with the FD results for vertical motions of four vertices of the barge. It furthermore shows how wave forces in this domain are calculated based on direct pressure integration after which results are given for including viscous damping effects for three $d$. A numerical example is subsequently given for including another $F_{ex}(t)$, namely the additional inertial force as discussed in Section 4-5-3. Lastly, the second order wave forces and motions are discussed and their importance on final vertical motions.

## 5-1  Frequency Domain Analysis

In the *Wave* - object specifics of the waves are user defined which act upon the *Vessel* - object. As described in Chapter 2, there is a range of applicability of the Linear Wave Theory (LWT), by Ursell Number (UR) and wave steepness $S$. The model shows for the range of $\omega$ used in the diffraction analysis, which waves can be described by the LWT by the input $H$ and $d$. For example, for a $H = 0.25$ m and $d = 5$ m, the majority falls within the limits of the LWT, only the lowest $\omega$ ($\omega$ =0.1, 0.2, 0.3 rad/s) can better be described by the cnoidal wave theory and the highest $\omega$ by Stokes second order theory. When the wave frequency $\omega = 1$ rad/s one can thus be sure that wave forces and subsequent ship motions can still be described by the LWT. The small amplitude assumption must be satisfied, and this is done by selecting a value of $S$ of 0.01. In the *Wave* - object a wave is created with $H = 0.25$ m and $\omega = 1$ rad/s in $d =$  5m. This gives the following values for the parameters which determine the validity:

|  | S | $\mu$ | $U_R$ |
|---|---|---|---|
| d = 5 m | 0.002 | 0.124 | 1.29 |

**Table 5-1:** Values for parameters for d = 5 m, H = 0.25 m and $\omega = 1\ rad/s$

In this section, the parameters are given numerically but in Chapter D the maximum wave height are given according to the limited values for UR and $S$ (for the LWT) in schematic

overview in Figure D-1. The hydrodynamic coefficients associated with this case, are obtained from the diffraction analysis in AQWA, and given in Table 5-2.

| $m$ | 410000 [kg] | $F_a$ | 1880 [kN/m] |
|---|---|---|---|
| $a$ | 2787100 [kg] | $\epsilon_{F,\zeta}$ | -1.28 [rad] |
| $b$ | 2562500 [kg $\cdot$ s] | RAO | 0.7 [m/m] |
| $c$ | 4020.7 [kN/m] | $\epsilon_{z,\zeta}$ | 0.08 [rad] |

**Table 5-2:** Hydrodynamic coefficients and displacement and load RAO with magnitude and phase at $d = 5$ m, $\omega = 1$ rad/s

In Section 4-6 it is shown that the calculation method for the first order forces is verified, and it is assumed that it can be modified by adding higher order wave pressure. When the wave height for example increases to $H = 1$ m, the wave should theoretically best be described by the Stokes second order wave theory, see values for the parameters in Table 5-3. How the wave pressure, and subsequent wave forces differs from the LWT description for the same input parameters, is shown in Figure 5-5.

|  | S | $\mu$ | $U_R$ |
|---|---|---|---|
| d = 5 m | 0.025 | 0.124 | 12.9 |

**Table 5-3:** Values for parameters for d = 5 m, H = 1 m and $\omega = 1$ rad/s

### 5-1-1   First Order Motions

With values from Table 5-1 it is established that the focal case can be described by the LWT, and the total motions of the barge can thus be calculated by superposition of motions due to multiple Degree of Freedom (DOF). Four points on the barge are chosen for evaluation, and quite logically these lie on the vertices of the rectangular barge as can be expected that these will hit the seabed first.

| | $x$ | $y$ | $z$ |
|---|---|---|---|
| $P_1$ | 10 | $-10$ | $-1$ |
| $P_2$ | 10 | 10 | $-1$ |
| $P_3$ | $-10$ | 10 | $-1$ |
| $P_4$ | $-10$ | $-10$ | $-1$ |
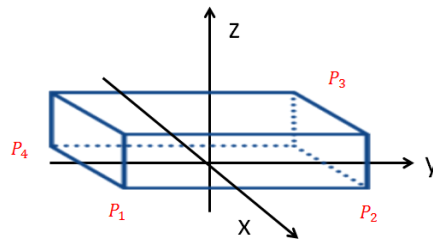


**Figure 5-1:** Points on barge

Based on model dimensions these points are modelled in Python and can be chosen accordingly. For the vertical motions three DOF are involved in the total vertical displacement:

$$z_p = z - x_p \cdot \theta + y_p \cdot \phi \tag{5-1}$$

The magnitude of vertical displacement for the focal points is shown in Figure 5-2. Those are plotted with the heave displacement only, to show what the effect of angular motions is

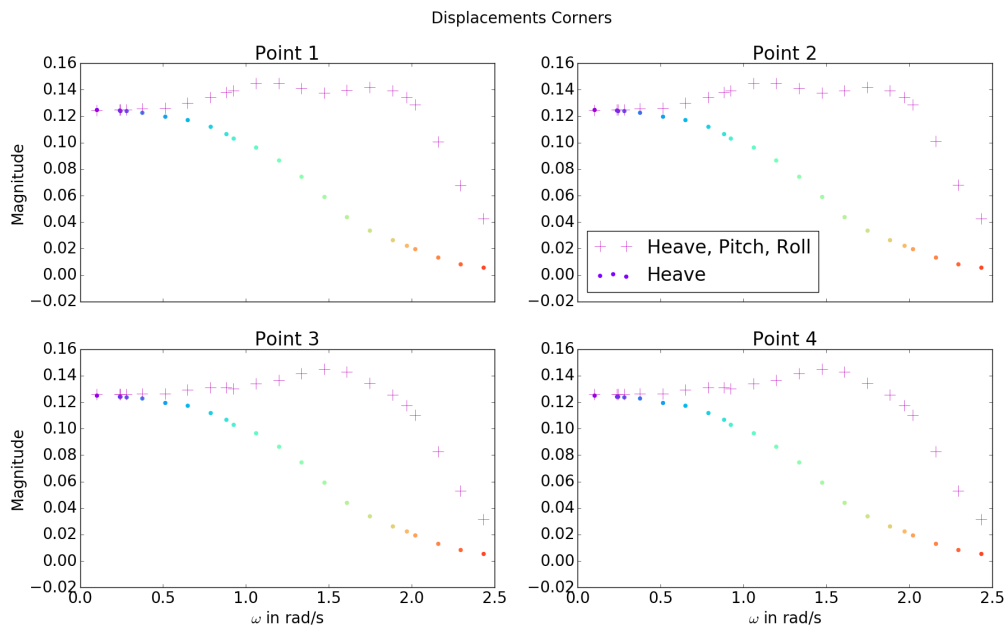in comparison to the motion of the Centre of Gravity (COG).



**Figure 5-2:** Vertical Displacement 4 Corners, $H = 0.25$ m.

The figure shows that the overall vertical motions of the barge has its largest amplitudes at the frequency range $[1.0 \leq \omega \leq 2.0]$ rad/s according to the LWT. For these input values, this range lies safely within the range of validity of the LWT, which means that theoretically this motion prediction is accurate. When wave height increases to input values of Table 5-3 though, the motion prediction increases linearly, i.e. the increase in $H$ can be recognized directly in magnitude of response. However, results are theoretically not to be trusted anymore, as the frequency range in which the LWT is applicable is exactly 1 frequency in this case, at $\omega = 0.8$ rad/s. For $[0.1 \leq \omega \leq 0.7]$ rad/s waves can better be described by the cnoidal wave theory, while for frequencies $[0.9 \leq \omega \leq 1.4]$ rad/s the waves are theoretically Stokes second order waves.

In the following section a numerical example is given for the calculation of direct pressure integration with second order pressures, described by this theory. The associated wave forces are given as well as the resulting motions.

## 5-1-2   Second Order Stokes Waves

When wave heights increase, and one should resort to the Second order stokes theory, where pressure differs than the one calculated by the linearised version in (2-21). For the values shown in Table 5-3, theoretically the wave forces should be described by this theory. In Figure 5-3 the blue dot shows this wave and that it meets validity limits.

The pressures can be calculated with Stokes second and the values are compared to the values as they are computed by the LWT, as well as those for the incoming wave forces. As one can see, the pressures and forces remain symmetric, but these are no longer sinusoidal.

The displacements as a result of these different pressures are calculated by assuming that the wave pressure can be multiplied by the wetted area and that subsequently the same
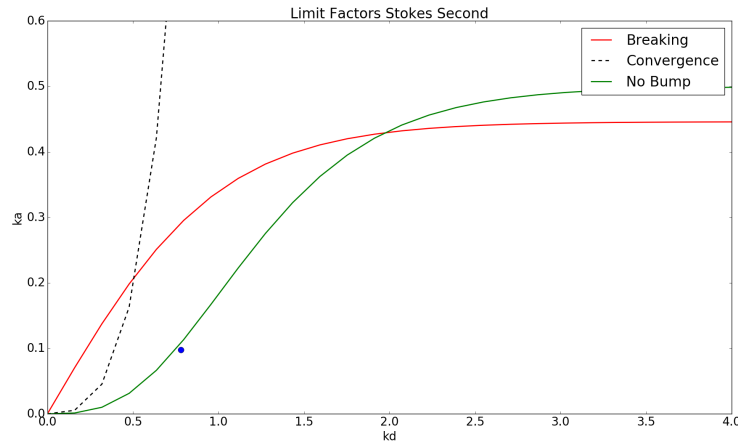
**Figure 5-3:** Position of Wave within limits of Stokes Second

procedure can be followed as if it were first order pressure. Based on input parameters the model gives for this $H$ and $d$ the validity frequency range is $[0.9 \leq \omega \leq 1.4 \text{rad/s}]$, for which the amplitudes of displacements are shown in Figure 5-6. However, as argued, these wave forces can not boldly be altered, firstly a transformation to TD needs to be done to include these in the Equation of Motion (EOM), for the calculation of associated displacement of the *Vessel*.
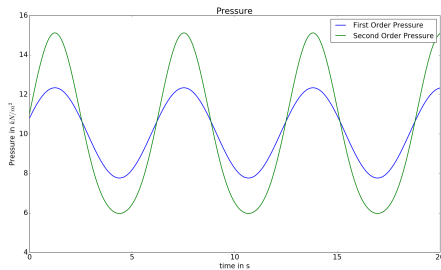


**Figure 5-4:** Pressure
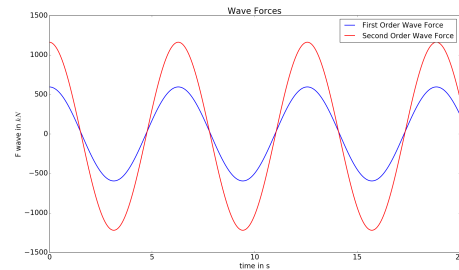


**Figure 5-5:** Wave Force

The difference with the first order results in Figure 5-6 are a result of the asymmetry in the vertical velocity component. The description of the pressure according to this theory consists of three terms, where the last (see (2-36) is a non-cyclic term which is zero at the bottom of the seabed. This meets the requirements that if $d = 0$, there can be no vertical momentum flux, i.e. the time averaged pressure must be in balance with the weight of the water above the seabed, also time-averaged. Moving away from the bottom, there is a vertical momentum owing to this asymmetry of the focal second order stokes waves (higher crests, flatter troughs), causing an dynamic pressure component larger than zero which adds to the usual higher frequency second order term.
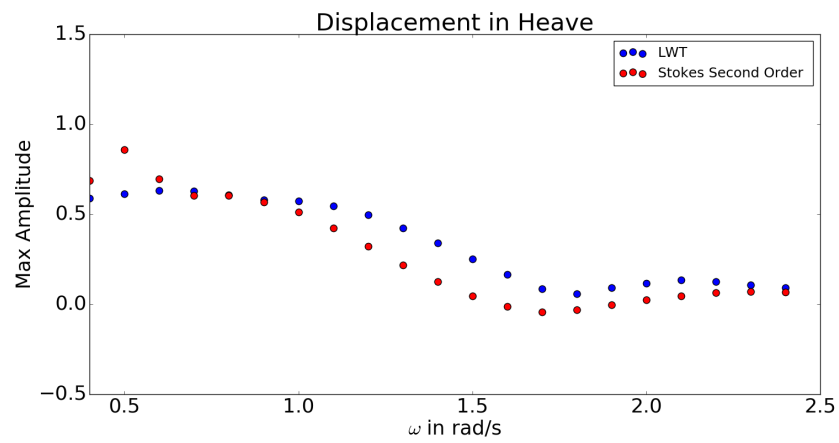
**Figure 5-6:** Linear Wave Theory and Stokes Second Order Theory

## 5-2   Time Domain Analysis

The vertical motions of the *Vessel* in TD can be evaluated at the desirable depth and wave height. For the values in Table 5-1 the amplitudes of the motions are given in Figure 5-7.
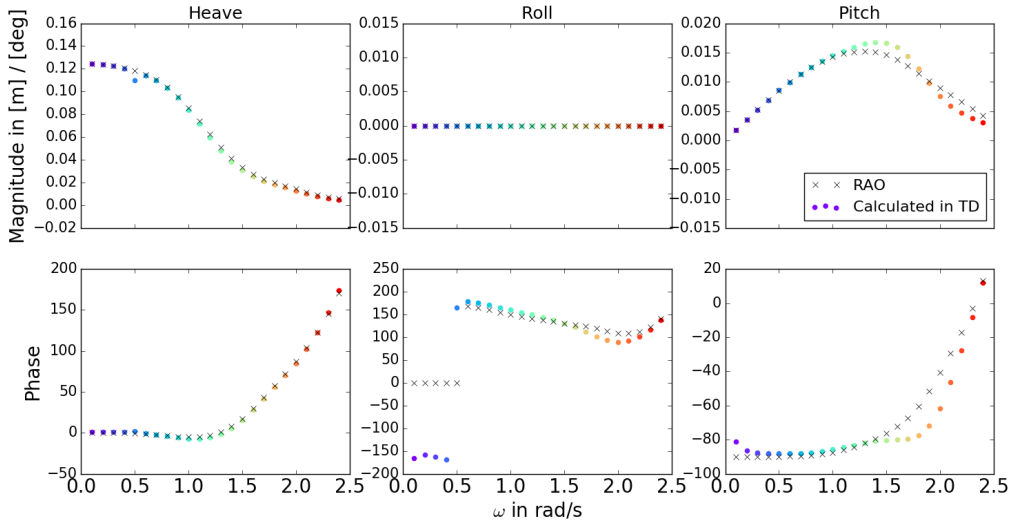


**Figure 5-7:** Magnitude and Phase of heave, roll and pitch in Time Domain. $H = 0.25$ m, $d = 5$ m.

The vertical motion of the four corners is calculated with the $R_{ij}$ and shown in comparison to the displacement RAO in Figure 5-8.
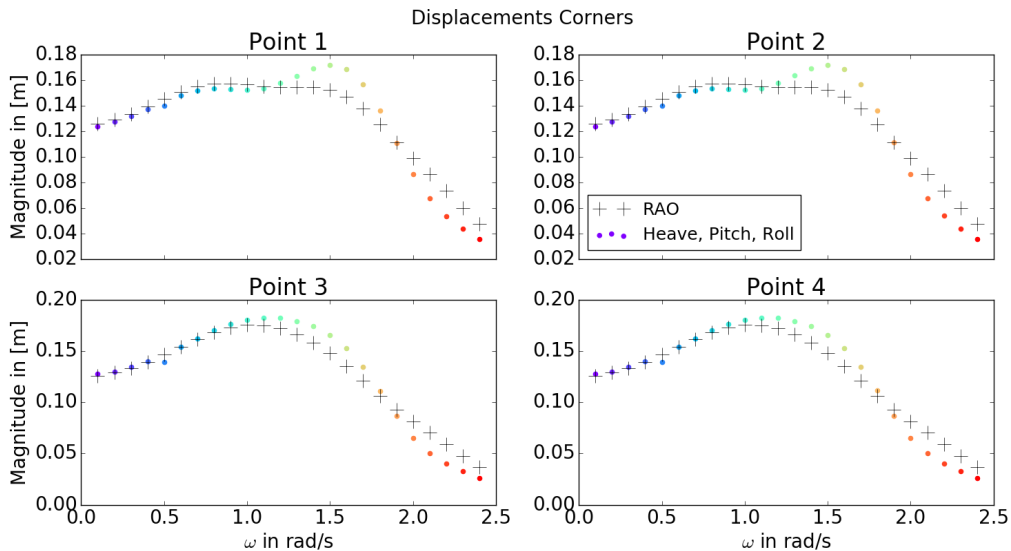


**Figure 5-8:** Points in Time Domain, $H = 0.25$ m, $d = 5$ m.

In the figure the black +'s highlight the displacement directly calculated from the RAO superposition of the three DOF, see (5-1). The coloured dots are the amplitudes calculated

in TD and one can see that values generally are in great agreement, although there are some slight differences. However, the damping as well as the added mass has changed due to the transformation to TD, so this is an expected result. Furthermore, in the calculations done in Python, all DOF are included, while the black crosses only represent the absolute values of amplitudes of $z, \phi, \theta$. Incoming waves come from direction $\mu = -180°$ in this situation, which explains why the two upper and two lower plots are similar because there is practically no roll moment, and the $x$ position are the same, creating the same pitch moment and overall same amplitude of displacement.

### 5-2-1 Motions with Force Model

The force model which calculates the incoming wave forces and resulting motions as a result of the water wave pressure is subsequently used to determine the incoming wave forces in TD. Two *Vessel* - objects are created and firstly motions are compared to assure these calculations are still valid. It is subsequently possible to determine the second order Stokes - pressure field and use the latter to evaluate motion behaviour. The resulting wave forces and motions still are comparable to RAOs, which makes it possible to use it to define other, non-linear, incoming waves as well. In Figure 5-9 the wave forces, pressures and resulting displacement are shown for one *Wave* - object of $\omega = 1$ rad/s and $H = 0.25$ m in $d = 5$ m. The upper left figure shows the wave forces prescribed by the load RAO and the restoring force, and the upper right figure shows the wave forces calculated with the pressure model, both in FD and TD. In Figure 5-10 the results are shown for all $\omega$, which shows that is predicts approximately same displacements. The pressure difference is marginal, where some deviations can be attributed to the differences in added mass and potential damping in FD and FD which has its effects on accelerations, velocities and displacements and since the latter are used to determine pressure on the barge at every time step, the values can be expected to not be exactly the same. The effect on the ultimate displacement is however still negligible and it can therefore be assumed that it is accurate.

Now, we want to see if we can calculate the incoming wave forces through the calculation of pressure with Stokes second order theory.

In Figure 5-14 the vertical displacement of one of the corners is shown. It is assumed that the incoming wave force are described by the Stokes second order pressure and subsequently the $z$, $\phi$ and $\theta$ are used to determine $z_p$ as previously done. In the upper plot only heave is shown, and the lower $z_p$.

| $\omega$ [rad/s] | $d$ [cm] |
|:---:|:---:|
| 0.7 | 2.75 |
| 0.8 | 3.87 |
| 0.9 | 5.2 |
| 1.0 | 6.8 |
| 1.1 | 8.3 |
| 1.2 | 9.3 |
| 1.3 | 10.7 |

**Table 5-4:** Differences with reference to LWT

A numerical example is given in Table 5-4. The largest increases are for this case 20% more
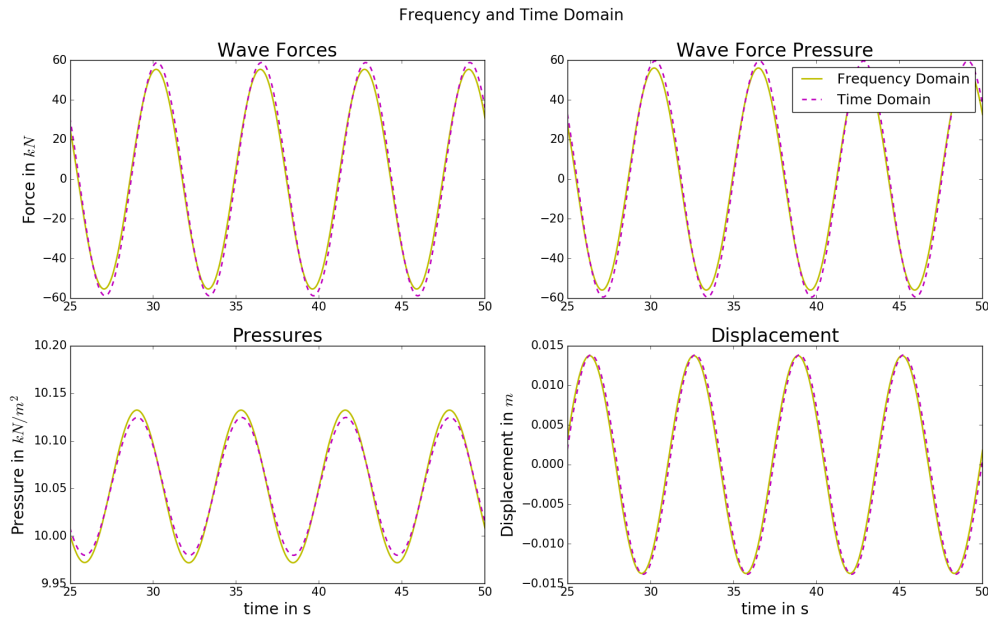
**Figure 5-9:** Wave Force, Pressure, Displacement in FD and TD for $\omega = 1\text{rad/s}$
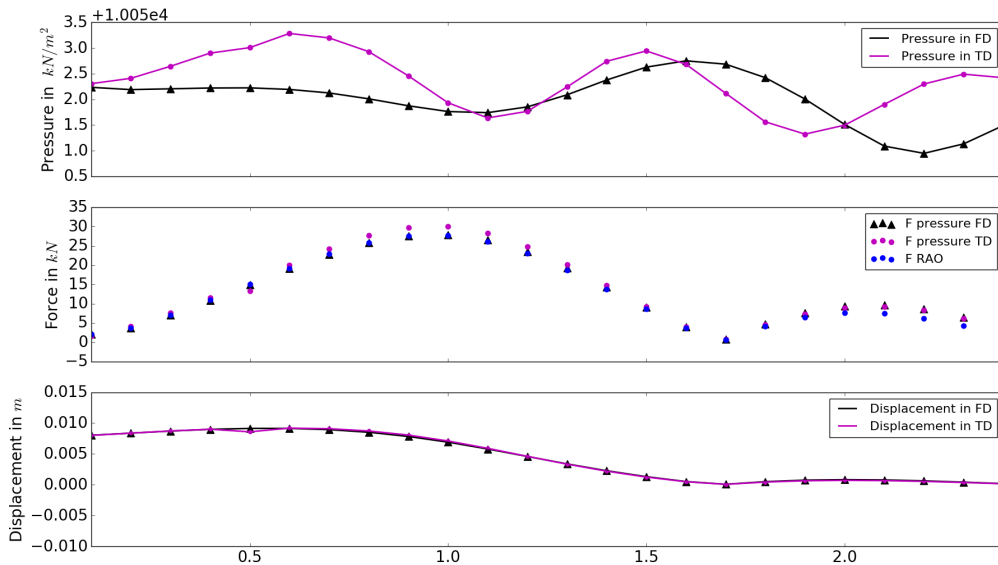


**Figure 5-10:** Wave Force, Pressure, Displacement in FD and TD for all $\omega$

than considered with Airy waves, the absolute values of the differences in displacement in cm are given for a frequency range in which the Stokes second order theory is valid. These are considerable values and can help to predict a safe workability range when these values are added to the first order displacement. When letting the depth decrease in the model, the results show similar graphs, but in these situations other effects will influence motion
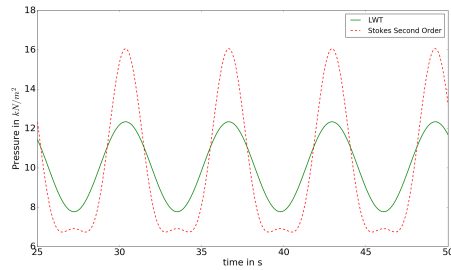
**Figure 5-11:** Pressure
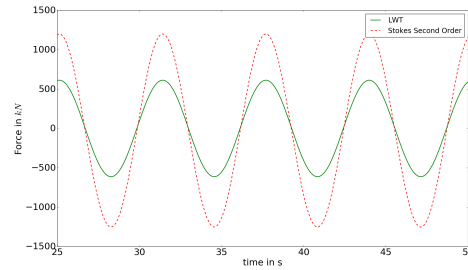


**Figure 5-12:** Wave Force
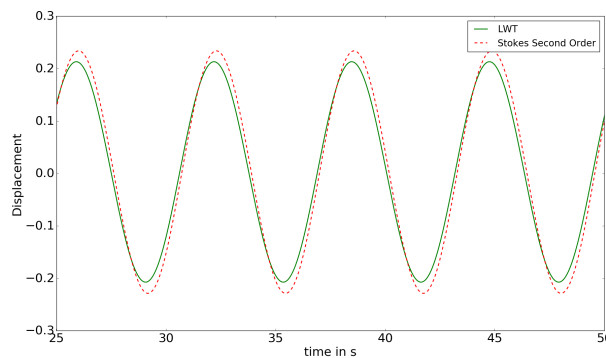


**Figure 5-13:** Heave Displacement $H = 1$ m, $\omega = 1$ rad/s with LWT and Stokes Second Order Theory

behaviour. Furthermore, waves can not only be considered individually, especially in shallow water where the second order effects become more and more significant. The viscous damping effects and bi-chromatic waves and the effects of these groups of waves are therefore discussed in the following.

### 5-2-2   Viscous Damping

As discussed in Chapter 3 in Section 3-3-2, research has shown that viscous effects need consideration in shallow water when $d/T \leq 1.3$. In this case, also a water depth of $d = 2$ m, i.e. $d/T \leq 2$ is evaluated, as damping has shown to increase significantly around this value, see Chapter 3. After the transformation to TD the $B_{crit}$ can be determined at the desired depth. With (3-21) the viscous damping $B_v$ is calculated.

One can see in Table 5-5 that the $\omega_n$ of the three DOF decrease, and that the $B_v$ increases. Furthermore, the relative magnitude of $B_{ij}$ versus the $B_{crit}$ is given in last column of the tables. These values are given to highlight the relative magnitude of viscous effects; as the $B_{ij}$ is approximately 30% of $B_{crit}$, the factor of $B_{crit}$ which determines the viscous part, is actually not that small with reference to the overall damping of the system. So for a preliminary analysis, this damping factor is used for determination of viscous damping.
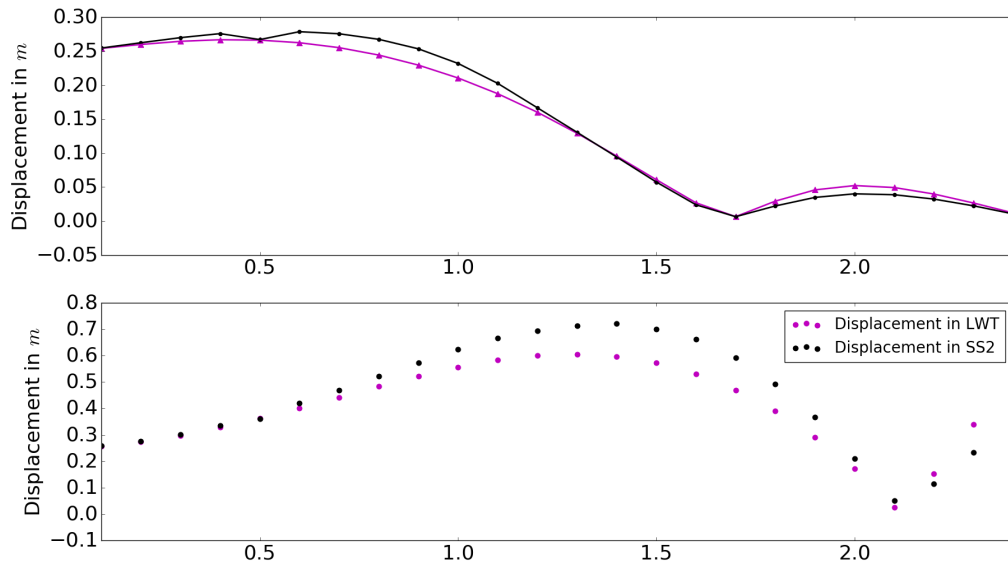
**Figure 5-14:** Vertical Displacement of one of the Corners of the Barge with LWT and Stokes Second Order Theory

| d<br>in [m] | $\omega_n$<br>in [rad/s] | $B_{crit}$<br>in [kN s/m] | $B_v$<br>in [kN s/m] | $B_{ij}/B_{crit}$<br>[-] |
|---|---|---|---|---|
| 5 | 1.0 | 7863.15 | 393.16 | 0.11 - 0.34 |
| 2 | 0.66 | 12219.45 | 610.9 | 0.16 - 0.39 |
| 1.09 | 0.26 | 31186.89 | 1559.34 | 0.013 - 0.24 |

| d<br>in [m] | $\omega_n$<br>in [rad/s] | $B_{crit}$<br>in [kN s/m] | $B_v$<br>in [kN s/m] | $B_{ij}/B_{crit}$<br>[-] |
|---|---|---|---|---|
| 5 | 1.6 | 1652738.7 | 8136.93 | 7.8 e-4 - 0.21 |
| 2 | 1.08 | 244604.41 | 12230.22 | 0.005 - 0.27 |
| 1.09 | 0.41 | 638120.31 | 31906.0 | 9.8 e-3 - 0.15 |

| d<br>in [m] | $\omega_n$<br>in [rad/s] | $B_{crit}$<br>in [kN s/m] | $B_v$<br>in [kN s/m] | $B_{ij}/B_{crit}$<br>[-] |
|---|---|---|---|---|
| 5 | 1.6 | 1652738.7 | 8137.30 | 7.8 e-4 - 0.21 |
| 2 | 1.08 | 244604.42 | 12230.22 | 0.005 - 0.27 |
| 1.09 | 0.41 | 638120.31 | 31906.0 | 9.8 e-3 - 0.15 |

**Table 5-5:** Damping, Critical Damping and Viscous Damping for Heave, Roll and Pitch at different depths

## Vertical Motions

In Figure 5-8 was shown how the model the vertical displacements calculates for an incoming wave of $\mu = -180°$. In this section, the situations is re-calculated, including an additional

damping accounting for the viscosity. The $B_v$ based on $B_{crit}$ is included in the EOM in TD and motion behaviour of the four corners is calculated. In the following figures the differences with reference to $z_p$ without viscosity are shown, for two wave directions, $\mu = -180°$ and $\mu = -145°$, for wave with wave height $H = 1$ m.
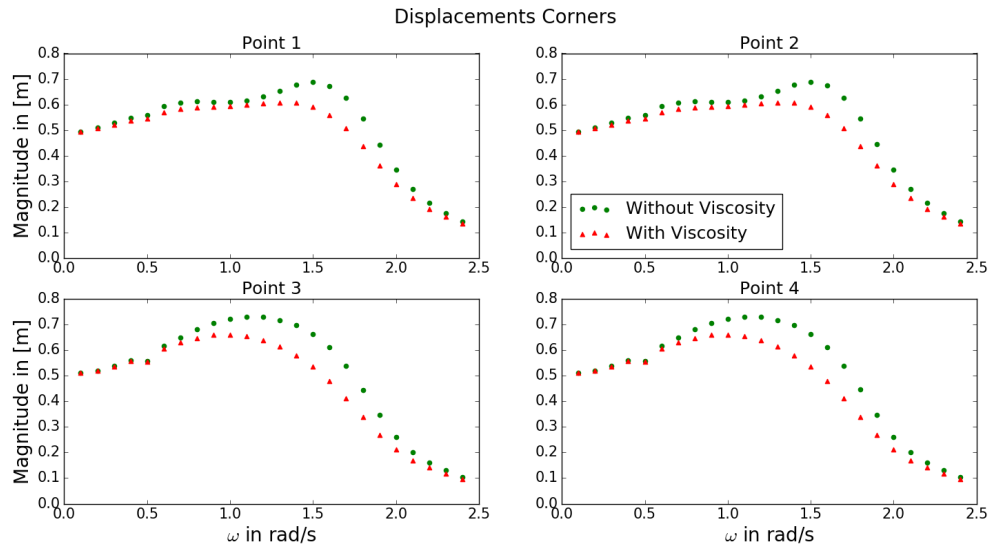


**Figure 5-15:** Vertical displacement of four corners at $d = 5$ m with and without viscosity, with $\mu = -180°$
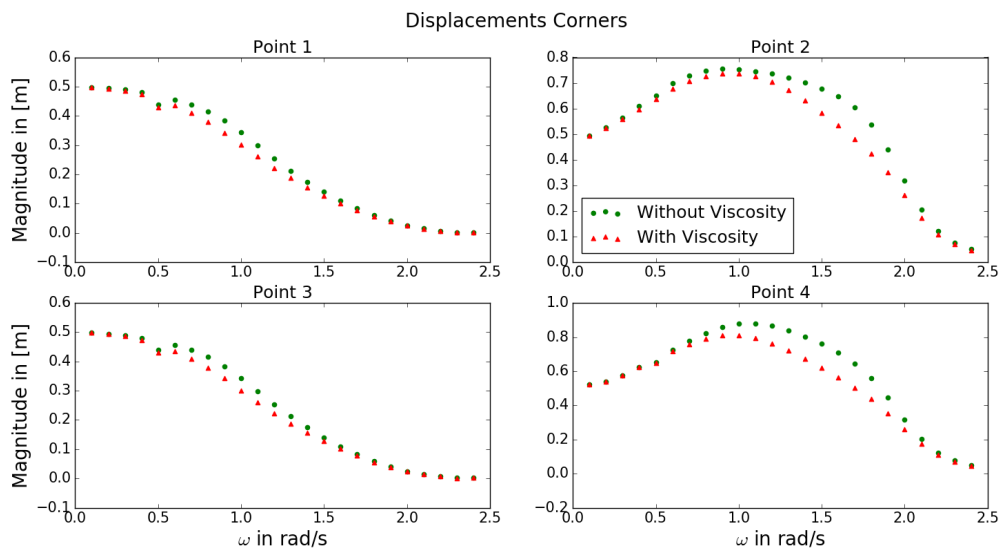


**Figure 5-16:** Vertical displacement of four corners at $d = 5$ m with and without viscosity, with $\mu = -145°$

In the figures can be recognized that the $z_p$ increases in shallow water, near the resonance of the pitch moment, which is lower for $d = 2$ m than for $d = 5$ m, which can be noticed in the maximum displacements at the different $\omega$. Because the case of $d = 2$ m can become more
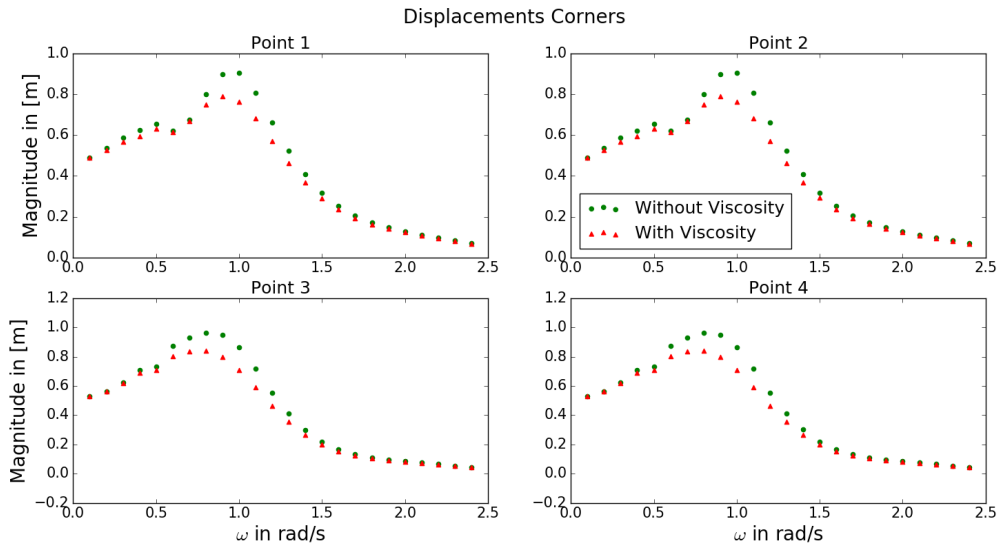
**Figure 5-17:** Vertical displacement of four corners at d = 2 m with and without viscosity, with $\mu = -180°$
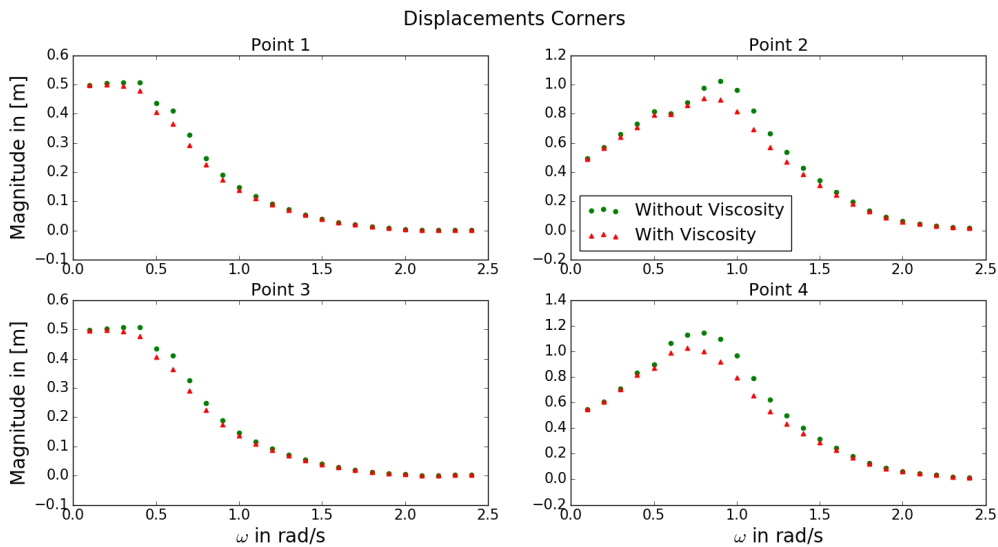


**Figure 5-18:** Vertical displacement of four corners at d = 2 m with and without viscosity, with $\mu = -145°$

problematic, this situations is numerically further investigated and discussed.

For an incoming wave from direction $\mu = -145°$, the points 1 and 3 are mainly displaced by the heave DOF, apparently a negative roll moment is counteracted by a positive pitch moment and vice versa. So for long $\lambda$, the vessel will follow the motions of the wave, and the displacement equals the wave amplitude. This effect is also recognized in Figure 5-16. The fact that point 2 and 4 do show an additional vertical displacement is explained by the fact that the wave travels underneath the bottom of the vessel, and has a different length than the dimension of the vessel. This is not the case in point 1 and 3, which are exactly in line with the

wave crests and trough for a wave coming from this direction. The results in the graphs and tables show however that when the incoming wave has direction $\mu = -180°$, the rotations due to $\phi$ and $\theta$ amplify the vertical motion behaviour. There is no roll moment, so the $\theta$ rotation causes the additional vertical displacement at the corners of the vessel. In Table 5-2-2 the numerical results for $d = 2$ m are given, for both with and without viscosity and for both wave directions. In the second and third columns the magnitudes of displacement are given, and in row four and five the $\Delta_{zp}$, which means the difference in vertical displacement when viscosity is considered. These values can arguably thus be subtracted from the values in row two and three for motion prediction.

For point 1, 3, in $\mu = -180°$ the vessel the largest displacements are around $\omega = 1$ and $\omega = 1.6$ rad/s, which is in line with the $\omega_{nh}$ and $\omega_{np}$ respectively. The displacement of points 3 and for is slightly bigger than those of 1 and 2, which can be explained by the fact that for these points lie on the negative x - axis and for a positive $\theta$ thus add to $z$. The largest displacement of these points is at $\omega = 0.8$ rad/s, while for points 1 and 2 this is at $\omega = 1.0$ rad/s. The largest $\Delta_{zp}$ is for these points found at the same frequencies.

For $\mu = -145°$ the maximum displacement is found at $\omega = 0.9$ rad/s, although the displacement at the frequencies $\omega = 0.8$ and $\omega = 1.0$ rad/s is still larger than the largest for $\mu = -180°$. The largest $\Delta z$ are also found in this range.

| $\omega$ | $z_{p1}$ | $z_{p2}$ | $\Delta z_{p1}$ | $\Delta z_{p3}$ | $\omega$ | $z_{p1}$ | $z_{p2}$ | $\Delta z_{p1}$ | $\Delta z_2$ |
|---|---|---|---|---|---|---|---|---|---|
| 0.5 | 0.65 | 0.73 | 0.02 | 0.03 | 0.5 | 0.44 | 0.82 | 0.03 | 0.02 |
| 0.6 | 0.62 | 0.87 | 0.01 | 0.07 | 0.6 | 0.41 | 0.80 | 0.05 | 0.01 |
| 0.7 | 0.68 | 0.93 | 0.01 | 0.09 | 0.7 | 0.33 | 0.87 | 0.04 | 0.02 |
| 0.8 | 0.80 | 0.97 | 0.05 | 0.12 | 0.8 | 0.25 | 0.98 | 0.02 | 0.07 |
| 0.9 | 0.90 | 0.95 | 0.11 | 0.15 | 0.9 | 0.19 | 1.0 | 0.01 | 0.13 |
| 1.0 | 0.90 | 0.87 | 0.14 | 0.16 | 1.0 | 0.15 | 0.96 | 0.01 | 0.15 |
| 1.1 | 0.91 | 0.72 | 0.13 | 0.13 | 1.1 | 0.12 | 0.82 | 0.01 | 0.13 |
| 1.2 | 0.81 | 0.55 | 0.09 | 0.09 | 1.2 | 0.09 | 0.66 | 0.00 | 0.09 |
| 1.3 | 0.66 | 0.41 | 0.06 | 0.06 | 1.3 | 0.07 | 0.54 | 0.00 | 0.07 |
| 1.4 | 0.52 | 0.3 | 0.04 | 0.03 | 1.4 | 0.05 | 0.43 | 0.00 | 0.05 |

**Table 5-6:** Left table: Vertical Displacements Point 1 and 3, for $d = 2$ m, $\mu = -180°$. Right table: Vertical Displacements Point 1 and 2, for $d = 2$ m, $\mu = -145°$

In the situation of $d = 1.09$ m, the model gives unrealistic results when $\Delta\omega = 0.1$. This is due to the fact that the retardation matrix gives negative damping values, because the $b_{ij}$ beyond a certain frequencies starts to give negative values, after which this 'damping' adds energy to the system and keeps doing time step after time step. In Figure 3-4 an example was given of $a_{ij}$ and $b_{ij}$ at three water depths, and where those damping coefficients approaches zero (which one would expect), those of the limit-case of $d = 1.09$ m cross this zero-line and give negative values (which one would not expect). Therefore, a $\Delta\omega = 0.05$ rad/s is evaluated for $d = 1.09$ m. Even with viscosity effects included, the increase of displacement around $\omega_n$ is large, and it would therefore arguably be necessary to do additional research on the cushioning and sticking effect, as well as the viscous forces, as these are expected to be quite important in this situations.

In Figure 5-19 it can be seen that the heave motion increases enormously around its $\omega_n$, causing the high peaks in the vertical motions of the four points in Figure 5-20 and Figure 5-21.

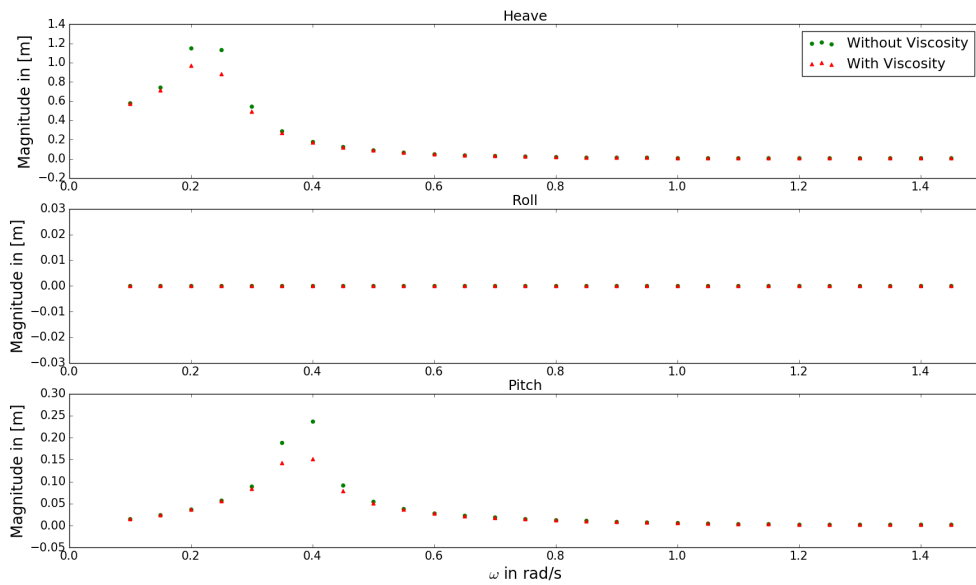**Figure 5-19:** Heave, roll and pitch at d = 1.09 m with and without viscosity
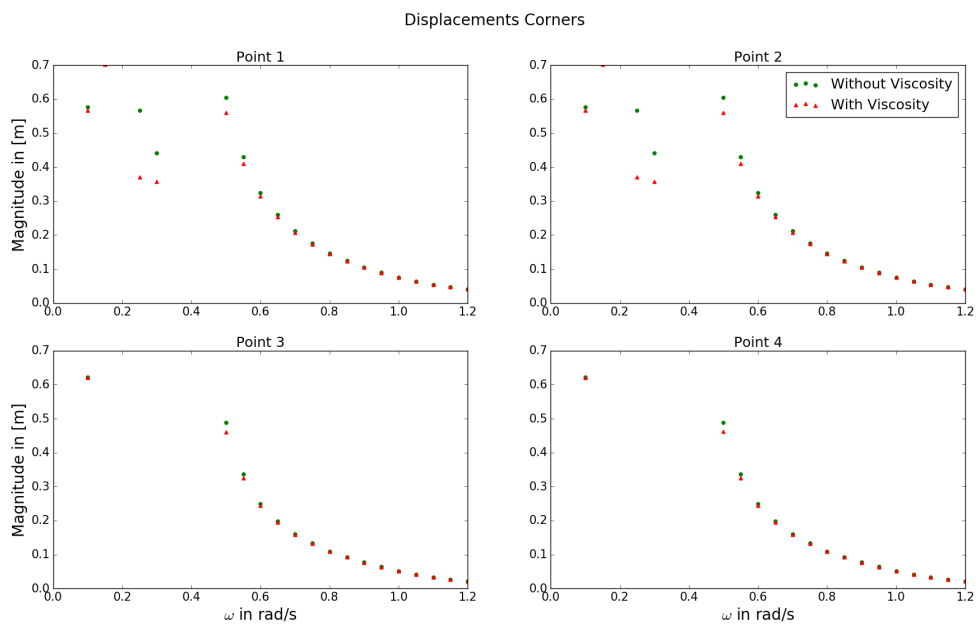


**Figure 5-20:** Vertical displacement of four corners at d = 1.09 m with and without viscosity, with $\mu = -180°$

For an Under Keel Clearance (UKC) of 0.09 cm, these results would have drastic consequences.
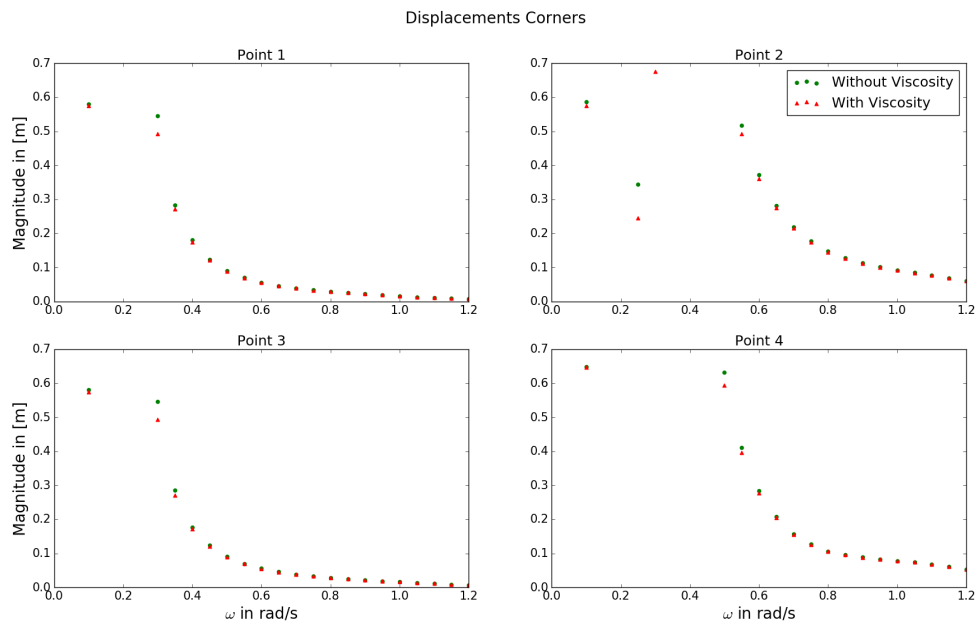
**Figure 5-21:** Vertical displacement of four corners at d = 1.09 m with and without viscosity, with $\mu = -145°$

### 5-2-3   Approaching Seabed

Because AQWA is at a certain point not capable anymore of calculating $a_{ij}$ and $b_{ij}$ when the UKC decreases, it is proposed that the additional forces which are present can be approximated by the argumentation of Brennen (1982) [31]. The results of the additional inertial force in the EOM are indeed such that heave responses decrease, and it could therefore arguably used to adjust for $a_{ij}$. Under the assumption that the focal model can be considered a flat plate as used in this paper, the results are shown here. To show what influence depth has on this, three different depths are analysed. The results show that for heave, the total force reduces, which could be used to account for an additional added mass term, i.e. the so-called 'Cushioning' effect.

In figreffig:resultFbrennen the additional force (4-20) is shown for three different water depths $d = 5, 2, 1.09$ m respectively:
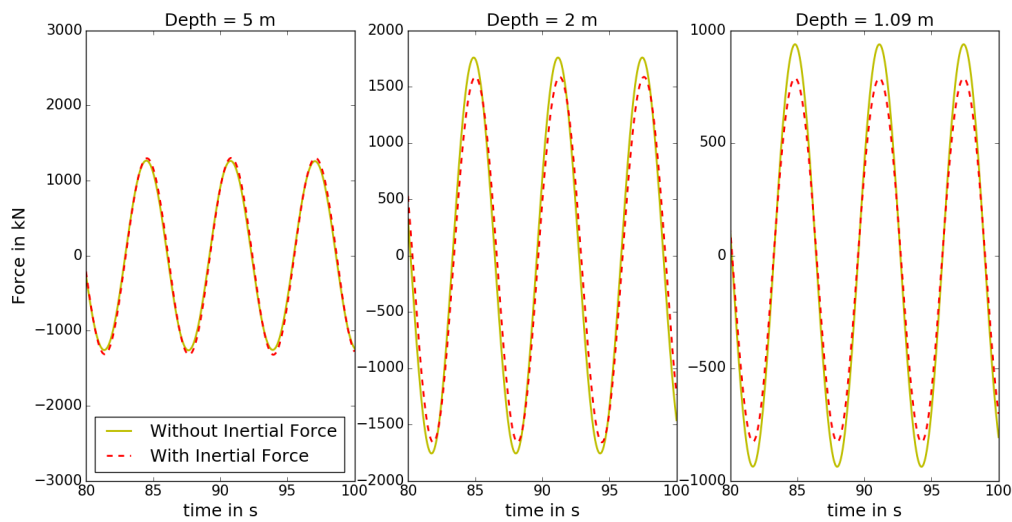


**Figure 5-22:** Additional force due to approaching seabed

It is clear that a lower UKC affects this force most. In Figure 5-23 the total forces are shown with and without the additional bottom force term taken into account. An incoming wave of $\omega = 1$ rad/s and $H = $ 1m is used.

|           | 5 m    | 2 m   | 1.09 m |
|-----------|--------|-------|--------|
| $F_{max}$ | 1.7 %  | 2 %   | 17 %   |
| $z_{max}$ | −2 %   | −1 %  | −2 %   |

**Table 5-7:** Differences with and without inertial force

|           | 5 m  | 2 m   | 1.09 m |
|-----------|------|-------|--------|
| $F_{min}$ | 3 %  | 5.5 % | 6.7 %  |
| $z_{min}$ | 1 %  | 1 %   | 23 %   |

**Table 5-8:** Differences with and without inertial force
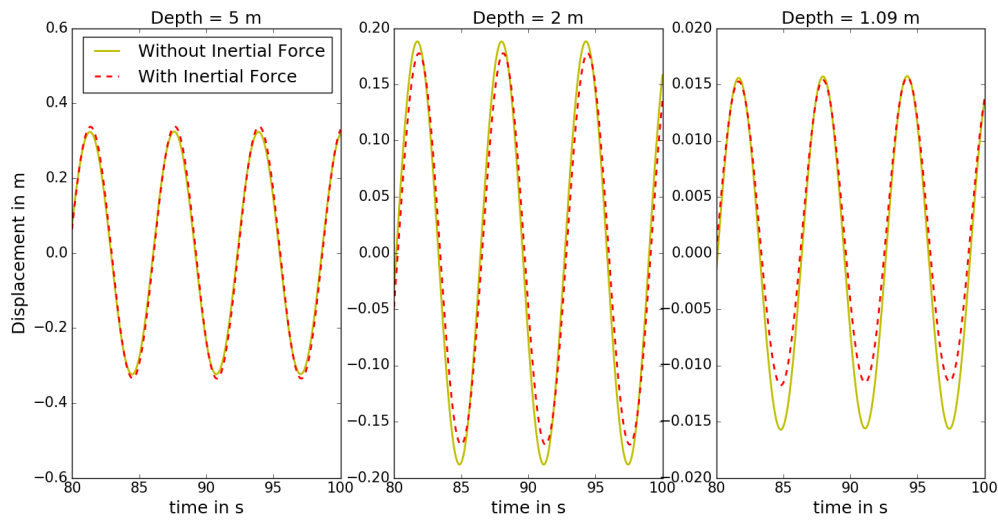
**Figure 5-23:** Displacement including the inertial force

In Table 5-7 and Table 5-8 the deviations are given. Especially for $d = 1.09$ m the difference is quite large: the displacement deviates 23% from the value as calculated without this inertial force. The deviation in motion response deviation is thus largest in the most shallow water situation. The steady state response in heave hence decreases by including this additional forces term. This would be in line with other research, which shows that heave motions decrease in shallow water. However, no verification nor validation data are available for these results, and since the focal method is based on some assumptions no general conclusions can be drawn based on these numerical results. It should be noticed though that in general the results are what can be expected, and that the model is thus capable of dealing with these external loads.

## 5-3   Second Order Wave Forces

When a bi-chromatic wave is considered, the presence of this regular wave group induces a long wave. The largest contribution in shallow water is due to the bound wave, with the frequency of the envelope, $\Delta\omega$. The forces associated with such a bi-chromatic wave group are calculated with Quadratic Transfer Function (QTF)s, which is shown in this part.

To assure the right set-down is added to the vertical motion behaviour, in this analysis two incoming regular waves are considered. This assures that no set-down is ignored, as argued by Chen [44].
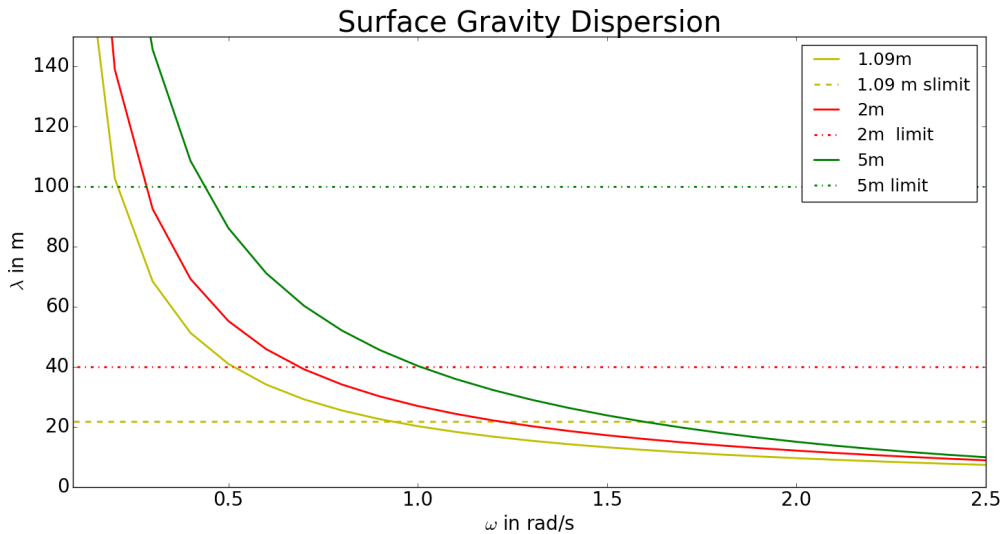


**Figure 5-24:** Dispersion Limits

The curves are in the figure the $\lambda$ as function of $\omega$ and the dashed lines are the dispersion limits, for shallow water ($d/\lambda = 1/20$). On the right of the intersection waves can be considered as deep water waves, and they propagate freely. On the left region of the intersection though, the dispersion relation does not hold, and interaction among waves becomes non-linear. Bound waves are in this region created. It is worth noting, that for the $\omega_n$ computed with the TD values for the hydrodynamic coefficients (see Table 5-5), the natural frequencies for both heave and pitch(and roll) for $d = 5$ m lie in the dispersion area. In in shallower water though, $d = 2$ m, bound waves become more important. For $d = 1.09$ m it is clear that the $\omega_n$ are one the left side of the intersection of the curve and the dashed line.

For values on the right hand side of these intersections it is reasonable to expect that there are no significant changes in the potential flow solution.

In (4-8) the equation for wave force of the bi-chromatic wave is given, which is used to calculate the second order wave forces. In Figure 5-25 these forces are shown, the mean drift part as well as the Low Frequency (LF) slowly varying part. It can be noticed from the graph that the new mean position is negative, and thus causes a negative offset of the equilibrium position of the vessel.

AQWA calculates the QTFs based on the approximation by Pinkster, as explained in Chapter 3, which is in good alignment with reality for small $\Delta\omega$. Therefore, it would not be reasonable to say something about motion behaviour $\Delta\omega = 1.0$ or even larger, so these are
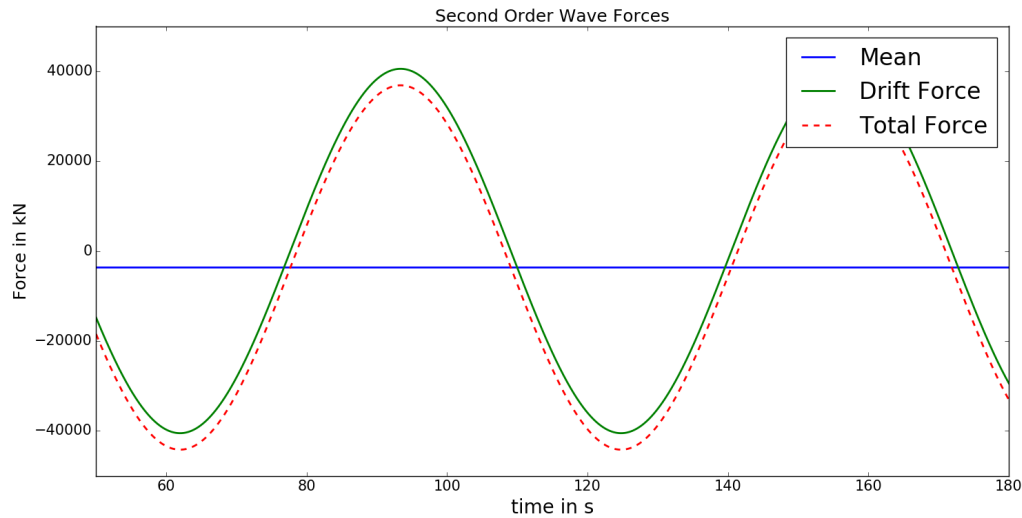
**Figure 5-25:** Second Order Forces of a bi-chromatic wave with $\Delta\omega = 0.1\text{rad/s}$

not considered here. And since the lower frequency $\omega_n$ are encountered in more shallow water conditions, this is not an issue for this thesis.

### 5-3-1   Set - Down

Set-down is as explained also referred to as 'mean drift forces', they thus cause a mean offset of the equilibrium position of the vessel in shallow water. In Figure 5-26 the first and second order wave forces of two waves in $d = 5$ m are plotted, including the set - down term as calculated by (3-24). This can also be seen in the deviation in height of the peaks of first and second order waves forces, as well as the resulting heave displacement. The fact that the set - down is lower under higher wave can be explained by means of radiation stress. The horizontal flux of momentum at given location is caused by the pressure acting on a vertical plane normal to the direction of flow, plus the transfer of momentum through that plane. This transfer of momentum is the momentum of the flow times the flow rate across the plane. The momentum flux will remain the same from one location to another, unless an external force acts upon the control volume, i.e. the fluid in the flow direction, which changes the flux of momentum. The radiation stress is given by:

$$S_{xx} = \frac{\rho g H^2}{8} \left( \frac{kd}{\sinh kd} \right) \tag{5-2}$$

Which is thus a function of $H$. The set down is caused by the increase in $S_{xx}$ in decreasing water depth. So before waves will break, i.e. their height increases, the radiation stress increases, inducing the set-down effect. This interaction is captured in the interaction kernel $K^-$ between two waves.

When the set - down term falls within the frequency range of slow drift motions of the focal vessel, which is often in the same range as the $\omega_n$ of offshore structures, it has major impact on resulting motions. As discussed, $\Phi^{(2)}$ is included in the determination of the QTFs, so the set - down term is implicitly included when these are used to determine the second order
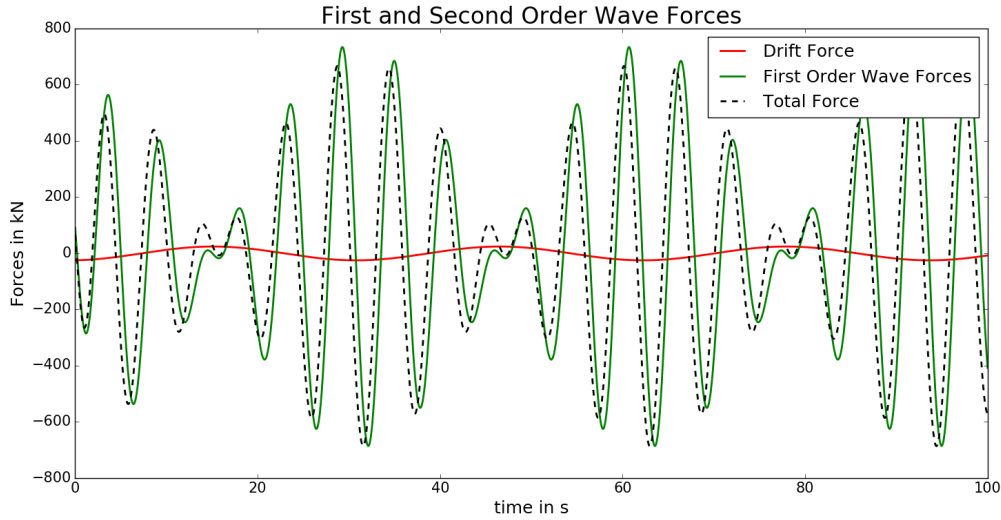
**Figure 5-26:** First and Second Order Wave Forces at $d = 5$ m.

wave forces and associated forces.

In Section 3-4-1 has been discussed how the set-down term is calculated. It is argued that $\Phi^{(2)}$ is the main contributor to this phenomenon in the LF drift forces in shallow water. The fact that the transfer function $D$ described by Voogt (2005) [43] uses the same parameters for its calculation of the term, endorses this. In the evaluations for the vertical motions of the four $z_p$ of the barge, it is shown that the model can accurately predict in both FD and TD. However, the set - down causes the mean water level to decrease, which needs to be included in the final vertical motion prediction. Because no validation data was available for this thesis, it the following some cases are defined, which calculate the set - down and show the resulting effect.

### Evaluation

Set - down is a quadratic effect, so increases drastically by changing wave heights. For the focal evaluations, $H = 0.1$ m is used, to assure the waves can still be described, or at least apporached, by the LWT.

For the $d = 2$ m case, we have seen in Figure 5-17 and Figure 5-18 that the largest vertical motions lie in the range of $[0.6 \leq \omega \leq 1.3]$, so in these situations the set - down term can cause most danger. These data are result of evaluations at $H = 1$ m, meaning that for this wave height, the $z_p$ would move the value given.

For the $d = 1.09$ m case, no really reliable data on the vertical motions are present. What can be noticed though, is that the area where most vertical motions occur, is in a much lower frequency part. Therefore, the set - down term is this situations is evaluated at these frequencies.

These values are indeed quite significant. What can be recognized, is that the set down is larger for shallow water, as well as that it magnifies for larger $\Delta\omega$, which was expected [43]. Considering the vertical displacements found in the previous, see for example Table 5-2-2, these values are in the same order of magnitude. For $d = 2$ m for instance, the set -

| | $\Delta\omega = 0.1$ | | | $\Delta\omega = 0.3$ | | | $\Delta\omega = 0.5$ | | |
|---|---|---|---|---|---|---|---|---|---|
| | $\omega_i$ | $\omega_j$ | Set - Down | $\omega_i$ | $\omega_j$ | Set - Down | $\omega_i$ | $\omega_j$ | Set - Down |
| d = 5 m | 0.1 | 0.2 | 0.01 | 0.1 | 0.4 | 0.02 | 0.1 | 0.6 | 0.12 |
| | 1 | 1.1 | 0.013 | 1 | 1.4 | 0.005 | 1 | 1.6 | 0.012 |
| d = 2 m | 0.6 | 0.7 | 0.011 | 0.6 | 0.9 | 0.033 | 0.6 | 1.3 | 0.007 |
| | 1.2 | 1.3 | 0.004 | 1 | 1.3 | 0.014 | | | |
| | $\Delta\omega = 0.1$ | | | $\Delta\omega = 0.2$ | | | $\Delta\omega = 0.4$ | | |
| | $\omega_i$ | $\omega_j$ | Set - Down | $\omega_i$ | $\omega_j$ | Set - Down | $\omega_i$ | $\omega_j$ | Set - Down |
| d = 1.09 m | 0.1 | 0.2 | 0.6 | 0.1 | 0.3 | 0.5 | 0.1 | 0.5 | 0.7 |
| | 0.2 | 0.3 | 0.64 | 0.3 | 0.5 | 0.32 | 0.3 | 0.7 | 0.18 |

**Table 5-9:** Set-Down Results

| | $\omega_i$ | $\omega_j$ | $z_{p1}$ | $z_{p12}$ | $\Delta_{p1}$ | | $z_{p3}$ | $z_{p32}$ | $\Delta_{p3}$ |
|---|---|---|---|---|---|---|---|---|---|
| $\Delta\omega 0.1$ | 0.6 | 0.7 | -0.134 | -0.156 | -0.022 | | -0.183 | -0.205 | -0.022 |
| | 1.2 | 1.3 | -0.115 | -0.124 | -0.009 | | -0.093 | -0.097 | -0.004 |
| $\Delta\omega = 0.3$ | 0.6 | 0.9 | -0.132 | -0.137 | -0.005 | | -0.156 | -0.165 | -0.009 |
| | 1 | 1.3 | -0.14 | -0.15 | -0.010 | | -0.127 | -0.134 | -0.007 |
| $\Delta\omega = 0.6$ | 0.6 | 1.2 | -0.111 | -0.124 | -0.013 | | -0.132 | -0.152 | -0.020 |

**Table 5-10:** Second Order Motions $d = 2$m

down is largest in the resonance area of the heave DOF of the *Vessel* - object, where thus motion behaviour is already largest. For $H = 0.1$ m, the maximum vertical displacement is approximately 0.09 m, so when the set - down is added of 0.033 m, the situation changes drastically. Adding these values to the vertical displacement of $z_p$, would provide an estimation of the difference in vertical motions of the vessel in shallow with reference to linear motion prediction.

### 5-3-2 Second Order Motions

The model is furthermore capable of calculating the motion behaviour of the vessel with QTFs. Firstly, it must be checked whether both waves are ones which can be described by LWT. Secondly, the $F_{ex}^{(2)}$ is calculated in accordance with (4-8), after with this force can be superimposed with $F_{ex}^{(1)}$ and the resulting motions can be computed, see (4-15). The resulting forces are subsequently used to determine the vertical motions of point 1 and point 3, as these show different motion behaviour for a monochromatic situation. Waves in the bi-chromatic case both come from direction $\mu = -180°$. Both waves have $H = 0.1$ m. In Figure 5-27 and example is given for point 1 and point 3 on the barge, and it is clear that indeed the second order effects act at the most extreme values. The numerical values for some $\Delta\omega$, for both $d$ = 2 m and $d = 1.09$ m are given in Table 5-10 and Table 5-11.

The values for $z_{p1}$ and $z_{p3}$ respectively are the vertical displacements induced by the two incoming monochromatic waves. The values for $z_{p12}$ and $z_{p32}$ represent the calculated displacement with including the second order wave forces, i.e. the quadratic interactions and the contribution due to $\Phi^{(2)}$ after calculating the forces with the QTFs. The $\Delta_{p1}$ and $\Delta_{p3}$ show the differences. From the latter values it can be concluded that these indeed increase
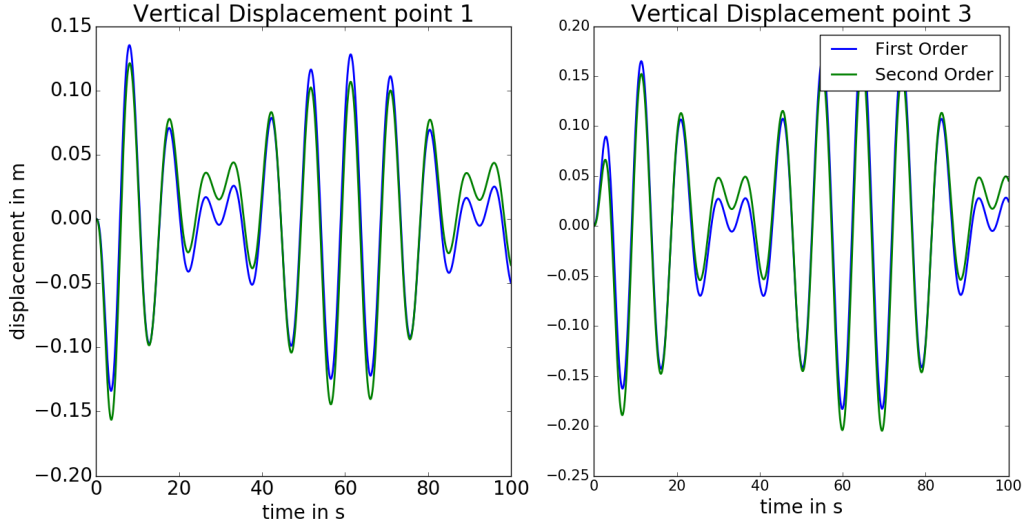
**Figure 5-27:** Vertical displacements points 1,3 at $d = 2$ m., $\omega_i = 0.6, \omega_j = 0.7$ rad/s

| | $\omega_i$ | $\omega_j$ | $z_{p1}$ | $z_{p12}$ | $\Delta_{p1}$ | $z_{p3}$ | $z_{p32}$ | $\Delta_{p3}$ |
|---|---|---|---|---|---|---|---|---|
| $\Delta\omega = 0.1$ | 0.1 | 0.2 | -0.145 | -0.163 | -0.018 | -0.178 | -0.185 | -0.007 |
| | 0.3 | 0.4 | -0.288 | -0.304 | -0.016 | -0.350 | -0.352 | -0.002 |
| $\Delta\omega = 0.2$ | 0.1 | 0.3 | -0.150 | -0.265 | -0.115 | -0.259 | -0.444 | -0.185 |
| | 0.3 | 0.5 | -0.230 | -0.226 | 0.003 | -0.281 | -0.301 | -0.021 |
| $\Delta\omega = 0.4$ | 0.1 | 0.5 | -0.144 | -0.276 | -0.133 | -0.172 | -0.297 | -0.125 |
| | 0.3 | 0.7 | -0.064 | -0.070 | -0.006 | -0.217 | -0.223 | -0.007 |

**Table 5-11:** Second Order Motions $d = 1.09$ m

when the water depth decreases. Furthermore, it can be concluded that the largest additional displacement for $d = 2$ m occurs around $\omega = 0.6 - 0.7$, where the longest $\lambda$ is considered, which thus causes the mean water level to drop. However, in the bottom row, where $\Delta\omega = 0.6$ rad/s, the additional motion is also larger, which can be attributed to the fact that this is arond the $\omega_n$ for the heave DOF. The $d = 1.09$ case shows larger $\Delta_{p1}$, especially for $\Delta\omega = 0.2$ rad/s. This can again be attributed to the $\omega_n$ of the heave DOF.

## 5-4 Resulting Vertical Motion

Consider the results of $z_p$ for the monochromatic case, where is shown that the maximum displacement occur in the range $[0.5 \leq \omega \leq 1.3]$ for a $d = 2$ m. These values are based on linearity, so when $H = 0.1$ m was used as input in the *Wave* - object, this implies that the results would have been one tenth of the values given. So when these numbers are then compared to the second order additional displacement shown in the previous section, the latter become quite appreciable. When a bi-chromatic wave group of $\omega_i = 0.6$ and $\omega_j = 0.7$ rad/s is for example considered, the set - down of this group makes the mean water level drop approximately 1.3cm, which adds substantially to the $z_p$ of approximately 7 cm. So for LF motion in shallow water, which are quite common for barge in this environment, the second

order effect should definitely be accounted for in motion prediction. The viscous damping displacement can have moderating effects on these vertical displacement, however, the second order wave forces and especially set - down are not yet concerned with a vessel within the waves and a viscous damping part does not change whether or not set - down will occur. The subsequent viscous damping could however differ from the calculated vessel, since the UKC would lower even more because of the set - down effect. This is however not considered in this thesis due to time constraints.

# Chapter 6

# Conclusions and Recommendations

## 6-1 Conclusion

For operations in shallow water, Van Oord faced issues with determination of vertical motions. The research therefore aimed to shed light on shallow water issues, in which the issue is divided in two parts; firstly the effects of shallow water on water waves and secondly the effects on hydrodynamic reactions. In this chapter a conclusion is given based on the objectives which were set in Chapter 1.

1. **Gain knowledge on wave theories and their applicability based on parameters which can describe certain sea states**
   Wave theories are divided in ranges of applicability based on three parameters:

   - Ursell Number (UR): the non-linearity parameter which indicates the degree of non-linearity with respect to the Linear Wave Theory (LWT)
   - $S$: wave steepness parameters
   - $\mu$: shallow water parameter

2. **Describe non-linearities and capture these effects to adapt linear results in such a manner that these effects are included to analyse the hydrodynamic loads on the structure in shallow water**

   - Wave exciting part: for higher $S$, the Stokes second order theory can give more reliable results for wave forces, which can be used in the Python model to determine the second order pressure and subsequent incoming wave forces based on the perturbation approach
   - Reaction part: added mass increases significantly in shallow water, and a reasonable amount of time of this project has been invested in describing this hydrodynamic coefficient based on its position, i.e. the position dependence of this coefficient instead of the usual frequency dependence. In Chapter **??** some results of these analyses are given, but unfortunately no reliable conclusions can be drawn from this phenomenon, as some very rough estimations had to be made which cannot be safely applied in accurate prediction. Another method which is used to

account for the added inertia due to increasing virtual mass is an additional external force. Based on the approaching seabed, an inertial force required to move the body away from the sea bed can be estimated in the model, to account for the so-called 'Cushioning' and 'Sticking' effect. The force is however developed based on several assumptions:

- Total fluid velocity can be obtained by linear additional of fluid velocities caused by each component of the body motion. Both equation for fluid flow and boundary conditions need therefore to be linear. This is not generally the case.

- The boundary (seabed) is rigid, which might not always be the case.

- It neglects viscous effects.

- Eddies and vortices are not taken into account (there are no frictional forces considered): the vertical upward velocity is directly related to the horizontal flow velocity.

- Free surface effects are neglected.

- The proposed formula for additional forces has not been proven by model tests.

The resulting force calculated should therefore be considered no more than a rough estimate to account for additional fluid forces in proximity of the seabed. On the damping part of the reaction, viscosity increases in importance with lower Under Keel Clearance (UKC) and therefore an additional damping factor based on $B_{crit}$ has been added to the Equation of Motion (EOM). This can account for the decrease in heave and pitch motion in shallow water, due to the damping of the water column, on top of the wave making damping as calculated by the potential damping

3. **Developed a parametric model which can predict motion behaviour and validate it with a deep water case**
A parametric model in Python is created, where objects can be user-identified: *Wave* - objects and *Vessel* - objects. With the model, firstly an analysis is done in Frequency Domain (FD), to make sure the output could be verified with the diffraction analysis from Ansys AQWA. Based on the hydrodynamic coefficients the Python model calculates the total forces. The incoming wave forces are calculated based on load Response Amplitude Operator (RAO)s, the damping forces based on potential damping and velocity of the *Vessel*, restoring forces based on stiffness and resulting motions. With these incoming forces the total force is obtained with which the acceleration, velocity and displacements can be calculated with the total mass of the focal *Vessel* - object. The resulting motions are verified with the displacement RAOs from AQWA.

Next, the incoming wave forces are calculated in the parametric model based on the fluid pressure. The *Vessel* - object is for this part subdivided in panels, on which the pressure is calculated and subsequently the incoming wave force on the *Vessel*. The resulting forces are compared to the incoming wave force based on load RAOs, and these correspond. Ultimately, the resulting motions are in agreement with the displacement RAOs. This calculation method allows for determining other wave forces than the incoming wave forces based on LWT. The second order pressure based on Stokes second order theory can be applied, which gives more flexibility than the hydrodynamic diffraction analysis of AQWA.

4. **Develop a parametric model which can calculate forces and moments and subsequent motion behaviour in Time Domain (TD) to account for non-linearities and/or other additional forces**
   Non-linearities which arise in shallow water, demand for a transformation to TD analysis. Therefore, a TD model is created, where a retardation kernel based on a inverse Fourier transformation, with $b_{ij}$ parameters is developed. The convolution with the history of velocities of the *Vessel* gives the damping in TD, and together with the re-evaluated added mass, the radiation force is transformed to TD. This model is verified by comparing motions calculated in TD versus those in FD with the same input parameters and these correspond as well. Subsequently, external forces can added on the right hand side of the EOM. Most importantly in this manner are the second order forces in shallow water situations. A full Quadratic Transfer Function (QTF) analysis has proven to be necessary and drift forces are calculated at several depths. This additional force and the accompanying excitation are verified by considering a deep water situation firstly, of which is expected that motions are dominated by first order wave forces. This is indeed the case and therefore the model can be used to calculate wave forces and resulting motions in more shallow water situations.

5. **Say something about vertical motions in shallow water, and how and if these differ from motion behaviour by linearised motion prediction**
   An analysis is executed on the vertical motions of four points on the bottom of the rectangular barge as can be expected that Ãŋf the barge hits the seabed, these will first. It is shown that the motions are indeed sensitive to water depth and that the inclusion of second order wave forces predict a much larger vertical displacement in shallow water. It is argued that this force is mainly created by the second order wave potential effect, which is calculated based on wave numbers and wave frequencies of the wave group of the bi-chromatic wave. This Low Frequency (LF) drift force causes the set-down of the mean water level, inducing larger vertical motions of the *Vessel* in negative heave direction. Both set - down as well as resulting vertical motions including second order wave forces are calculated, and both show that an additional displacement can be expected due to the LF shallow water wave drift forces. This would mean that based on first order motion prediction, the estimated vertical motion is smaller than would occur in reality. Bottom touching would therefore happen sooner than expected. It is therefore necessary to include these second order contributions in the EOM.

## 6-2   Recommendations

- In the current study, a parametric numerical model is created in Python. In addition to linear RAOs in FD, second order wave forces are evaluated after a model is created in TD with the retardation functions. It would be interesting for further research to test whether motions predicted by the model, thus when the depth decreases further than AQWA can handle, are in line with the numerical results.

- The convolution integral can become computationally very demanding, as for every time step the entire FD analysis needs to be evaluated. The convolution integral representing the memory effect is frequently found to be a problem in solving the dynamic equation. To overcome difficulties, some methods are developed, of which the Prony method and state-space realisation method [3, 52] are two most popular methods [59], which are shortly explained in Chapter A. the convolution integral representing the memory effect can become computationally very demanding and require significant amounts of computer memory. It could therefore be very interesting to model this by approximation the fluid-memory effects by a linear time invariant parametric model in state-space, see Chapter A.

- As discussed in Chapter 2, the Cnoidal Theory can be applied in shallow water, while the Stokes theory is generally more applicable in deep water. Some preliminary study in done on this Cnoidal theory, which on first sight seems hard, but actually it should be interesting the see if waves can described by means of this theory instead of regular, sinusoidal waves. Some information on it is given in, as well as on Solitary Waves Chapter D.

- Viscous damping is now estimated based on $B_{crit}$ and a factor based on literature. Model tests could more accurately find the viscous damping, by calculating the $B_{crit}$ based on $B_{ij}$ and find the resulting damping which can then be ascribed to viscosity $B_v$. These can then be added to the equation, just like in (3-23) proposed by [36].

- Include wave spreading. Second-order low frequency loads in shallow water are sensitive to wave angular spreading [40, 47]. A next step could thus be to apply it to multi-directional wave systems.

- Ansys AQWA is capable of a Time Response analysis for regular and irregular wave responses. The calculated forces with the numeric model in Python could be validated.

- Do additional research on the position dependency of the vessel and the associated hydrodynamic coefficients, and $a_{ij}$ in particular as this is highly sensitive to water depth changes. The results shown in this thesis have shown some interesting values, which demand for more in depth and thorough analyses.

# Appendix A

# Fourier Transforms

The basis of Fourier transformations is the assumption that random signals can be represented by the sum of a number of sinusoids or wavelets, each with a specific amplitude, frequency and phase angle. A spectrum can also be used to recreate a time signal. By assuming that the phase angle is distributed randomly, harmonic waves can be created based on the power spectral density at each separate frequency, combined with a randomly picked phase angle
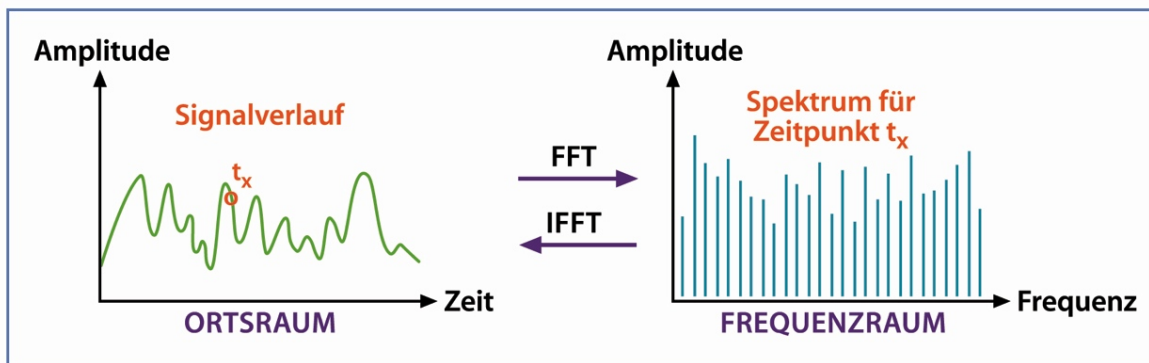


**Figure A-1:** FFT and IFFT

When the power spectral density is plotted as a function of frequency, we find a power (or energy) density spectrum, psd, auto spectrum or just spectrum.
Non-linear effects are usually analysed by time series analysis, and for more information on wave height associated with different wave periods, a time series analysis can be applied. For a sinusoidal wave, travelling in x-direction, the description in terms of wave height and period is te following:

$$\eta(x,t) = a\sin(kx - \omega t + \epsilon) \tag{A-1}$$

In which $\epsilon$ is the phase angle.
As mentioned, the random sea can be described as a summation of individual linear waves.

$$\eta(x,t) = \sum i = 1^n a_n \sin(k_n x - \omega_n t + \epsilon_n) \tag{A-2}$$
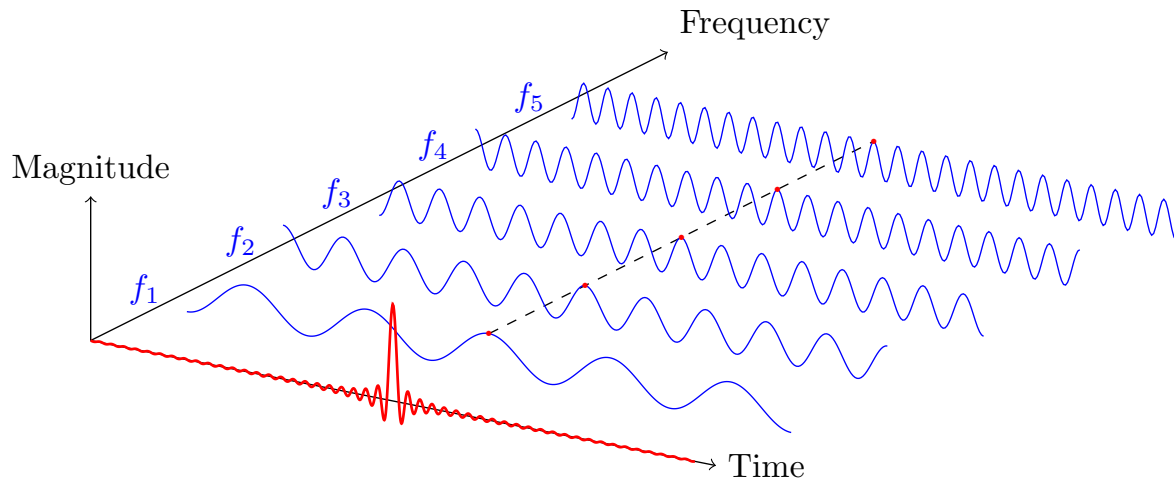
**Figure A-2:** Fourier Transform

This time series x(t) can be transformed to the frequency domain by the Fourier Transform:

$$x(\omega) = \frac{1}{2\pi} \int x(t) e^{-\omega t} dt \tag{A-3}$$

And its inverse:

$$x(t) = \int x(\omega) e^{i\omega t} dt \tag{A-4}$$

Fourier analysis of a discretely sampled signal (e.g. a wave record) can erroneously introduce a component with a higher frequency, an alias of the original wave component. To prevent this aliasing effect, a cut-off frequency must be defined, above which no frequencies should be included in the Fourier series. This is the so-called Nyquist frequency. The highest frequency component of the frequency domain representation should be limited to q = N/2.

## A-1    Convolution

Given two discrete time signals $x[n]$ and $v[n]$, the convolution of those is defined by:

$$x[n] * v[n] = \sum_{i=-\infty}^{\infty} x[i]v[n-1] \tag{A-5}$$

The sum on the right hand side is calle the convolution sum. It is important to note that the convolution operation is commutative, i.e.:

$$\sum_{i=-\infty}^{\infty} x[i]v[n-1] = \sum_{i=-\infty}^{\infty} v[i]x[n-i] \tag{A-6}$$

For a causal system, i.e. $x$ and $v$ are zero for integers $n < 0$, the $x[i] = 0$ for all integers $i < 0$ and $v[n-i] = 0$ for all integers $n - i < 0$. This means:

$$x[n] * v[n] = \begin{cases} 0 & \text{if } n = -1, -2, .. \\ \sum\limits_{0}^{\infty} x[i]v[n-1] & \text{if } n = 0, 1, 2, .. \end{cases} \tag{A-7}$$

### A-1-1    Non Causal

For noncausal lsystems, the unit pulse response $h[n]$ will not be zero for $n < 0$ and the summation for comuting $y[n]$ must run from i=0 to $i = \infty$. Furtermore, it must start at $i = \infty$. The input/output convolution expression becomes [57]

$$y[n] = h[n] * x[n] = \sum_{i=\infty}^{\infty} h[i]x[n-i] \tag{A-8}$$

## A-2    Approximations Convolution Integral

In this section approximations are given for the time consuming convolution integral. These could be interesting for future research on the topic.

**Prony's Method**

Prony's method can be used to approximate the impulse response function in every Degree of Freedom (DOF) with a sum of damped complex exponential. It extracts information from an uniformly distributed signal and constructs series of damped complex exponentials (or sinusoids). Prony's function will add equations to the dynamic system. The memory effect is:

$$\begin{aligned} F_{rad}(\dot{x}, t) &= \int_{-\infty}^{t} \mathbf{R}_{kj}(t-\tau) \cdot \dot{x}_j(\tau)d\tau \\ &= \int_{0}^{t} \sum_{k=1}^{N} \alpha_k e^{\beta_k(t-\tau)} \dot{x}_j(\tau)d\tau \end{aligned} \tag{A-9}$$

The impulse response function has large function for small values of $t$, and approaches zero for large enough time. This type of impulse response function can be approximated by exponential fitting:

$$R(t) \approx R(n) \approx \sum_{r=1}^{N} \alpha_r e^{\beta_r n} = \sum_{r=1}^{N} \alpha_r \cdot \mu_r^n \tag{A-10}$$

Where n = 0, 1, 2 .. $N-1$, the number of equally space samples of the impulse response function, $N$ is the order of the Prony function and $\alpha_r$ and $\mu_r$ are complex coefficients [?]. These are calculated in three steps, in the first the linear prediction model

$$\mathbf{d} = \mathbf{D} \ \mathbf{a} \tag{A-11}$$

is solved. Vector $\mathbf{d}$ and matrix $\mathbf{D}$ are created from the impulse response function to be approximated:

$$\mathbf{d} = \begin{bmatrix} R_{ij}(n) \\ R_{ij}(n+1) \\ \vdots \\ R_{ij}(N-1) \end{bmatrix} \tag{A-12}$$

$$\mathbf{D} = \begin{bmatrix} R_{ij}(N-1) & R_{ij}(N-2) & .. & R_{ij}(0) \\ R_{ij}(N) & R_{ij}(N-1) & .. & R_{ij}(1) \\ \vdots & \vdots & \ddots & \vdots \\ R_{ij}(n-2) & R_{ij}(n-3) & .. & R_{ij}(n-N-1) \end{bmatrix} \tag{A-13}$$

The system in (A-11) is usually overdetermined, and it can be solved by approximation for $\mathbf{a}$ by a least-squares method. The components of the vector $\mathbf{a}$ are components of the polynomial:

$$\mu^N - a_1 \mu^{N-1} - a_2 \mu^{N-2} - .. - a_{N-1}\mu - a_N = 0 \tag{A-14}$$

Find the roots $\mu_r$ is the second step in the analysis. These roots are subsequently used to build a system of linear equations:

$$\begin{bmatrix} R_{ij}(0) \\ R_{ij}(1) \\ \vdots \\ R_{ij}(n-1) \end{bmatrix} = \begin{bmatrix} \mu_1^0 & \mu_2^0 & .. & \mu_N^0 \\ \mu_1^1 & \mu_2^1 & .. & \mu_L^1 \\ \vdots & \vdots & \ddots & \vdots \\ \mu_1^{n-1} & \mu_2^{n-1} & .. & \mu_N^{n-1} \end{bmatrix} \begin{bmatrix} \alpha_1 \\ \alpha_2 \\ \vdots \\ \alpha_N \end{bmatrix} \tag{A-15}$$

Solving this for $\alpha$ is the final step. Again, the least squares methods can be applied [59]
The main disadvantage of the Prony method is that additional equations required additional calculating time for solving the dynamic equations.
Sheng et al. [59] found a new method based on the above, but calculated the memory effect through a recursive approach. Only one step previous value is of the memory integral and velocity are used.

$$R(t)(n+1) = R_k(n)e^{\beta_k \triangle t} + \dot{x} \triangle \alpha_k \triangle e^{\beta_k \triangle t/2} \tag{A-16}$$

**State Space Approximation**

Another method is to approximate the convolution integral by a state-space model. The concept of convolution in time-domain is well established in linear system for linear time-invariant systems. Convolution integrals are closely related to Laplace transforms and state-space models [56, 55]. Equation of motion for a surface vessel can be reformulated in such a state-space force, which can not only decrease calculation time but also provides additional insight into the radiation problem [3, 56]

The convolution term in (3-37) is replaced by $\tau_{rad}$, which is the output of a linear system with input $\dot{\mathbf{x}}$ and kernel $R_{kj}(t)$, which is calculated from (3-41).

$$(M_{kj} + A_{kj}) \cdot \ddot{\mathbf{x}}_{\mathbf{j}} \cdot \tau_{\mathbf{rad}}(\dot{\mathbf{x}}, t) + C_{kj} \cdot x_j\} = \mathbf{F}_{\mathbf{ext}}(t)$$
$$\dot{\mathbf{z}}(\mathbf{z}, \dot{\mathbf{x}}, t) = A'\mathbf{z}(t) + B'\dot{\mathbf{x}}(t) \qquad (A\text{-}17)$$
$$\tau_{\mathbf{rad}}(\mathbf{z}, \dot{\mathbf{x}}, t) = C'\mathbf{z}(t) + D'\dot{\mathbf{x}}(t)$$

Where $z$ and $\dot{z}$ are initial state vectors and $\mathbf{A'}, \mathbf{B'}, \mathbf{C'}, \mathbf{D'}$ constant matrices. The convolution integral in (3-36) is approximated by a state space, where the memory of the fluid is transformed using a Laplace transformation. This results in a transfer function $R(s)$ in frequency domain, which can be written as a parametric function $\hat{R}(\omega)$.

The approximation state space model can be obtained by system identification. This can be solved in either time or frequency domain, depending on the value for $R_{kj}$ as represented in (3-41).

When the retardation function is identify in frequency domain, the model obtained is the following. After the convolution term is formulated in state-space, the transfer function can be derived as:

$$H(s) = \mathbf{C}(s\mathbf{I} - \mathbf{A})^{-1} + D \qquad (A\text{-}18)$$

Where $s$ is the complex frequency $s = j\omega$. It can also be expressed in system identification. The associated approximate transfer function of the state space model is then a rational transfer function approximation:

$$R(s) \approx \hat{R}(s) = \frac{P_{kj}(s, \omega)}{Q_{kj}(s, \omega)} = \frac{p_m s^m + p_{m-1} s^{m-1} + .. + p_0}{s^n + q_{n-1} s^{n-1} + .. + q_0} \qquad (A\text{-}19)$$

An important aspect of any identification is the *a priori* knowledge available about the system, which can be used to set constraints on the model structure and parameters. For the identification of the parameters in (A-19), some properties are discussed in detail by Taghipour et al. [3] which help identify the parameters of the approximating model.

Once the parameters in (A-19) are known, a state space realisation can be obtained. The unknown matrices can be identified in several manners, as outlined by Taghipour et al. [3]. The convolution terms are replaced by alternative models based on the complex hydrodynamic coefficients $A(j\omega)$ and $B(j\omega)$ the retardation functions $R_{kj}(t)$ and $R_{kj}(\omega)$, the force to motion frequency response function $H^{FM}(j\omega)$. Depending on type of data, the identification either is done in frequency or time-domain.

**Frequency Domain Identification of Fluid Memory Model**

The constraints discussed above and in more detail by Taghipour et al. and Perez et al. [3, 52] are more easily incorporated in the frequency domain identification of the parameters,
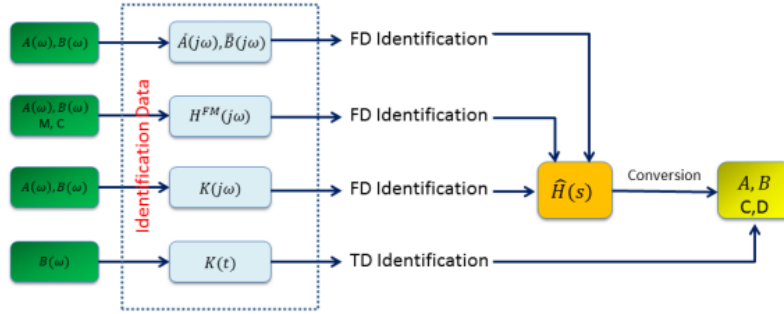
**Figure A-3:** System Identification. From Taghipour et al. [3]

while these are not easy to impose in the time domain identification methods. By curve fitting of the frequency response of fluid memory models to obtain these parameters, the frequency response function $R_{ij}$ can be computed for a finite set of frequencies. One way to obtain the parameters for the identification methods is the impulse response curve fitting. The coefficients of the state-space representation are parametrized in terms of the vector of parameters $\theta$.

$$\dot{\mathbf{z}}(t) = A'(\theta)\mathbf{z}(t) + B'(\theta)\dot{\mathbf{x}}(t)$$
$$y(t) = C'(\theta)\mathbf{z}(t)$$
(A-20)

This approximated can be characterized, in least-squares:

$$\theta* = \operatorname{argmin} \sum_l w_l \epsilon_l^* \epsilon_l$$
(A-21)

Where the notation * means the transpose complex conjugate, $w_l$ are weight coefficients and $\epsilon_l$:

$$\epsilon_l = R_{ij}(j\omega_l) - \frac{P_{ij}, \theta}{Q_{ij}, \theta}$$
(A-22)

And $\theta$ is the vector of parameters which is defined as:

$$\theta = [p_r, .., p_0, q_{n-1}, .., q_0]^T$$
(A-23)

Once the approximation for $R_{ij}$ is found, the added mass and damping terms can be found [3, 52, 59]

As it is an approximation to the convolution integral, it is important io identify errors involved and if they are small enough to be acceptable. Frequency dependent hydrodynamic coefficients are required for obtaining the state space models. The Frequency Domain (FD) identification method is carried out by establishment of the frequency response function of the convolution integrals, which are beforehand constructed from frequency dependent hydrodynamic coefficients. Rational transfer functions are then fitted to the frequency response functions by regression which are then converted into the state-space model [3].

# Appendix B

# ANSYS AQWA

## B-1 Calculation of the potential

For the incoming wave potential (3-8), as well as potentials $\phi_j$ at a point $(x, y, z)$ on the mean wetted surface $S_H$ can be represented by continuous distribution of source on this body surface. At each panel, a source strength $\sigma$ is calculated, taking influences of other panel into account with the use of the Green's function. Potential software program Ansys AQWA is used for this manner. Ultimately, all $\sigma$ are determined, and the $\Phi$, $a_{ij}$ and $b_{ij}$ and wave forces are calculated. With these values, the motions are determined.

Green functions, containing interactions between the source and field points (be it on the surface of the hull itself or on the seabed), are usually calculated on the same position. Meaning, that it should be noted that these influence functions are calculated with respect to the initial body position and distance from the seabed, while the linearised free surface conditions are used.

### B-1-1 Mass Matrix

The mass matrix defines the mass coefficients of the body in six Degree of Freedom (DOF). The masses consist of the solid mass or solid mass moments of inertia of the ship and the added mass masses or added mass moments of inertia by the disturbed water. The added mass is discussed in Section 3-3-1.

### B-1-2 Stiffness Matrix

The stiffness matrix represents the restoring terms which affect motions in the vertical plane (i.e. heave, roll and pitch motions). The spring terms for these 3 DOF are:

$$
\begin{aligned}
c_{zz} &= \rho g A_{WL} \\
c_{\phi\phi} &= \rho g \bigtriangledown \cdot G\bar{M} \\
c_{\theta\theta} &= \rho g \bigtriangledown \cdot G\bar{M}_L
\end{aligned}
\tag{B-1}
$$

Hydrostatic stability due to the righting moments, see Journee [2] .

Three dimensional panel methods are commonly used numerical tools to find the hydrodynamic behaviour of structure with large volume in waves. It is based on the potential theory, and the surface of the strucutre is represented by series of diffraction panels. AQWA employs a method where it combines modelling large-volume components by diffraction panels and small cross sectional components by Morison elements.

**Mesh**  This mesh discretizes the geometry using diffracting panels. The user can manually control the size of these panels. Too many panels will increase calculation time and will only give unnecessary details and too little panels will not give a good representation of the geometry. This inaccuracy is caused by the fact that Aqwa averages the source and potential strengths over the area of the panel.

The next step is to choose wave directions and frequencies to evaluate and options regarding QTF and drift forces can be included.

## B-2  Limits

Non-linear forces have an inertia and a lift part. As the body oscillates close to the seabed, the non-linear force is due to high accelerations of flow in the gap, which induces the inertia part. Furthermore, the movement with reference to the actual under keel clearance is relatively high, while AQWA assumes these movements to be small. Source panels are in this assumed to be move only slightly, and the seabed is assumed to be distant. For computations, the equations in the software are linearised and the time variation of source strength is neglected, which makes the software unable to calculate non linear parts of the inertia force near the seabed.

### Theoretical Limitations

- Fluid assumed irrotational

- Fluid is assumed incompressible

- Fluid is assumed inviscid.

### B-2-1  Green's Theorem

The panel method, also known as the boundary integral equation method, has been widely used for the purpose of finding the radiation and diffraction potentials. Fundamentally, it is a form of Green's theorem, in which the velocity at any point in the fluid is represented by surface distributions of singularities over the hull surfaces. The essential steps are:

1. The potential is represented by a source distribution of unknown strength.

2. The body surface is subdivided in a large number N panels, which approaches its shape.

3. the source strength and dipole strength are assumed constant on each panel individually. This gives a total of N unknowns.

4. when formulated in source terms, the normal derivative of the potential is evaluated at the center of the panels, each one individually, and set equal to the normal velocity at

that point. The potential is formulated at the same point directly, which gives a total number of N linear equations for the unknown source strengths (/potentials).

5. After the potential is found through these evaluations, the pressure is evaluated and integrated over the wetted surface to find the required forces and moments.

The function by Green which calculates these source strengths:

$$G(\vec{x}, \vec{\xi}) = \frac{1}{\sqrt{(x - \xi)^2 + (y - \eta)^2 + (z - \varsigma)^2}} + \frac{1}{\sqrt{(x - \xi)^2 + (y - \eta)^2 + (z + 2d + \varsigma)^2}} \quad \text{(B-2)}$$

## B-2-2 Mesh

To use the panel method a right mesh is needed. The diffraction software AQWA uses the following 'rules' to generate a mesh.

- The aspect ratio

- The size difference between the panels is as low as possible

- The centroid of one panel should not be close to those of other panels: $d_{min} = \sqrt{\frac{area}{\pi}}$

- Panels must be regular

- Panel size must be small compared to the wave lengths: $d_{min} \leq \frac{1}{7}\lambda$

- Center must be above the seabed at a minimal distance

# Appendix C

# Coefficients as Function of Depth

In this chapter some values and graphs are given for the preliminary study of the effect of position / wave height on the hydrodynamic coefficients added mass and potential damping. As discussed in the main file, more research is necessary to draw general conclusions on these results.

| M | 410000 [kg] |     | $F_a$ | 3090000 [N/m] |
|---|---|---|---|---|
| A | 3211100 [kg] |   | $\epsilon_{F,\zeta}$ | -0.11 [rad] |
| B | 679930 [kg $\cdot$ s] | | RAO | 0.99 [m/m] |
| C | 4020700 [N/m] | | $\epsilon_{z,\zeta}$ | 0 [rad] |

**Table C-1:** Hydrodynamic coefficients and RAOs

| $A_{max}$ | 3218000 [kg] |
|---|---|
| $A_{min}$ | 3208800 [kg] |
| $B_{max}$ | 687670 [kg $\cdot$ s] |
| $B_{min}$ | 669870 [kg $\cdot$ s] |

**Table C-2:** Max/min values for added mass and damping at depth = 30 m and $\omega = 0.5$ rad/s

| A max | 3094000 [kg] @ 4.3 m |
|---|---|
| A min | 2591200 [kg] @ 5.7 m |
| B max | 2812700 [kg $\cdot$ s] |
| B min | 2364600 [kg $\cdot$ s] |

**Table C-3:** Max/min values for added mass and damping at depth = 5 m and $\omega = 1$ rad/s

Heave motion of the vessel with different added mass values, which starts at a water depth of 5 meter is shown in Figure C-1. The maximum displacement as a result of the changing added mass values, and the difference with respect to the original added mass value in percentage is given in Table C-4.
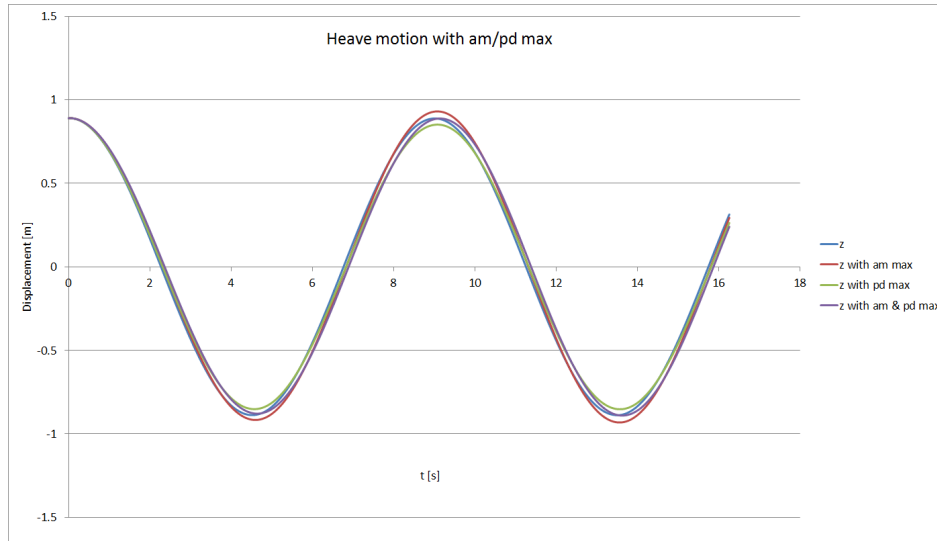
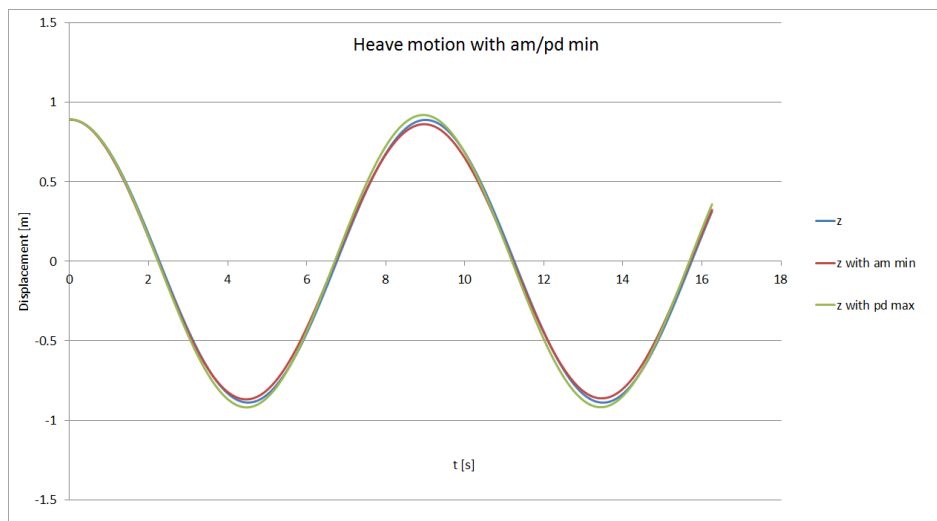**Figure C-1:** Heave motion of the barge with am and pd values as function of position at $\omega = 0.7$ rad/s



**Figure C-2:** Heave motion of the barge with am and pd values as function of position at $\omega = 0.7$ rad/s

| Added mass [kg] | z(max) [m] | difference [%] |
|---|---|---|
| A | 0.69888 | 0 |
| A max | 0.718266 | 2.77 |
| A (z) | 0.708351 | 1.36 |

**Table C-4:** Relative effect of changing the added mass values of those at the extreme positions in heave motion



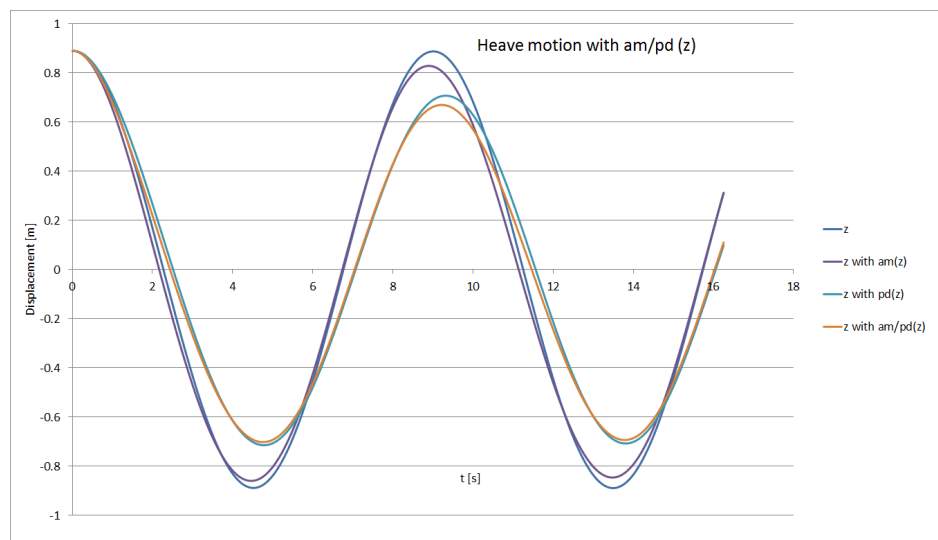**Figure C-3:** Heave motion of the barge with am and pd values as function of position at $\omega = 0.7$ rad/s

# Appendix D

# Additional Information

## D-1 Wave Theory

In the results section it is described that the Linear Wave Theory (LWT) limits the wave height $H$ based on Ursell Number (UR) and $S$. The maximum values for specific cases are shown in Figure D-1. Based on these values it can be established where the LWT can safely be applied. The limiting values are shown in color scale, where red means that the waves cannot be described by the linear wave theory, where the values in the green cells fall within the limits of UR and $S$. The limiting steepness for the linear wave theory to be applicable is set at $S_{max} = 0.01$

| Limited by S | | Limited by URSELL | | | | | | | | |
| | | depth [m] | | | | | | | | |
| max H [m] | Lambda [m] | 1 | 2 | 3 | 4 | 5 | 10 | 15 | 20 | 30 |
|---|---|---|---|---|---|---|---|---|---|---|
| 0.1 | 10 | 0.10 | 0.10 | 0.10 | 0.10 | 0.10 | 0.10 | 0.10 | 0.10 | 0.10 |
| 0.2 | 20 | 0.07 | 0.20 | 0.20 | 0.20 | 0.20 | 0.20 | 0.20 | 0.20 | 0.20 |
| 0.3 | 30 | 0.03 | 0.23 | 0.30 | 0.30 | 0.30 | 0.30 | 0.30 | 0.30 | 0.30 |
| 0.4 | 40 | 0.02 | 0.13 | 0.40 | 0.40 | 0.40 | 0.40 | 0.40 | 0.40 | 0.40 |
| 0.5 | 50 | 0.01 | 0.08 | 0.28 | 0.50 | 0.50 | 0.50 | 0.50 | 0.50 | 0.50 |
| 0.6 | 60 | 0.01 | 0.06 | 0.20 | 0.46 | 0.60 | 0.60 | 0.60 | 0.60 | 0.60 |
| 0.7 | 70 | 0.01 | 0.04 | 0.14 | 0.34 | 0.66 | 0.70 | 0.70 | 0.70 | 0.70 |
| 0.8 | 80 | 0.00 | 0.03 | 0.11 | 0.26 | 0.51 | 0.80 | 0.80 | 0.80 | 0.80 |
| 0.9 | 90 | 0.00 | 0.03 | 0.09 | 0.21 | 0.40 | 0.90 | 0.90 | 0.90 | 0.90 |
| 1 | 100 | 0.00 | 0.02 | 0.07 | 0.17 | 0.33 | 1.00 | 1.00 | 1.00 | 1.00 |
| 1.1 | 110 | 0.00 | 0.02 | 0.06 | 0.14 | 0.27 | 1.10 | 1.10 | 1.10 | 1.10 |
| 1.2 | 120 | 0.00 | 0.01 | 0.05 | 0.12 | 0.23 | 1.20 | 1.20 | 1.20 | 1.20 |
| 1.3 | 130 | 0.00 | 0.01 | 0.04 | 0.10 | 0.19 | 1.30 | 1.30 | 1.30 | 1.30 |

**Figure D-1:** Maximum Wave Height, limited by $U_R$ and $S$

## D-1-1 Orbital Motion

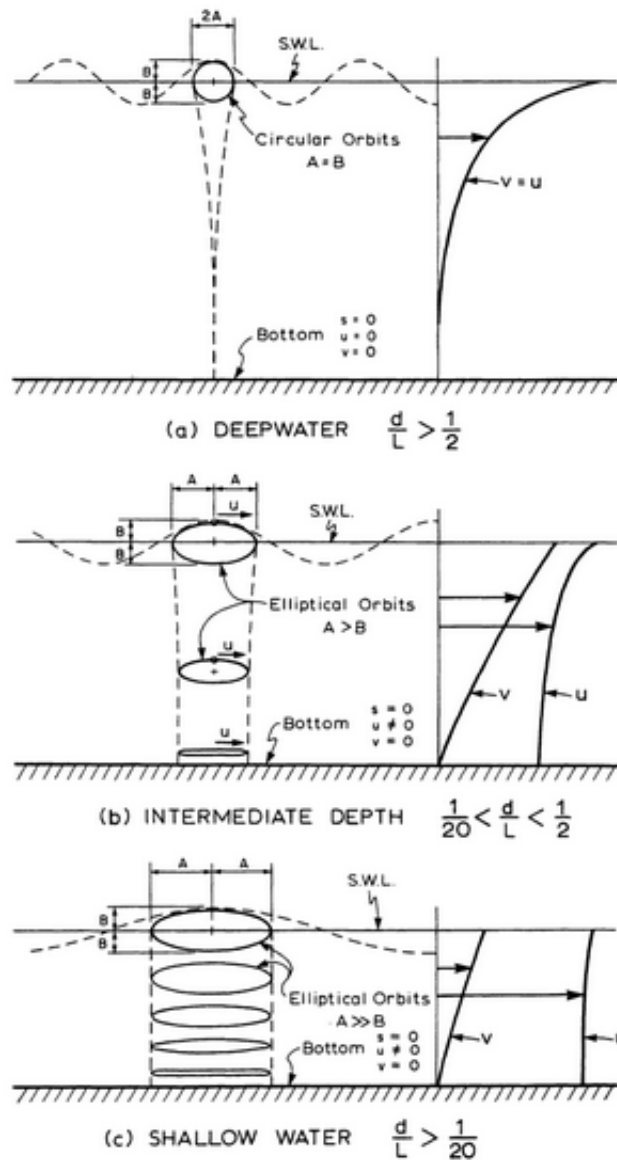Orbital motions of water particles under the assumption of LWT.

**Figure D-2:** Orbital motion of wave particles. Obtained from Chakrabarti (1987)

## D-1-2   Trochoidal or Gerstner Waves

The trochoidal waves or Gerstner wave is a non-linear wave, which is not irrotational. It was the first exact non-linear solution for waves of finite amplitude on deep water. The trochoidal wave satisfies continuity and surface conditions. It is used to describe the surface profile and particle orbits of finite amplitude, non-sinusoidal waves. The profile is a trochoid and the fluid particle motion is rotational versus the usual irrotational motion for waves. A trochoid is the curve traced out by a point inside a circle when the circle is rolled along a straight line, and if the circle is below the line it will be found that the resulting curve is sharper at the crest than at the trough.

$$\zeta = \zeta_a \cos kx + \frac{1}{2}k\zeta_2^2 \cos 2kx - \frac{1}{2}k\zeta_a^2 \tag{D-1}$$

$$P(x, z, t) = x + \Sigma(Q_i A_i \cdot D_i x \cdot \cos(\omega_i D_i \cdot (x, y) + \phi_i t)) \tag{D-2}$$

In which $Q_i$ is a parameter for the steepness of the wave. For $Q_i = 0$ it gives an usual sine wave, while $Q_i = 1/(\omega_i A_i)$ gives a sharp crest. In figreffig:Trochoid and example of the shape of a trochoidal wave is given.

The fact that the flow field is rotational, makes finding a solution for waves difficult because vorticity has to be taken into account. Furthermore, the phase speed is independent of the amplitude of the wave. From hydordynamic point of view the trochoid is not convenient as there is a mass transport in fintie amplitudes. Furthermore, the flow field is rotational, which makes the Stokes wave more applicable [4].

### D-1-3   Cnoidal Wave Theory

For very shallow water, the LWT is not applicable and one could possible resort to the Cnoidal theory to describe waves. Short procedure is given in Figure D-4

An extreme Cnoidal wave, where the elliptic equals zero, the wave becomes translatory and can be described by the Solitary Wave theory. The $m$ in the figure is the elliptic parameter, which determines the shape of the Cnoidal wave.

### D-1-4   Solitary Wave

At the limit case of the Cnoidal wave where crest amplitude equals wave height, the surface profile given in (2-39) defines the profile of the solitary wave [18]:

$$\eta = H\text{sech}^2[\sqrt{\frac{3H}{4d^3}}(x - ct)] \tag{D-3}$$

Where celerity $c$ is given as:

$$c = \sqrt{gd\left(1 + \frac{H}{2d}\right)} \tag{D-4}$$

### D-1-5   Stream Theory

**Regular Stream Function**

The boundary value problem solution is sought in the same way as with the LWT, as a function of the Laplace equation:

$$\frac{\partial^2 \Psi}{\partial x^2} + \frac{\partial^2 \Psi}{\partial z^2} = 0 \tag{D-5}$$

The boundary conditions in terms of this stream function are:

$$\frac{\partial \Psi}{\partial x} = 0 \quad \text{at} \quad z = -d \tag{D-6}$$

$$\frac{\partial \Psi}{\partial x} = \left( \frac{\partial \Psi}{\partial z} - c \right) \cdot \frac{\partial \eta}{\partial x} \quad \text{at} \quad z = \eta \tag{D-7}$$

$$\frac{1}{2} \left[ \left( \frac{\partial \Psi}{\partial x} \right)^2 + \left( \frac{\partial \phi}{\partial z} - c \right)^2 \right] + g \cdot \eta = Q \quad \text{at} \quad z = \eta \tag{D-8}$$

Where $Q$ is the total energy with respect to still water elevation. The stream function for small-amplitude waves becomes:

$$\Psi(x, z) = c \cdot z + \sum_{n=1}^{N} X_n \sinh nk(z + d) \cos(nkx) \tag{D-9}$$

In which $c$ = celerity, $N$ the order aimed of the theory, determined by the wave steepness $S$ and $\mu$. $X(n)$ is the coefficient for each specific order required to require the dynamics free surface condition (D-8). The closer to the breaking limit, the more terms needed to find accurate results. In Figure D-6 it is graphically shown which order $N$ is needed.

The free surface form is found by substituting $z = \eta$ in (D-9) which becomes:

$$\eta = \frac{\Psi(x, \eta)}{c} - \frac{1}{c} \sum_{n=1}^{N} X_n \sinh nk(z + d) \cos nkx \tag{D-10}$$

The problem is to evaluate $X(n)$ to the desired order, find $k$ and a value for $\Psi$ to satisfy the boundary condition in (D-8). This is done by finding the right value for $Q$ along the certain points on the wave through trial and error [18]. The theory is consistent over most of the wave parameter domain except at the very low region where values of $H/T^2$ and $d/T^2$ are small. In Figure D-6 one can see that the stream theory has a wider range of applicability than Stokes waves, up to nearly breaking. However, the stream function applicability is not ideal for design purposes [4, 19, 18].

### D-1-6   Shoaling

In Chapter 2 it was argued that a preliminary modification could be the change in $H$ due to shoaling [14]. The effect of shoaling is checked by calculating the shoaling coefficient $K_s$ from (2-22) for two different frequencies, $\omega = 1\text{rad/s}$ and $\omega = 0.5\text{rad/s}$ in $d = 5\text{m}$. These values are chosen within the limits of LWT shown in Table 2-1. The pressure and forces are given as percentages of those calculated without the shoaling coefficient. As one can see in Table D-1, is deviates less than 0.1% and is not considered further.

| $\omega in[\text{rad/s}]$ | $\mu$ | $K_s$ | $p_s/p$ | $F_{p,s}/F_p$ |
|---|---|---|---|---|
| 1 | 0.12 | 0.95 | 100.02 % | 100.04 % |
| 0.4 | 0.058 | 1.22 | 0.999 % | 0.98 % |

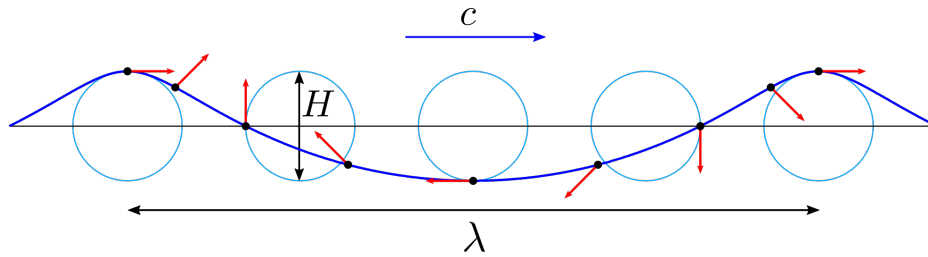**Table D-1:** Pressures and Forces including Shoaling Coefficient $K_s$

**Figure D-3:** Shape of a Trochoid

**Elliptic integrals**

Complete elliptic integral of the first kind $K(m)$

$$K(m) \approx \frac{2}{\left(1+m^{1/4}\right)^2} \log \frac{2\left(1+m^{1/4}\right)}{1-m^{1/4}}$$

Complementary elliptic integral of the first kind $K'(m)$

$$K'(m) \approx \frac{2\pi}{\left(1+m^{1/4}\right)^2}$$

Complete elliptic integral of the second kind $E(m)$

$$E(m) = K(m)\, e(m), \text{ where}$$

$$e(m) \approx \frac{2-m}{3} + \frac{\pi}{2KK'} + 2\left(\frac{\pi}{K'}\right)^2 \left(-\frac{1}{24} + \frac{q_1^2}{\left(1-q_1^2\right)^2}\right),$$

where $q_1(m)$ is the complementary nome $q_1 = e^{-\pi K/K'}$.

**Jacobian elliptic functions**

$$\text{sn}(z|m) \approx m^{-1/4} \frac{\sinh w - q_1^2 \sinh 3w}{\cosh w + q_1^2 \cosh 3w},$$

$$\text{cn}(z|m) \approx \frac{1}{2} \left(\frac{m_1}{m\, q_1}\right)^{1/4} \frac{1 - 2q_1 \cosh 2w}{\cosh w + q_1^2 \cosh 3w},$$

$$\text{dn}(z|m) \approx \frac{1}{2} \left(\frac{m_1}{q_1}\right)^{1/4} \frac{1 + 2q_1 \cosh 2w}{\cosh w + q_1^2 \cosh 3w},$$

in which $w = \pi z / 2K'$.

**Figure D-4:** Approximation for elliptic integrals for m > 1/2. Obtained from Fenton [4]
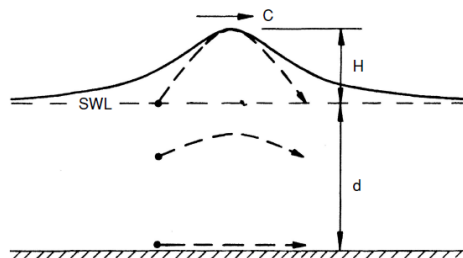


**Figure D-5:** Surface profile for a Solitary Wave. From: Sorenson (2006) [?]
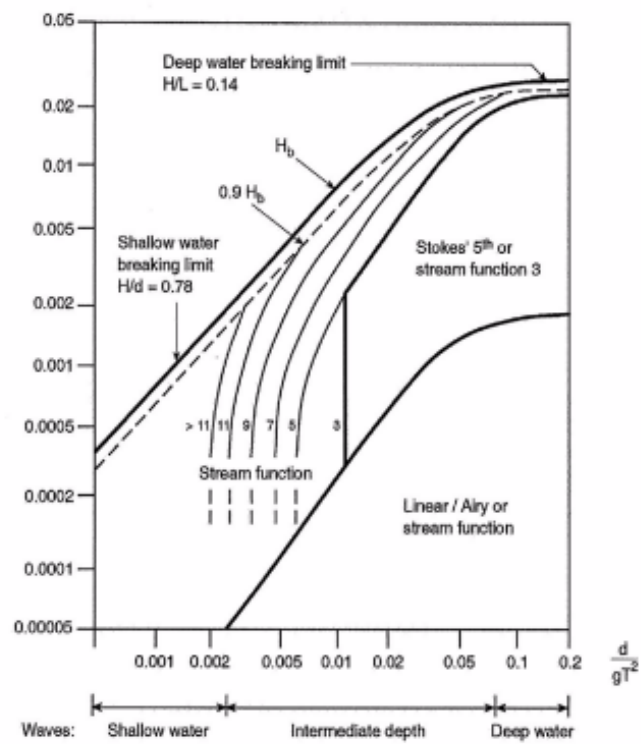
**Figure D-6:** The required order of N, such that the stream function wave theory is best applicable. Obtained from DNV [5]

## D-2    Damping

### D-2-1    Ikeda's Method

Unlike other Degree of Freedom (DOF), roll damping is known to be highly non-linear. The viscous roll damping is particularly significant at a frequency near the roll natural frequency. An often used method for these non-potential parts of the roll damping, is the so-called 'Ikeda-method'. All contributions to this damping are shown in Figure D-7.
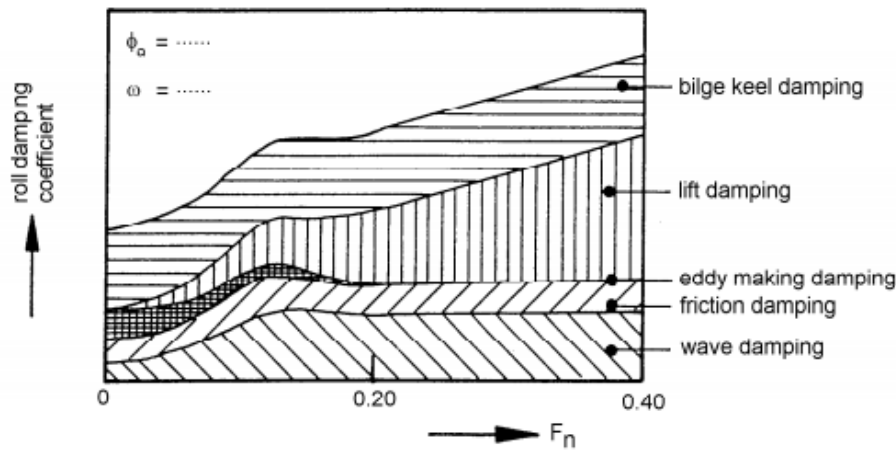


**Figure D-7:** Roll damping contributions as a function of forward speed. Obtained from Journee (2001)

Ikeda's method is a widely used method to predict the roll damping in the design state. The method divides roll damping into several components shown in Table D-2.

| Abbreviation | Component | Linearity |
|---|---|---|
| $B_F$ | Friction damping | Non-linear |
| $B_W$ | Wave making damping | Linear |
| $B_E$ | Eddy damping | Non-linear |
| $B_{BK}$ | Bilge Keel damping | Non-linear |
| $B_L$ | Lift damping | Linear |

**Table D-2:** Components of damping according to the Ikeda Method

$B_F$, $B_E$ and $B_{BK}$ are non-linear terms can't be used in the frequency domain equations, so an equivalent is found;

$$b_{eq} = b_{44}^{(1)} + \frac{8}{3\pi} \cdot x_4 \cdot \omega \cdot b_{44}^{(2)} \tag{D-11}$$

In which $b_{44}^{(1)}$ is the linear lift damping + linear forward speed correction and $b_{44}^{(2)}$ the summation of non-linear friction damping, the non-linear eddy damping and the non-linear bilge keel damping.

The lift damping $B_L$ is only applied in the case of forward speed, and thus not considered here. Furthermore, no bilge keel is used in this model, so this term is also not taken into consideration.

**Skin Friction**    Skin friction accounts for for both laminar and turbulent flow and can become appreciable in non-circular bodies in motion [32]. Kato's formulation is used by Himeno and Ikeda to find a damping term expressed in terms of an equivalent linear damping coefficient $B_F$ [60, 2]:

$$B_{friction} = 0.787 \cdot \rho \cdot S \cdot r_e^2 \cdot \sqrt{\omega \nu} \cdot \left(1 + 0.00814 \left(\frac{r_f^2 \cdot R_0^2 \cdot \omega}{\nu}\right)^{0.386}\right) \tag{D-12}$$

In which $\nu$ is the kinematic viscosity, $R_0$ the roll radius of rotation, $c_f$ is a frictional coefficient, $r_f$ the average radius from the axis of rolling, $S_f$ the wetted surface area. The kinematic viscosity is chosen based on $\rho = 1025 \ kg/m^3$ based on the following figure:
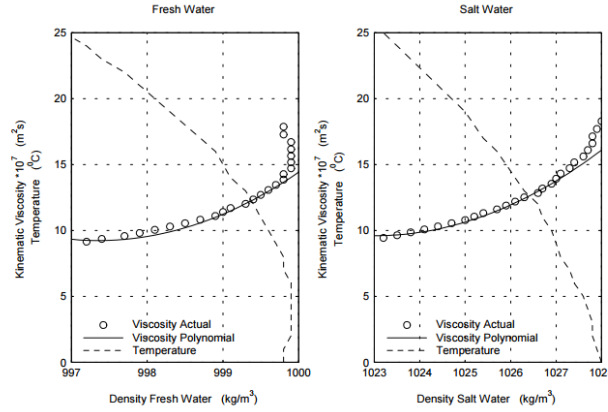


**Figure D-8:** Eddy damping value

These parameters can be calculated by the following equations [**?**]:

$$c_f = 1.328 \left(\frac{3.22 \cdot r_f^2 \cdot \phi_a^2}{T_\phi \cdot \nu}\right)^{\frac{1}{2}}$$
$$r_f = \frac{(0.887 + 0.145 \cdot C_b)(1.7 \cdot W + C_b \cdot B) - 2 \cdot OG}{\pi} \tag{D-13}$$
$$S_f = L_p p \cdot (1.75 \cdot d + C_b \cdot B)$$

Where $\phi_a$ is the roll amplitude, $C_b$ the block coefficient ($=1$) $T_\phi$ the roll period, $\nu$ the dynamic coefficient of viscosity, $OG$ the vertical distance from water surface Centre of Gravity (COG) (downward is positive) and $W$ the draft.

**Eddy Damping**    Eddies can have substantial circulation around them which makes them a concern for operations at sea. It rises from pressure variation due to separation at sharp corners of a body in water. Damping for the barge geometry due to eddy making at zero forward speeds can become very large. The area coefficient affects this eddy making, meaning

that the sharper the corner, the more fluid seperation and eddy making. Taking a closer look at Figure D-7, it is clear that eddy damping can become a large contributor to the total damping [60, 2].

A formula which is suitable for rectangular shaped barges:

$$B_{eddy} = \frac{2}{\pi} \cdot \rho \cdot L \cdot D^4 \cdot \left( H_0^2 + 1 - \frac{OG}{D} \right) \cdot \left( H_0^2 + \left( 1 - \frac{OG}{D} \right)^2 \right) \cdot R_0 \cdot \omega \qquad \text{(D-14)}$$

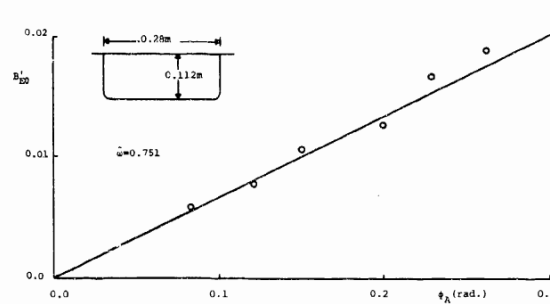$H_0$ is 1/2 Beam-to-draft ratio, $R_0$ amplitude of roll [61]



Figure 4.3. Eddy component of roll damping force for midship section, with area coefficient of 0.997.

**Figure D-9:** Eddy damping value

**Lift Damping**   The lift damping is another factor, which will increase when the roll centre is above the mean water level. It occurs in the form of a lift moment when the ship moves with a forward speed [15, 60].

### D-2-2   Morison's Equation

The Morison equation is usually applied for long, slender structures, like vertical piles, in oscillatory flow [2]. The structure is small compared to the wave particle orbit dimension, so that the assumed flow past the structure is reasonably valid. Otherwise, force are for the largest part best described by diffraction [62]. The drag force $F_{DRAG}$ can be described by:

$$F_{DRAG} = \frac{1}{2}\rho C_d \cdot A \cdot u \cdot |u| \qquad \text{(D-15)}$$

**Drag Coefficient**

In Chapter 3 it is discussed that an additional force can be added to the Equation of Motion (EOM) based on a drag coefficient. The velocity in vertical direction for a point on the barge, when viscous forces are included is:

$$v_{visc}(t) = \dot{z} - x_b \cdot \dot{\theta} + y_b \cdot \dot{\phi} \qquad \text{(D-16)}$$

Viscous drag acts both in horizontal and vertical direction as a function of the fluid velocity along the vessel's hull. The drag load $\mathrm{d}F_{drag}$ on area $\mathrm{d}A$ can then be calculated with (**??**)

$$F_{drag}(t) = -\frac{1}{2} \cdot \rho \cdot C_d \cdot \int_A v_{visc}(t) \cdot | v_{visc}(t) | \cdot \mathrm{d}A$$

$$M_{drag}(t) = \frac{1}{2} \cdot \rho \cdot C_d \cdot R \cdot \int_A v_{visc}(t) \cdot | v_{visc}(t) | \cdot \mathrm{d}A$$

(D-17)

$C_D$ typically depends on motion amplitude of structure under consideration [13]. For shallow water, the equation from Seelig et al. (1992) [63] is can be used [64, 63]:

$$C_{D_t} = C_D + (C_{D1} - C_D) \cdot \left(\frac{T}{d}\right)^K$$

$$C_{D0} = 0.22 \cdot L \cdot \sqrt{\frac{A}{B \cdot \nabla}}$$

(D-18)

In which $K$ is a dimensionless coefficient and from labatory tests it is shown that a value of 2 is applicable for most barges. $C_{Dl}$ is suggested to be 3.2 for most cases [63]. In Figure D-11 in Chapter **??** the values for $C_{D_t}$ for various values of $C_{D0}$ are shown [63]. Using this figure, it can be concluded that $C_{D_t} \geq 1$, From this figure: $C_{D_t} \geq 1$. Experiments have shown the sensitivity of $C_D$ to depth in current, as shown in Figure D-10. It can be concluded from the figure, even though in this study no current is considered, the $C_D$ could be estimated in the range of $1.5 - 2$. Other literature has shown values for $C_D$ which are of same order of magnitude [65, **?**, 66]
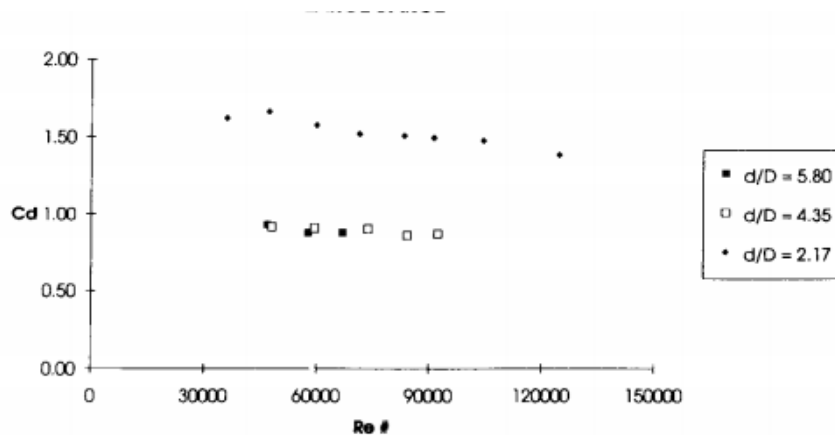


**Figure D-10:** $C_D$ Values for Various Depths

In Chapter **??** some other estimation methods are shown, which would give very rough guesses as the shapes used are not submitted to the same boundary conditions as the barge in water (it for example shows long slender structures, or flat plates).

Even though no current is accounted for in this study, it could be argued that a current drag is present based on increased flow velocities due to lower Under Keel Clearance (UKC). In Figure D-11 drag coefficient are given for given ship dimensions ($\xi$) and shallow water parameter. $\xi = \sqrt{\frac{A}{B \cdot \nabla}}$ and is 20 for the model in this study. It can be seen that $C_{D_t} \geq 1$ approximately [63].
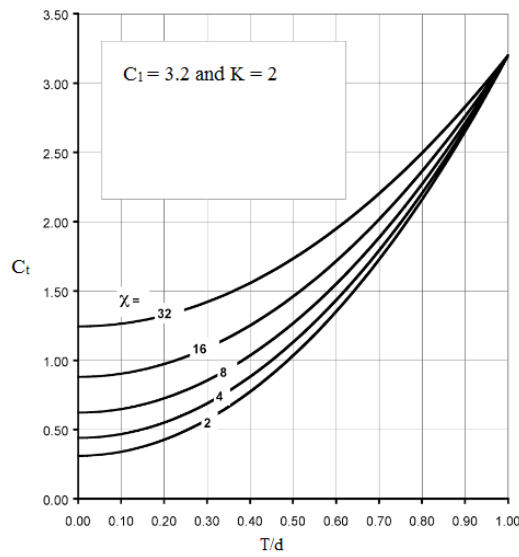
**Figure D-11:** Drag Coefficient Estimation



**Figure D-12:** CD by DNV

**Estimation of $C_D$ based on standards**

Shapes for estimation of $C_D$ values as proposed by DNV [65]

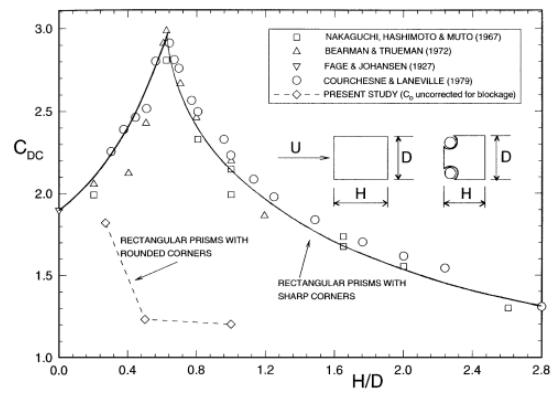| Geometry | Dimensions | $C_{DS}$ |
|----------|------------|----------|
| Rectangular plate normal to flow direction | B/H | |
| | 1 | 1.16 |
| | 5 | 1.20 |
| | 10 | 1.50 |
| | ∞ | 1.90 |
| | | $R_e > 10^3$ |
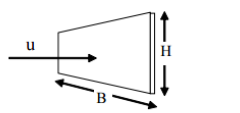
**Figure D-13:** CD by DNV



**Figure D-14:** CD by DNV

## D-3   Second Order

### D-3-1   Approximation Second Order Potential

In shallow water difference frequency drift force can increase significantly due to this second order potential and cannot be ignored [39, 38]. The non-linear nature of free surface condition and complexity of body boundary conditions makes calculation of the contribution due to the second order potential difficult. There have been succesful effort though which can estimate the velocity potential of incoming second order Low Frequency (LF) bound wave that belongs to the bi-chromatic wave group as a function of first order wave numbers, frequencies and water depth [37, 47].

The second order potential force contribution (part 5) can be approximated based on the assumption that it is dominated by the undisturbed incoming waves. The method is based on the transformation of first order force in a wave with the same wave number as the associated force with a set-down wave. The first order diffraction and radiation $\Phi_D$ and $\Phi_R$ potentials are small compared to the undisturbed wave potential $\Phi_w$. The amplitude of wave load is modified to estimate wave forces related to set-down of the incoming wave; the combination of two first order waves carry a second order wave with wavenumber $k_i - k_j$. The second order wave potential can then be approximated by [37, 39]:

$$
\begin{aligned}
\Phi^{(2)} &= -\sum_{i=1}^{2}\sum_{j=1}^{2} \zeta_i \cdot \zeta_j \cdot A_{ij} \cdot \frac{\cosh((k_i - k_j) \cdot (z - d))}{\cosh((k_i - k_j) \cdot d)} \\
&\times \sin\left[(k_i - k_j)x - (\omega_i - \omega_j)t + (\varepsilon_i - \varepsilon_j)\right]
\end{aligned}
$$

Where $\Phi^{(2)}$ is the LF part of the second order incoming wave potential, $(k_i - k_j)$ the wave number of the LF bound wave and $A_{ij}$ defined as:

$$
A_{ij} = \frac{1}{2} \cdot g^2 \cdot \frac{B_{ij} + C_{ij}}{(\omega_i - \omega_j)^2 - (k_i - k_j) \cdot g \cdot \tanh((k_i - k_j) \cdot d)} \tag{D-19}
$$

In which $B_{ij}$ and $C_{ij}$ are:

$$
B_{ij} = \frac{k_i^2}{\omega_i \cdot \cosh^2(k_i \cdot d)} - \frac{k_j^2}{\omega_j \cdot \cosh^2(k_j \cdot d)}
$$

$$\tag{D-20}$$

$$
C_{ij} = \frac{2 \cdot k_i k_j (\omega_i - \omega_j) \cdot (1 + (\tanh(k_i \cdot d)(\tanh(k_j \cdot d))))}{\omega_i \cdot \omega_j}
$$

The LF part represents a long wave induced by the presence of the regular wave group. It is assumed that a first order wave of which the frequency equals the difference frequency of a bound wave can be used to describe this bound wave. The incoming waves due to LF second order potential have a wave number equal to $k_i - k_j$ and frequency $\omega_i - \omega_j$, which doesn't meet the dispersion relationship (2-18). To overcome this issue, the diffracted waves are allowed to have the same wave number as the incoming waves. Differences will occur in diffracted waves further away from the body. The ordinary first order wave exciting force on the body in a regular wave is then solved for a wave number $k_i - k_j$.

The frequency for this bound wave will satisfy the dispersion relationship in shallow water. Furthermore, the gravitational acceleration constant $g$ is also altered:
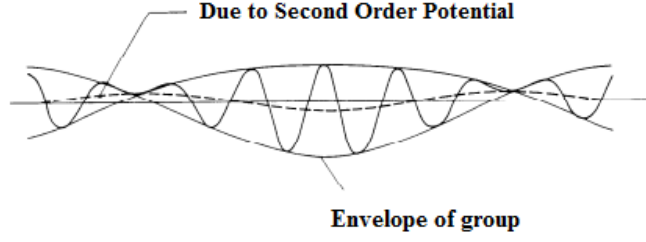
**Figure D-15:** Second Order Potential Contribution

$$g_{ij} = \frac{(\omega_i - \omega_j)^2}{(k_i - k_j) \cdot \tanh((k_i - k_j) \cdot d)} \tag{D-21}$$

This factor must be taken into account when transforming the initial force $F^{(1)}$ to a second order wave force with frequency $\omega_i - \omega_j$. Another requirement to be met is that the amplitudes of the potential must be equal. This means that a first order wave potential must be selected so that:

$$\zeta_a^{(1)} = \zeta_i \cdot \zeta_j \cdot \frac{A_{ij}(\omega_i - \omega_j)}{g_{ij}} \tag{D-22}$$

Which is a second correction factor to $F^{(1)}$ to give $F^{(2)}$. Ultimately, the fifth contribution, the vertical drift force due to incoming and diffracted second order potential can be approximated by:

$$F_z^{(2)}(\omega_i - \omega_j) \approx \zeta_i \cdot \zeta_j \cdot \frac{A_{ij}(\omega_i - \omega_j)}{g} \cdot F_z^{(1)}(k_i - k_j) \tag{D-23}$$

Where $F_z^{(1)}(k_i - k_j)$ is the first order vertical wave induced force [39].

**Python**  To validate calculation method to find the approximation $\Phi^{(2)}$, the first order vertical wave induced force for a wave number of $\Delta k = k_i - k_j$ is plotted against a first order wave with wave number $k_i$ where the latter $k_i$ equals $\Delta k$.
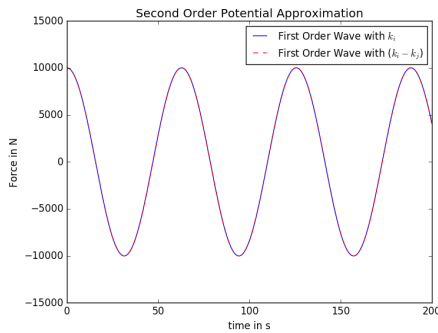


**Figure D-16:** Vertical Drift Force for difference wavenumber $(k_i - k_j)$
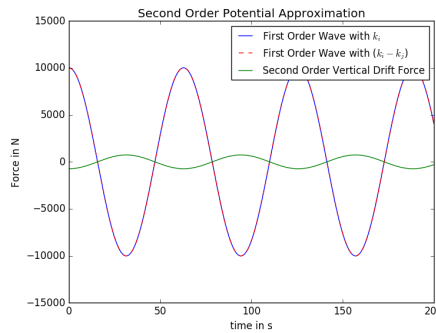


**Figure D-17:** Vertical drift force for difference frequency $(\omega_i - \omega_j)$

Now the drift force can be calculated by the transformation parameters $A_{ij}, B_{ij}, C_{ij}$ in (D-19) and (D-20), which is shown in Figure D-17 for a water depth of $d = 5$m, and frequencies $\omega_i = 0.2$rad/s and $\omega_j = 0.1$ rad/s. The depth effects on these second order drift forces is shown in Figure D-18.
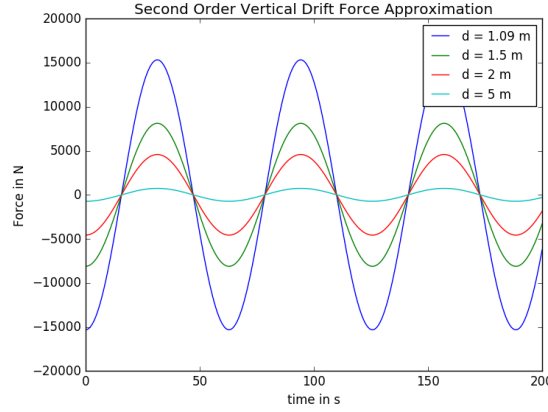


**Figure D-18:** Vertical drift force at different depths

## Set-down Correction

In the case of difference frequency second order loads in heave DOF, there appears an inconsistency which is sometimes ignored. In Stokes second order waves there is often a term neglected which accounts for an additional free surface decrease, i.e. set-down, which adds to the set-down resulting from quadratic product of the first order potential. When second order Stokes waves are considered and this term is ignored, the estimated set-down will be smaller and the steady vertical second order force will subsequently be underestimated. Ignoring this additional set-down related to a monochromatic second order Stokes wave causes inconsistency in the vertical drift force where the difference frequency is zero [38, 44].

It can be proven that the contribution to set-down is much more significant than classical Stokes derivation [44]. The classical correction for set-down in the second order Stokes wave is the following:

$$D = -\frac{k \cdot \zeta_a^2}{2 \cdot \sinh(2kd)} \tag{D-24}$$

The correction by Chen (2005) [44] is found as an addition to this $D$ through the derivation of the second order incident bi-chromatic wave potential.

$$
\begin{aligned}
\Phi^{(2)} &= \mathrm{Re}\left\{\phi_1^{(2)} \cdot e^{(-i2\omega_1 t)}\right\} + \mathrm{Re}\left\{\phi_2^{(2)} \cdot e^{(-i2\omega_2 t)}\right\} \\
&= -(C_1 + C_2)gt + \mathrm{Re}\left\{\phi_+^{(2)} \cdot e^{(-i(\omega_1 + \omega_2)t)}\right\} + \mathrm{Re}\left\{\phi_-^{(2)} \cdot e^{(-i(\omega_1 - \omega_2)t)}\right\}
\end{aligned}
\tag{D-25}
$$

The first order potential of a bi-chromatic wave become the potential of a regular wave with the amplitude doubled, when $\omega_1 \to \omega_2$ and $\epsilon_1 \to \epsilon_2$ performed at the same time. When the difference approaches zero, the results are matched with the classical form of the second order stokes elevation (2-34). To keep consistency, the components at double frequency and

set-down of second-order potential in bi-chromatic waves are quadruple of those in regular waves:

$$\phi_1^{(2)} + \phi_2^{(2)} + \phi_+^{(2)} \rightarrow 4 \cdot \phi^{(2)} \tag{D-26}$$

In the limit, where $\omega_i - \omega_j \rightarrow 0$, this constant $C$ can be found:

$$C = \frac{k\zeta_a^2}{4} \left[ \frac{4S + 1 - \tanh^2(kd)}{4S^2 kd - \tanh(kd)} \right] \tag{D-27}$$

With:

$$S = \frac{\sinh(2kd)}{2kd + \sinh(2kd)} \tag{D-28}$$

The vertical mean drift force in monochromatic wave accounting for bi-chromatic wave set-down effects is then given by:

$$T_{3jj}(\omega_j) = P_3(\omega_j) + R_3 \tag{D-29}$$

Thus when a bi-chromatic wave is considered of two second order stokes waves, this additional set-down term needs to be include in the determination of vertical motions of the vessel. It is important to take account for both set-down terms to maintain consistency between second-order mean vertical fore in regular wave and low-frequency forces in bichromatic waves [**?**]. The additional steady vertical second order force is then simply given by:

$$R_3(\omega) = \rho g A_{WL} \eta_c \tag{D-30}$$

# Bibliography

[1] L. Wang, H. Tang, and Y. Wu, "Wave interaction with a surface-piercing body in water of finite depth," *Engineering Applications of Computational Fluid Mechanics*, 2016.

[2] W. Journée, Johan M.J & Massie, *Offshore Hydrodynamics*. Delft: University of Technology, 2001.

[3] R. Taghipour, T. Perez, and T. Moan, "Hybrid frequency-time domain mmodel for dynamic response analysis of marine structures," *Ocean Engineering*, vol. 35, pp. 685–705, 2008.

[4] J. D. Fenton, "Nonlinear wave theories," *Ocean Engineering Science*, vol. 9, 1990.

[5] DNV, *Environmental Conditons and Environmental Loads*. Det Norske Veritas, April 2007.

[6] L. Xiong, L. Haining, J. Yang, and W. Zhao, "Motion responses of a moored barge in shallow water," *Ocean Engineering*, vol. 97, pp. 207–217, 2015.

[7] J. You and O. M. Faltinsen, "A numerical investigation of second-order differnece frequency forces and motions of a moored ship in shallow water," *Journal Ocean Engineering Maritime Energy*, vol. 1, pp. 157–179, 2015.

[8] O. A. Peters and R. Huijsmans, "Assessing hydrodynamic behavior during offshore loading and discharge in the heavy marine transport," in *Proceedings of the ASME 2011 30th International Conference on Ocean, Offshore and Arctic Engineering*, (Rotterdam, The Netherlands), OMAE2011, 19-24 June 2011.

[9] T. Tezdogan, A. Incecik, and O. Turan, "Full-scale unsteady rans simulations of vertical ship motions in shallow water," *Ocean Engineering*, vol. 123, pp. 131–145, July 2016.

[10] Y. Drobyshevski, "Hydrodynamic coefficients of a two-dimensional, truncated rectangular floating structure in shallow water," *Ocean Engineering*, vol. 31, pp. 305–341, 2004.

[11] B. Buchner, "The motions of a ship on a sloped seabed," in *International Conference on Offshore Mechanics and Arctic Engineering*, no. 25th, (Hamburg, Germany), 4-9 June 2006.

[12] F. Ursell, "The long-wave paradox in the theory of gravity waves," *Mathematical Proceedings of the Cambridge Philosophical Society*, vol. 49, no. 4, p. 685âĂŞ694, 1953.

[13] H. Cozijn, R. Uittenbogaard, and E. ter Brake, "Heave, roll and pitch damping of a deepwater clam buoy with a skirt," in *The International Society of Offshore and Polar Engineers*, Proceedings of the Fifteenth International Offshore and Polar Engineering Conference, June 19-24 2005.

[14] G. Clauss, F. Stempinski, M. Dudek, and M. Klein, "Water depth influence on wave-structure-interaction," *Ocean Engineering*, vol. 36, pp. 1396 – 1403, 2009.

[15] Z.-M. Yuan, A. Incecik, S. Dai, and S. Day, "Hydrodynamic interactions between two ships travelling or stationary in shallow waters," *Ocean Engineering*, pp. 620–635, August 2015.

[16] L. Roald, J. Jonkman, and A. Robertson, "The effect of second-order hydrodynamics on a floating offshore wind turbine," Tech. Rep. 5000-61452, National Renewable Energy Laboratory, May 2014.

[17] I. Bayati, S. Gueydon, and M. Belloli, "Study of the effect of water depth on potential flow solution of the oc4 semisubmersible floating offshore wind turbine," *Energy Procedia*, vol. 80, pp. 168–176, 2015.

[18] R. M. Sorensen, *Basic Coastal Engineering.* Springer, 3 ed., 2006.

[19] S. K. Chakrabarti, *Hydrodynamics of Offshore Structures.* Ashurst Lodge, Ashurst, Southampton, SO40 7AA, United Kingdom: WIT Press, 1987.

[20] G. Z. Forristall, "Wave crest distributions: Observations and second-order theory," *Journal of Physical Oceanography*, vol. 30, no. 8, pp. 1931–1943, 2000.

[21] D. Peregrine, "Breaking waves on beaches," *Annual Review Fluid Mechanics*, vol. 15, pp. 149–178, 1983.

[22] R. W. Yeung and Y. Jiang, "Shape effect on viscous damping and motion of heaving cylinders," *Journal of Offshore Mechanics and Arctic Engineering*, vol. 136, November 2014.

[23] S. K. Chakrabarti, *Handbook of Offshore Engineering.* Elsevier, 2005.

[24] D. Hasson and C. Crowe, *Materials for Marine Systems and Structures*, vol. 28 of *Treatise on Materials Science and Technology.* Academic Press, Inc., 1988.

[25] O. Kimmoun, B. Molin, and E. Fontainel, "Experimental study of the wave response of a two-dimensional rectangular barge in very shallow water.," tech. rep., International Workshop on water waves and floating bodies, 2005.

[26] O. M. Faltinsen, *Sea Loads on Ships and Offshore Structures.* Cambridge University Press, 1990.

[27] Z. Zhou, E. Y. Lo, and S. Tan, "Effect of shallow and narrow water on added mass of cylinders with various cross-sectional shapes," *Ocean Engineering*, vol. 32, pp. 1199–1215, 2005.

[28] W. Koo and J.-D. Kim, "Simplified formulas of heave added mass coefficients at high frequency for various two-dimensional bodies in a finite water depth," *International Journal of Naval Architecture and Ocean Engineering*, vol. 7, pp. 115–127, 2015.

[29] B. Boer, Gerrit de & Buchner, ed., *Viscous Damping of Vessels Moored in Close Proximity of Another Object*, (Seoul, Korea), Internatioal Offshore and Polar Engineering Conference, June 19-24 2005.

[30] J. Pinkster and R. Huijsmans, "Wave drift forces in shallow water," in *Proceedings of the 1992 BOSS Conference*, (London, UK), 1992.

[31] C. Brennen, "A review of added mass and fluid inertial forces," *Naval Civil Engineering Laboratory*, 1982.

[32] B. Molin, "On the frictional damping in roll of ship sections," *International Shipbuilding Program*, vol. 51, pp. 59–85, January 2004.

[33] M. Borg and M. Collu, "Offshore floating vertical axis wind tturbine, dynamics modelling state of the art. part iii: Hydrodynamics and coupled modelling approaches," *Renewable and Sustainable Energy Reviews*, 2014.

[34] B. Pena and A. McDougall, eds., *An Investigation into the Limitation of the Panel Method and the Gap Effect for a Fixed and a Floating Structure subject to Waves*, no. 35th, (Busan, South Korea), International Conference on Ocean, Offshore and Arctic Engineering, June 19-24 2016.

[35] A. Subulakshmi, J. Jose, R. Sundaravadivelu, and P. Selvam, "Effect of viscous damping on hydrodynamic response of spar with heave plate," *Aquatic Procedia. International conference on Water Resources, Coastal and Ocean Engineering*, vol. 4, pp. 508–515, 2015.

[36] J. M. J. Journée, *Theoretical Manual of SEAWAY*. Delft University of Technology, Mekelweg 2, 2628 CD Delft, February 2001.

[37] J. Pinkster, *Low frequency second order wave exciting forces on floating structures*. PhD thesis, Delft University of Technology, 1980.

[38] J. Pessoa, N. Fonseca, and C. Soares, "Analysis of the first order and slowly varying motions of an axisymmetric floating body in bichromatic waves," *Journal of Offshore Mechanics and Arctic Engineering*, vol. 13, 2013.

[39] International Workshop on Ship and Platform Motions, *Non-Linear Ship Motions in Shallow Water*, October 1983.

[40] Y. Liu, B. Molin, O. Kimmoun, F. Remy, and M.-C. Roualt, "Experimental and numerical study of the effect of variable bathymetry on the slow-drift wave response of floating bodies," *Applied Ocean Research*, no. 33, pp. 199–207, 2011.

[41] B. Molin and V. Fauveau, "Effect of wave-directionality on second-order loads induced by the set-down," *Applied Ocean Research*, vol. 6, no. 2, pp. 66–72, 1984.

[42] J. N. Sharma and R. G. Dean, *Development and evaluation of a procedure for simulating a random directional second order sea surface and associated wave forces.* University of Delaware, 1979.

[43] A. Voogt, "Second order effect in extreme waves and shallow water waves," in *2nd International Workshop on Applied Offshore Hydrodynamics*, (Rio de Janeiro, Brazil), April 2005.

[44] X. B. Chen, "The set-down in the second-order stokes waves," tech. rep., Bureau Veritas, Paris, France, 2005.

[45] S. Rajendran, N. Fonseca, and C. Soares, "Body nonlinear time domain calculation of vertical ship responses in extreme eseas accounting for 2nd order froude-krylov pressure," *Applied Ocean Research*, vol. 54, pp. 39–52, 2016.

[46] J. Pessoa and N. Fonseca, "Investigation of depth effects on the wave exciting low frequency drift forces by different approximation methods," *Applied Ocean Research*, vol. 42, pp. 182–199, 2013.

[47] O. J. Waals, "The effect of wave directionality on low frequency motions and mooring forces," in *28th International Conference on Ocean, Offshore and Arctic Engineering*, (Honolulu, Hawaii), May 31 - June 5 2009.

[48] X. Chen and W. Duan, "Formula of low-frequency qtf by $o(\bigtriangledown\omega)$ approximation," tech. rep., International Workshop on Water Waves and Floating Bodies, Plitvice, Croatia, 2007.

[49] S. Rajendran, N. Fonseca, and G. Soares, "Effect of surge motion on the vertical repsonses of ships in waves," *Ocean Engineering*, vol. 96, pp. 125–138, March 2015.

[50] J. Journée, "Hydromechanic coefficients for calculating time domain motions of cutter suction dredgers by cummins equations," tech. rep., Delft University of Technology, Mekelweg 2,2628 CV Delft, 1993.

[51] M. H. Meylan, "The time-dependent motion of a floating elastic or rigid body in two dimensions," *Applied Ocean Research*, vol. 46, pp. 54–61, 2014.

[52] T. Perez and T. I. Fossen, "Identification of dynamic mdels of marine structures from frequency-domain data enforcing model structure and parameter constraints," tech. rep., ARC Centre of Excellence for Complex Dynamic Systems and Control, 2009.

[53] W. Cummins, "The impulse response function and ship motions," in *Symposium on Strip Theory*, vol. 9, (Hamburg, Germany), pp. 101–109, InstitÃijt fÃijr Schiffbau der UniverstiÃďt Hamburg, Schiffstechnik, January 1962.

[54] T. Ogilvie, "First and second order forces on a cylinder submerged under a free surface," *Journal of Fluid Mechanics*, pp. 451–472, 1963.

[55] J. A. Armesto, R. Guanche, F. d. Jesus, A. Iturrioz, and I. J. Losada, "Comparative analsysi of the method to compute the radiation term in cummins' equation," *Journal Ocean Engineering Maritime Energy*, vol. 1, pp. 377–393, 2015.

[56] E. Kristiansen, A. Hjulstad, and O. Egeland, "State-space representation of radiation forces in time-domain vessel models," *Modeling, Identification and Control*, vol. 27, no. 1, pp. 23–41, 2006.

[57] E. W. Kamen and B. S. Heck, *Fundamentals of Signals and Systems*. Pearson Prentice Hall, 3 ed., 2007.

[58] W. van der Molen and W. Ivo, "Time-domain calculation of moored ship motions in nonlinear waves," *Coastal Engineering*, vol. 55, pp. 409–422, March 2008.

[59] W. Sheng, R. Alcorn, and A. Lewis, "A new method for radiation forces for floating platforms in waves," *Ocean Engineering*, pp. 43–53, 2015.

[60] S. K. Chakrabarti, *The Theory and Practice of Hydrodynamics and Vibration*, vol. 20 of *Advanced Series on Ocean Engineering*. 5 Toh Tuck Link, SIngapore 596224: World Scientific, 2002.

[61] ASME 28th International Conference on Ocean, Offshore and Arctic Engineering, *Estimation of Roll Damping for Transportation Barges*, (Honolulu, Hawaii), May 31- June 5 2009.

[62] M. Patel and J. Witz, *Compliant Offshore Structures, Elsevier, pp. 80âĂŞ83,*. Elsevier, 2013. pp. 80-83.

[63] E. N. Seelig, D. Kriebel, and J. Headland, "Broadside current forces on moored ships.," *In Proceedings of Civil Engineering in the Oceans*, 1992.

[64] P. Sammarco and M. Risio, "Effect of moored boats on the gradully varied free-surface profiles of river flow," *Journal of Waterway, Port, Coastal, and Ocean Engineering*, October 2016.

[65] DNV, *Modelling and Analysis of Marine Operations*. Det Norske Veritas, dnv-rp-h103 ed., April 2011.

[66] S. Munshi, V. Modi, and T. Yokomizo, "Fluid dynamics of flat plates and rectangular prisms in the presence of moving surface boundary layer control," *Journal of Wind Engineering and Industrial Aerodynamics*, vol. 79, pp. 37–60, 1999.